

75348

NATIONAL LIBRARY  
OTTAWA



BIBLIOTHÈQUE NATIONALE  
OTTAWA

NAME OF AUTHOR..... Kathleen A. Simpson  
 TITLE OF THESIS..... Some Crystal Structures  
 ..... of Transition Metal Hydrides  
 .....  
 UNIVERSITY..... Alberta (Edmonton)  
 DEGREE FOR WHICH THESIS WAS PRESENTED..... Ph.D  
 YEAR THIS DEGREE GRANTED..... 1973

Permission is hereby granted to THE NATIONAL LIBRARY  
 OF CANADA to microfilm this thesis and to lend or sell copies  
 of the film.

The author reserves other publication rights, and  
 neither the thesis nor extensive extracts from it may be  
 printed or otherwise reproduced without the author's  
 written permission.

(Signed)..... Kathleen Simpson

PERMANENT ADDRESS:

..... 10803 63 Ave.  
 .....  
 .....

DATED..... April 27 ..... 19 73

NL-91 (10-68)

THE UNIVERSITY OF ALBERTA

SOME CRYSTAL STRUCTURES OF TRANSITION METAL HYDRIDES

by



KATHLEEN A. SIMPSON

A THESIS

SUBMITTED TO THE FACULTY OF GRADUATE STUDIES AND RESEARCH  
IN PARTIAL FULFILMENT OF THE REQUIREMENTS FOR THE DEGREE  
OF DOCTOR OF PHILOSOPHY

DEPARTMENT OF CHEMISTRY

EDMONTON, ALBERTA

SPRING, 1973

THE UNIVERSITY OF ALBERTA  
FACULTY OF GRADUATE STUDIES AND RESEARCH

The undersigned certify that they have read, and recommend to the Faculty of Graduate Studies and Research, for acceptance, a thesis entitled SOME CRYSTAL STRUCTURES OF TRANSITION METAL HYDRIDES submitted by KATHLEEN A. SIMPSON in partial fulfilment of the requirements for the degree of Doctor of Philosophy.

*M. J. Bennett*  
.....  
M. J. Bennett, Supervisor

*F. W. Birss*  
.....  
F. W. Birss

*W. A. G. Graham*  
.....  
W. A. G. Graham

*R. E. D. McClung*  
.....  
R. E. D. McClung

*D. Rankin*  
.....  
D. Rankin

*Frederick W. B. Fainstein*  
.....  
External Examiner

Date .. *April 26, 1973* .....

## ABSTRACT

A rudimentary discussion of crystal symmetry includes unit cells, symmetry elements and operations, space group notation and general position definitions. Using the Laue equations and Bragg's law, the geometry of film diffraction patterns is discussed including the idea of reciprocal space. An expression is developed which shows the structure factor to be a Fourier transform of electron density. Modifications to the structure factor expression using Friedel's law and symmetry operations are illustrated. Two methods, direct and Patterson, for locating atoms within the unit cell are explained. The basic experimental and computational techniques used are given.

The history of transition metal hydrides is briefly traced from the earliest preparation of  $\text{Fe}(\text{CO})_4\text{H}_2$  through the NMR characterization of  $\text{HRe}(\text{C}_5\text{H}_5)_2$  to the determination of the hydride position by neutron diffraction in  $\text{HMn}(\text{CO})_5$ , and the formulation of bridged hydride species as in  $\text{HMnRe}_2(\text{CO})_{14}$ . The preparation and structural properties of Group IV substituted carbonyl hydrides of transition metals are given.

The compound  $\text{H}_2\text{W}_2(\text{CO})_4\text{Si}_2(\text{C}_2\text{H}_5)_2$  crystallizes in space group  $\text{P}2_1/n$  ( $Z = 2$ ) with cell dimensions  $a = 9.212(1)$ ,  $b = 10.131(1)$ ,  $c = 12.749(1)$  Å,  $\beta = 99.07(1)^\circ$ . The structure was refined to an R factor of 0.038 for 945 reflec-

tions. The tungsten atoms are held together by a W-W bond and by two silicon bridges. There are two distinct W-Si bond lengths, the longer being interpreted as a three-centre two-electron bond involving the hydrogen atom.

The compound  $\text{HFe}(\text{CO})_4\text{Si}(\text{C}_6\text{H}_5)_3$ , crystallizes in the triclinic space group  $P\bar{1}$  with  $a = 10.062(1)$ ,  $b = 10.377(1)$ ,  $c = 10.800(6)$  Å,  $\alpha = 90.96(3)$ ,  $\beta = 111.43(1)$ ,  $\gamma = 98.55(1)^\circ$  and  $Z = 2$ . The structure was refined using data from eight crystals to an R factor of 0.061 based on 1612 reflections. The terminal hydridic hydrogen is at a normal covalent distance from iron.

The compound  $(\pi\text{-C}_5\text{H}_5)\text{HMn}(\text{CO})_2\text{Si}(\text{C}_6\text{H}_5)\text{Cl}_2$  crystallizes in space group  $P\bar{1}$  with  $a = 10.995(1)$ ,  $b = 8.171(1)$ ,  $c = 8.486(1)$  Å,  $\alpha = 98.25(1)$ ,  $\beta = 98.06(1)$ ,  $\gamma = 100.26(1)^\circ$  and  $Z = 2$ . Its structure was refined to an R factor of 0.039 using 968 reflections. The hydridic hydrogen atom is located in a bridging position with respect to manganese and silicon forming a bent three-centre two-electron bond with  $\text{Mn-H} = 1.49$  and  $\text{Si-H} = 1.79$  Å.

The compound  $(\pi\text{-C}_5\text{H}_5)\text{HFe}(\text{CO})(\text{Si}(\text{CH}_3)_2\text{C}_6\text{H}_5)_2$  crystallizes in the orthorhombic space group  $Pbca$  with  $Z = 8$  and  $a = 19.028(3)$ ,  $b = 13.320(2)$ ,  $c = 17.316(2)$  Å. The structure was refined to an R factor of 0.055 with 1180 reflections. The structure may be viewed as a distorted tetragonal pyramid with the centroid of the cyclopentadienyl

v.

ring at the apex, the carbonyl and dimethylphenylsilyl ligands in the basal plane with the latter trans to each other and the iron displaced toward the cyclopentadienyl ring. The remaining position in the basal plane of the pyramid is assumed to be occupied by the hydridic hydrogen which was not conclusively located.

ACKNOWLEDGEMENTS

I would like to express my sincere appreciation to:

Professor M. J. Bennett for his patient guidance and friendly tutoring throughout my apprenticeship in crystallography and pursuit of this research.

Professor W. A. G. Graham for steering me into crystallography, and his research group for providing most of the crystals used in these studies.

Professor W. E. Harris for generously employing me as a teaching assistant in an outstanding course.

The X-ray crystallographic group, past and present, especially W. L. Hutcheon, for comradeship and support.

And the National Research Council and the University of Alberta for financial assistance.

## TABLE OF CONTENTS

	Page
<u>Chapter 1:</u> General Crystallographic Introduction	
Crystals and Symmetry . . . . .	1
X-Ray Diffraction . . . . .	8
Determination of Atom Positions . . . . .	23
Experimental . . . . .	28
<u>Chapter 2:</u> General Chemical Introduction . . . . .	33
<u>Chapter 3:</u> The Crystal and Molecular Structure of $\text{H}_2\text{W}_2(\text{CO})_8\text{Si}_2(\text{C}_2\text{H}_5)_4$	
Introduction . . . . .	40
Experimental . . . . .	42
Solution and Refinement . . . . .	46
Results . . . . .	50
Discussion . . . . .	61
<u>Chapter 4:</u> The Crystal and Molecular Structure of $\text{HFe}(\text{CO})_4\text{Si}(\text{C}_6\text{H}_5)_3$	
Introduction . . . . .	66
Experimental . . . . .	68
Solution and Refinement . . . . .	73
Results . . . . .	86
Discussion . . . . .	95



## Table of Contents

	Page
<u>Chapter 5:</u> The Crystal and Molecular Structure of $(\pi\text{-C}_5\text{H}_5)\text{HMn}(\text{CO})_2\text{SiCl}_2(\text{C}_6\text{H}_5)$	
Introduction . . . . .	100
Experimental . . . . .	102
Solution and Refinement . . . . .	106
Results . . . . .	117
Discussion . . . . .	128
 <u>Chapter 6:</u> The Crystal Structure of $(\pi\text{-C}_5\text{H}_5)\text{HFe}(\text{CO})$ $[\text{Si}(\text{CH}_3)_2\text{C}_6\text{H}_5]_2$	
Introduction . . . . .	140
Experimental . . . . .	141
Solution and Refinement . . . . .	147
Results . . . . .	161
Discussion . . . . .	172
 <u>Chapter 7:</u> Summary and Conclusions . . . . .	181
 <u>References</u> . . . . .	187
 <u>Appendix A:</u> Structure of $\text{Sn}(\text{Fe}(\text{CO})_4\text{SiCl}_3)_2\text{Cl}_2$	
Experimental . . . . .	194
Discussion . . . . .	195
 <u>Appendix B:</u> Redetermination of the Crystal Structure of Ferrocene	
Introduction . . . . .	196

## Table of Contents

	Page
Experimental . . . . .	197
Solution and Refinement . . . . .	199
Discussion . . . . .	204
<u>Appendix C:</u> DREFINE, a Program in FORTRAN to Obtain Accurate Cell Parameters . . . . .	208

LIST OF TABLES

	Page
<u>Chapter 1:</u>	
Table I: Symmetry operations . . . . .	3
Table II: Crystal systems . . . . .	5
Table III: Bravais lattices . . . . .	6
Table IV: Direct, reciprocal lattice relationships . . . . .	12
Table V: Systematic absences . . . . .	22
 <u>Chapter 2:</u>	
Table VI: Transition metal silicon hydrides . . . . .	37
 <u>Chapter 3:</u>	
Table VII: % composition of $H_2W_2(CO)_8$ [Si(C <sub>2</sub> H <sub>5</sub> ) <sub>2</sub> ] <sub>2</sub> . . . . .	45
Table VIII: Observed and calculated structure factor amplitudes . . . . .	48
Table IX: Final coordinate and thermal parameters . . . . .	49
Table X: Bond lengths . . . . .	56
Table XI: Bond angles . . . . .	57
Table XII: Intramolecular contacts . . . . .	58
Table XIII: Intermolecular contacts . . . . .	59

List of Tables (Continued)

	Page
Table XIV: Least squares planes and distances of selected atoms from these planes . . . . .	60
 <u>Chapter 4:</u>	
Table XV: Crystal information . . . . .	70
Table XVI: Patterson vectors . . . . .	74
Table XVII: Patterson solutions . . . . .	75
Table XVIII: Statistical distribution of E's	76
Table XIX: Calculated and observed hydride peak heights . . . . .	77
Table XX: Final coordinate and thermal parameters . . . . .	82
Table XXI: Rigid body parameters. . . . .	83
Table XXII: Derived parameters for rigid bodies . . . . .	84
Table XXIII: Observed and calculated structure factor amplitudes . . . . .	85
Table XXIV: Bond lengths . . . . .	91
Table XXV: Bond angles . . . . .	92
Table XXVI: Non-bonding intramolecular distances . . . . .	93
Table XXVII: Intermolecular contacts . . . . .	94

## List of Tables (Continued)

	Page
<u>Chapter 5:</u>	
Table XXVIII:	Chemical data on hydrides . . . 99
Table XXIX:	Statistical distribution of E's 105
Table XXX:	Calculated and observed hydride peak heights . . . . . 110
Table XXXI:	Observed and calculated struc- ture factor amplitudes . . . . 111
Table XXXII:	Final positional and thermal parameters . . . . . 112
Table XXXIII:	Parameters for the rigid bodies and hindered rotors . . . . . 113
Table XXXIV:	Derived parameters for rigid bodies and hindered rotors . . 114
Table XXXV:	Bond lengths and angles . . . . 123
Table XXXVI:	Intramolecular contacts . . . . 125
Table XXXVII:	Intermolecular contacts . . . . 126
Table XXXVIII:	Comparison of silicon-chlorine bond lengths . . . . . 136
Table XXXIX:	Comparison of hindered rotors . 137
Table XL:	Comparison of cyclopentadienyl manganese carbonyl compounds . 138

List of Tables (Continued)

	Page
<u>Chapter 6:</u>	
Table XLI:	Patterson vectors . . . . . 144
Table XLII:	Patterson solutions . . . . . 145
Table XLIII:	Phasing planes in direct solution . . . . . 150
Table XLIV:	Comparison of solutions . . . . 150
Table XLV:	Calculated and observed hydride peak heights . . . . . 153
Table XLVI:	Observed and calculated struc- ture factor amplitudes . . . . 156
Table XLVII:	Positional and thermal para- meters of individual atoms . . 157
Table XLVIII:	Parameters for rigid bodies and hindered rotors . . . . . 158
Table XLIX:	Derived individual atom para- meters for rigid bodies and hindered rotors . . . . . 159
Table L:	Bond lengths and angles . . . . 164
Table LI:	Intramolecular distances with models for thermal motion . . . 166
Table LII:	Intramolecular contacts . . . . 167
Table LIII:	Intermolecular contacts . . . . 168

## List of Tables (Continued)

	Page
Table LIV: Comparison of bond lengths, angles . . . . .	171
<u>Appendix B:</u>	
Table LV: Positional coordinates . . . .	201
Table LVI: Observed and calculated struc- ture factor amplitudes . . . .	202
Table LVII: Positional and thermal parameters . . . . .	203
Table LVIII: Comparison of bond lengths . .	207

## LIST OF FIGURES

	Page
<u>Chapter 1:</u>	
Figure 1: Laue equation: definitions in one dimension . . . . .	10
Figure 2: Bragg's law definitions . . . . .	10
Figure 3: A and B terms in the structure factor . . . . .	17
<u>Chapter 3:</u>	
Figure 4: A perspective view of $H_2W_2(CO)_8[Si(C_2H_5)_2]_2$ . . . . .	51
Figure 5: $W_2Si_2$ structural fragment . . . . .	52
Figure 6: Packing of $H_2W_2(CO)_8[Si(C_2H_5)_2]_2$ down the a axis . . . . .	53
Figure 7: Packing of $H_2W_2(CO)_8[Si(C_2H_5)_2]_2$ down the b axis . . . . .	54
Figure 8: Packing of $H_2W_2(CO)_8[Si(C_2H_5)_2]_2$ down the c axis . . . . .	55
<u>Chapter 4:</u>	
Figure 9: Perspective view of $HFe(CO)_4Si(C_6H_5)_3$ . . . . .	87
Figure 10: Packing of $HFe(CO)_4Si(C_6H_5)_3$ down the a axis . . . . .	88



List of Figures

	Page
Figure 11: Packing of $\text{HFe}(\text{CO})_4\text{Si}(\text{C}_6\text{H}_5)_3$ down the b axis . . . . .	89
Figure 12: Packing of $\text{HFe}(\text{CO})_4\text{Si}(\text{C}_6\text{H}_5)_3$ down the c axis . . . . .	90

Chapter 5:

Figure 13: Slant Fourier through the phenyl ring plane . . . . .	115
Figure 14: Slant Fourier through the cyclo- pentadienyl ring plane . . . . .	116
Figure 15: Perspective view of $(\pi\text{-C}_5\text{H}_5)\text{HMn}$ $(\text{CO})_2\text{SiCl}_2(\text{C}_6\text{H}_5)$ . . . . .	118
Figure 16: Geometry of the manganese atom surroundings . . . . .	119
Figure 17: Packing of $(\pi\text{-C}_5\text{H}_5)\text{HMn}(\text{CO})_2$ $\text{SiCl}_2(\text{C}_6\text{H}_5)$ down the a axis . . . . .	120
Figure 18: Packing of $(\pi\text{-C}_5\text{H}_5)\text{HMn}(\text{CO})_2\text{SiCl}_2$ $(\text{C}_6\text{H}_5)$ down the b axis . . . . .	121
Figure 19: Packing of $(\pi\text{-C}_5\text{H}_5)\text{HMn}(\text{CO})_2\text{SiCl}_2$ $(\text{C}_6\text{H}_5)$ down the c axis . . . . .	122
Figure 20: a) Typical anharmonic potential function	

## List of Figures

	Page
b) Scattering density distribution corresponding to the anharmonic stretching vibration in a) . . . . .	139
 <u>Chapter 6:</u>	
Figure 21: Perspective view of $(\pi\text{-C}_5\text{H}_5)\text{HFe}$ $(\text{CO})[\text{Si}(\text{CH}_3)_2\text{C}_6\text{H}_5]_2$ . . . . .	162
Figure 22: Geometry of the iron atom surroundings . . . . .	163
Figure 23: Silicon-hydrogen distances for $(\pi\text{-C}_5\text{H}_5)\text{HFe}(\text{CO})[\text{Si}(\text{CH}_3)_2\text{C}_6\text{H}_5]_2$ . . . . .	179
Figure 24: Silicon-hydrogen distances for $(\pi\text{-C}_5\text{H}_5)\text{HFe}(\text{CO})(\text{SiCl}_3)_2$ . . . . .	180
 <u>Chapter 7:</u>	
Figure 25: Potential energy diagram showing a double minimum . . . . .	187
 <u>Appendix B:</u>	
Figure 26: Perspective drawing of ferrocene . . . . .	206

CHAPTER I

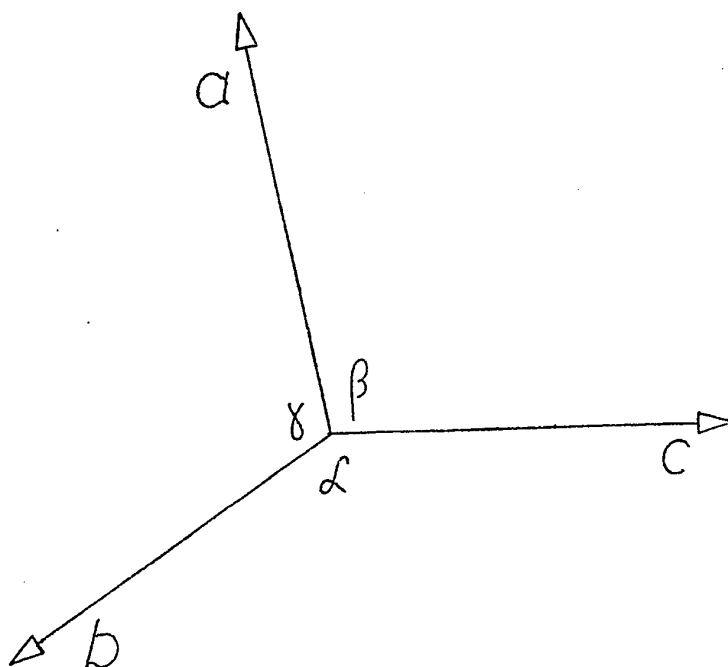
General Crystallographic Introduction

GENERAL CRYSTALLOGRAPHIC INTRODUCTION<sup>1,2</sup>

I. Crystals and Symmetry

A. The Unit Cell

A crystal consists of atoms arranged in a pattern which can contain a single atom, a group of atoms, a molecule or a group of molecules and which repeats periodically in three dimensions. To discuss the pattern quantitatively, a system of reference points is necessary and so one point is chosen at random. All points with identical environment and orientation to this point constitute a lattice. By connecting the lattice points with straight lines a parallelepiped or unit cell can be formed which can be repeated by translation from one lattice point to another to generate the entire lattice. If the positions of the atoms within one unit cell are known, by extension, the atom positions throughout the crystal are determined. The size and shape of the unit cell are specified by the lengths of the three independent edges,  $a$ ,  $b$ ,  $c$  and by the three angles  $\alpha$ ,  $\beta$ ,  $\gamma$  between these edges as shown in the figure below. The axes  $a$ ,  $b$ ,  $c$  define a coordinate system appropriate to the crystal. The location of a point within a unit cell may be specified by means of three fractional coordinates  $(x, y, z)$  defined by starting at an origin  $(0, 0, 0)$  and moving  $xa$  along the  $a$  axis,  $yb$  along the  $b$  axis and  $zc$  along the  $c$  axis.



General Crystallographic Coordinate System

### B. Symmetry Elements and Operations

The three-dimensional repeating unit in the lattice can show symmetry. An object is said to have symmetry if some movement of the object or operation on the object leaves it in a position indistinguishable from its original position. Some symmetry elements and their corresponding symmetry operations along with the Hermann-Mauguin symbol are given in Table I. The collection of symmetry elements possessed by a molecule is called a point group, while a study of the characteristics of point groups is called group theory and will not be treated further here.

In principle, the unit cell which is picked as

Table I  
Symmetry Operations

<u>Symmetry Element</u>	<u>Symmetry Operation</u>	<u>Hermann-Mauguin Symbol</u>
Identity	Rotate by $360^\circ$	I
Rotation axis	Rotate by $\left(\frac{360}{n}\right)^\circ$	n
Mirror plane	Reflection	m
Centre of symmetry	Invert through a point	$\bar{1}$
Rotary inversion	Rotate by $\left(\frac{360}{n}\right)^\circ$ ; Invert through a point	$\bar{n}$

outlined above may be chosen in an infinite number of ways. However, in practice, symmetry may be used to restrict the number of choices for the unit cell. In describing crystals, seven three-dimensional coordinate systems are used (Table II). It can be seen that symmetry considerations dictate some of the relationships between, and values of, the six parameters  $a$ ,  $b$ ,  $c$ ,  $\alpha$ ,  $\beta$ ,  $\gamma$ .

In addition, in order to preserve the advantages of a unit cell chosen on the basis of symmetry, a centred cell in one of the basic crystal systems can be chosen. As shown in Table III fourteen Bravais lattices are then possible. The symbols used in the diagrams are Hermann-Mauguin symbols: P, primitive; C, c-faced centred; I, body-centred; F, all faces centred. Each component of a symbol refers to a different direction except if used in conjunction with a slash, so that for example,  $mmm$  implies three mutually perpendicular mirror planes while  $4/m$  indicates a mirror plane perpendicular to a four-fold rotation axis.

#### C. Translational Symmetry Elements and Space Groups

So far, symmetry as it applies to the repeating pattern or unit cell contents has been considered, but the repetition of the unit of pattern in space also can result in symmetry. There are three new symmetry elements involved, the first of which is the lattice translation

Table II  
Crystal Systems

<u>Crystal System</u>	<u>No. of Independent Parameters</u>	<u>Parameters</u>
Triclinic	6	$a \neq b \neq c$ $\alpha \neq \beta \neq \gamma$
Monoclinic	4	$a \neq b \neq c$ $\alpha = \gamma = 90^\circ \quad \beta \neq 90^\circ$
Orthorhombic	3	$a \neq b \neq c$ $\alpha = \beta = \gamma = 90^\circ$
Tetragonal	2	$a = b \neq c$ $\alpha = \beta = \gamma = 90^\circ$
Rhombohedral	2	$a = b = c$ $\alpha = \beta = \gamma \neq 90^\circ$
Hexagonal	2	$a = b \neq c$ $\alpha = \beta = 90^\circ \quad \gamma = 120^\circ$
Cubic	1	$a = b = c$ $\alpha = \beta = \gamma = 90^\circ$



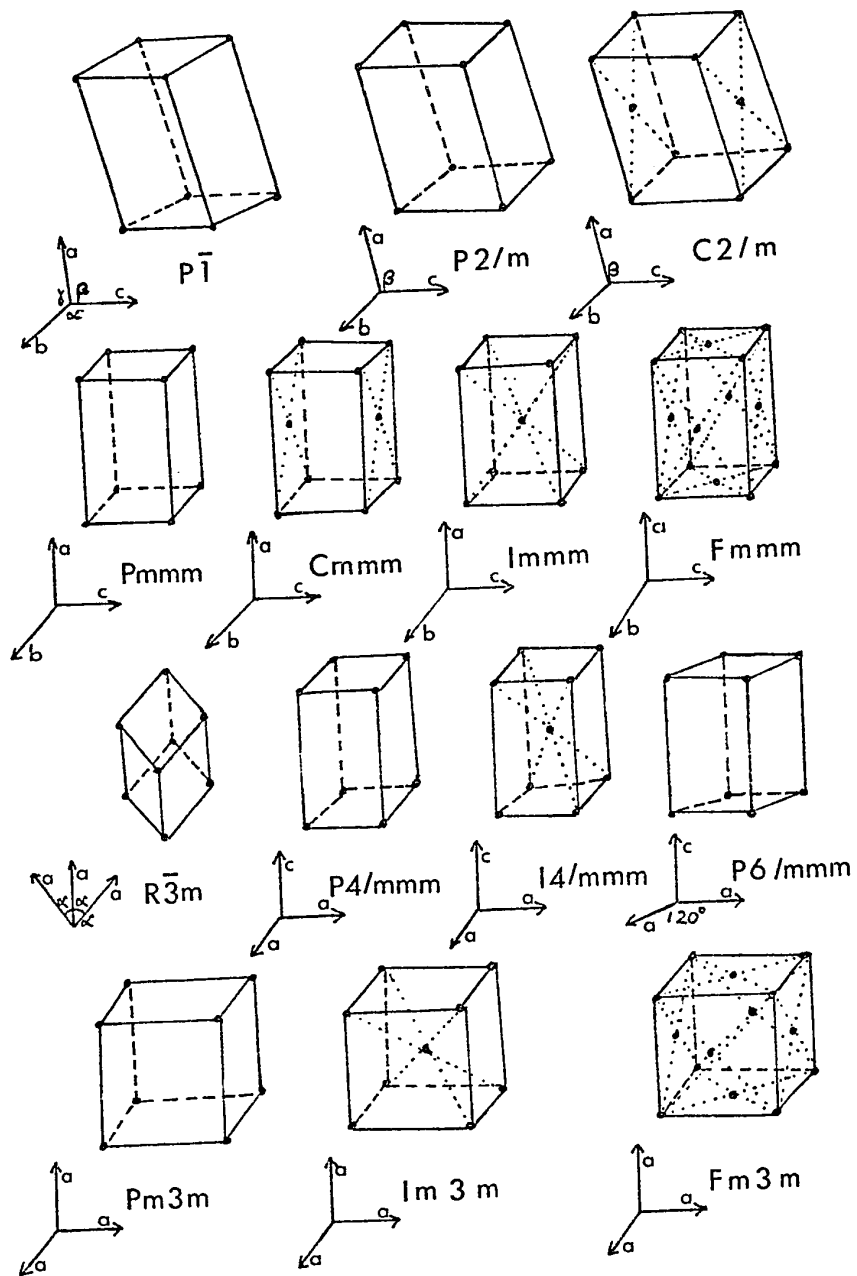


Table III  
Bravais Lattices

itself. Then, there are screw axes,  $n_p$  which constitute a rotation of  $360/n^\circ$  followed by a translation of  $p/n$  in the direction of the axis. Thirdly, there are glide planes consisting of reflection in a plane followed by translation. Thus, "a" implies reflection in the plane followed by translation of  $a/2$  in the a axis direction. There are 230 ways, called space groups, in which motifs may be repeated, which can be symbolized by Hermann-Mauguin symbols as already described. Thus,  $P2_1/c$  implies a primitive monoclinic cell, with a 2-fold screw axis parallel to the b axis, and with a glide plane perpendicular to b, with a translation of  $c/2$ .

#### D. General Positions

Equivalent or general positions refer to the positions generated within the unit cell by the actions of the symmetry elements. So, using the previous example of  $P2_1/c$ , if there is one position at fractional coordinates  $(x, y, z)$ , there is a second position related to this by a two-fold screw along the b axis, that is at  $(\bar{x}, y+\frac{1}{2}, \bar{z})$ . A third position related to the first by a c glide is at  $(x, \bar{y}, z+\frac{1}{2})$ , and finally, there is a position with fractional coordinates  $(\bar{x}, \frac{1}{2}-y, \frac{1}{2}-z)$ , that can be described either as a c glide performed on the second position, or a  $2_1$  performed on the third position. These four posi-

tions are called the equivalent positions for the space group  $P2_1/c$ . (The standard notation places the centre of symmetry at the origin.) Special positions are sets of particular locations which are related by the symmetry elements, and at which objects (molecules) may be placed if and only if they have symmetry which is identical to that of the cell.

## II. X-Ray Diffraction

### A. Laue Equations

X-rays are electromagnetic radiation with wavelengths in the range 0.1 to 100 Å. They are produced for diffraction purposes by decelerating rapidly moving electrons very quickly by collision with a metal target, and converting their energy of motion into a quantum of radiation. The most useful X-rays for studying molecular structure have wavelengths in the vicinity of 1 Å which is comparable to interatomic distances in crystals. The periodic structure of a crystal can be used to diffract X-rays just as gratings are used to produce diffraction patterns with visible light. Diffracted X-rays are observed only in certain allowed directions determined by the repeat distance of the periodic structure and the wavelength of the radiation. The direction for which diffraction occurs may be defined by three equations called the Laue equations:

$$\begin{aligned}
 a(\cos\mu_1 - \cos\nu_1) &= h\lambda \\
 b(\cos\mu_2 - \cos\nu_2) &= k\lambda \\
 c(\cos\mu_3 - \cos\nu_3) &= l\lambda
 \end{aligned}
 \tag{1}$$

where  $a$ ,  $b$ ,  $c$  are the repeat distances in the unit cell;  $\mu_1$ ,  $\mu_2$ ,  $\mu_3$  are the angles between the incident beam and the  $a$ ,  $b$  and  $c$  axes respectively;  $\nu_1$ ,  $\nu_2$ ,  $\nu_3$  are the angles between the diffracted beam and the axes;  $\lambda$  is the wavelength of the X-radiation;  $h$ ,  $k$ ,  $l$  must be integers if constructive interference is to occur. See Figure 1 for 1-dimensional case.

#### B. Bragg's Law and the Reciprocal Lattice

Another way of defining the conditions for constructive interference in the diffraction process is by Bragg's law:

$$2d\sin\theta = n\lambda \tag{2}$$

Here  $d$  is the perpendicular distance between successive planes in the crystal;  $\theta$  is the angle between the incident X-ray beam and these planes;  $n$  is an integer and  $\lambda$  is the wavelength of the radiation. (Figure 2)

At this point it is convenient to introduce the concept of reciprocal space and the reciprocal lattice, since information available in interpreting X-ray diffraction geometry is often in terms of reciprocal parameters. By considering Bragg's law in the form  $\sin\theta = n\lambda/2d$  it is

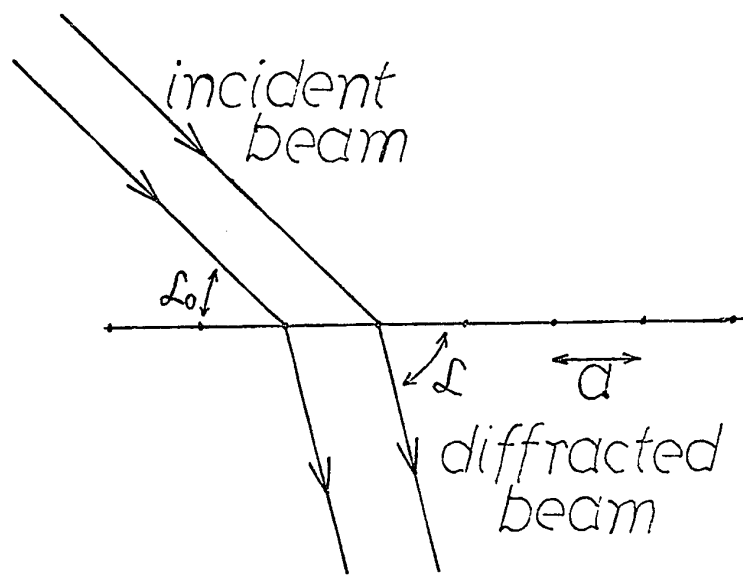


Figure 1

Laue Equation: Definitions in One Dimension

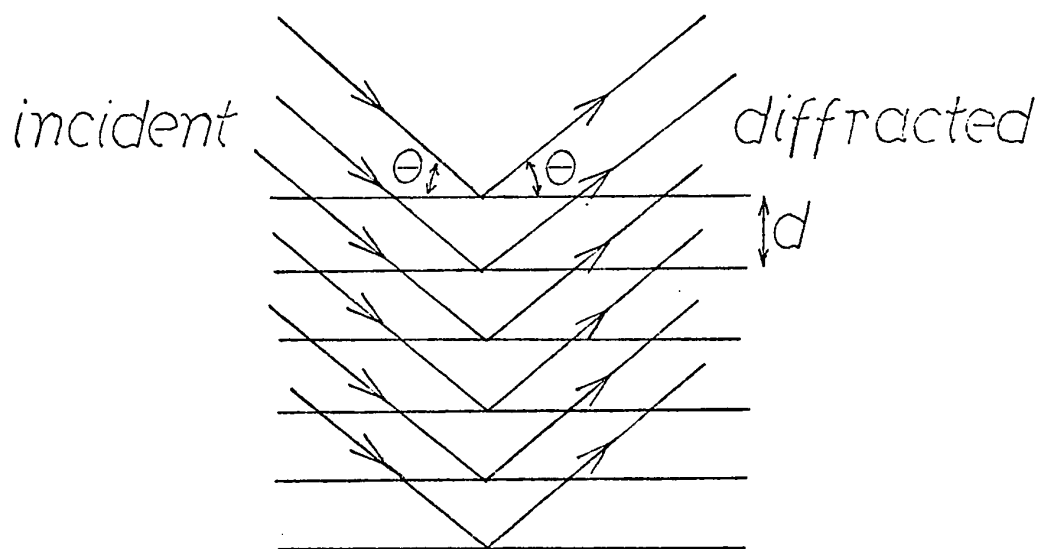


Figure 2

Bragg's Law Definitions

seen that  $\sin\theta$  which measures the deviation of the diffracted beam from the direct beam varies directly as  $1/d$ . The reciprocal lattice is based on this quantity  $1/d$ : from an arbitrarily chosen origin, normals to all possible direct lattice planes  $hkl$  of length  $1/d_{hkl}$  are drawn with  $d_{hkl}$  equal to the perpendicular distance between planes in the  $hkl$  set. The set of points so determined constitutes the reciprocal lattice. Some of the relationships between the direct and reciprocal lattices for the triclinic case are given in Table IV.

### C. Geometry of X-Ray Diffraction

The Laue equations may be applied directly in interpreting the geometry of X-ray diffraction. If a crystal rotates about one of the unit cell axes, say the  $a$  axis, with the incident X-ray beam normal to this axis,  $\mu_1 = 90^\circ$  and  $\cos\mu_1 = 0$ . If  $h = 0$ , the first Laue equation is satisfied for  $\nu_1 = 90^\circ$ . As the crystal rotates, positions are reached such that the remaining two Laue equations are simultaneously satisfied and constructive interference occurs. The allowed directions ( $\nu_1 = 90^\circ$ ) are always in a plane normal to the axis of rotation. For values of  $h$  other than 0 there is a cone of diffracted radiation with a half-angle of  $(90 - \nu_1)^\circ$ . The diffraction pattern may be seen by wrapping a cylinder of film around the crystal.

Table IV

Direct, Reciprocal Lattice Relationships

$$a^* = \frac{bc \sin \alpha}{V} \qquad b^* = \frac{ac \sin \beta}{V} \qquad c^* = \frac{ab \sin \gamma}{V}$$

$$V = abc(1 - \cos^2 \alpha - \cos^2 \beta - \cos^2 \gamma + 2 \cos \alpha \cos \beta \cos \gamma)^{\frac{1}{2}}$$

$$\cos \alpha^* = \frac{\cos \beta \cos \gamma - \cos \alpha}{\sin \beta \sin \gamma} \qquad \cos \beta^* = \frac{\cos \alpha \cos \gamma - \cos \beta}{\sin \alpha \sin \gamma} \qquad \cos \gamma^* = \frac{\cos \alpha \cos \beta - \cos \gamma}{\sin \alpha \sin \beta}$$

\*Refers to reciprocal space.

The resulting photograph consists of a series of spots on straight lines, one line per value of  $h$ , whose separation can be used to calculate the length of the crystal axis,  $a$ :

$$a = \frac{h\lambda}{\sin \tan^{-1}(y/r)}$$

where  $\lambda$  is the wavelength of the X-rays,  $r$  is the radius of the cylinder of film and  $y$  is the film distance from row 0 to row  $h$ .

The lengths of the other axes, the angles between these axes, as well as the crystal system and space group are best obtained with the aid of Weissenberg and precession photographs. The Weissenberg camera allows each row of the rotation photograph (corresponding to one value of  $h$ ) to be expanded to cover the entire cylindrical film. From these films it is possible to deduce two reciprocal cell dimensions and the reciprocal angle between them, thus being able to calculate the unit cell volume. The symmetry of the oscillation and Weissenberg photographs as well as systematic absences (discussed below) allows assignment of the crystal system and the possible space group or groups. The precession camera gives an undistorted view of the reciprocal lattice, and can be used to provide the cell constants not readily obtained from Weissenberg photographs, while using the crystal in the same orientation as for the



Weissenberg photographs.

#### D. The Structure Factor

To be able to relate the intensities of the diffraction patterns observed on films to the contents of the unit cell, it is necessary to develop some mathematical descriptions.

A simple harmonic wave may be described in terms of a point moving on a circle at a constant angular velocity, that is, a rotating vector. Since waves scattered by an atom will have the same velocity but different amplitudes and phases, they may be represented as static vectors in the complex plane. (see Figure 3). The vector representation for a wave of amplitude  $f_1$  and phase angle  $\phi_1$  (measured with respect to the wave scattered by hypothetical electrons at the cell origin) is  $f_1 \exp(i\phi_1)$ . The resultant sum of  $j$  waves scattered by  $j$  atoms in the direction of the scattering vector to the  $hkl$  plane is given by

$$F(hkl) = \sum_j f_j \exp(i\phi_j) \quad (3)$$

with  $F(hkl)$  termed the structure factor. The phase angle,  $\phi_j$ , may be expressed in terms of  $hkl$  and the fractional coordinates  $(x_j, y_j, z_j)$  of the atoms in the cell as

$$\phi_j = 2\pi(hx_j + ky_j + lz_j) \quad (4)$$

so that

$$F(hk\ell) = \sum_j f_j \exp 2\pi i (hx_j + ky_j + \ell z_j) \quad (5)$$

Equation (5) may be resolved into real and imaginary components such that

$$F(hk\ell) = \sum_j f_j \cos 2\pi (hx_j + ky_j + \ell z_j) + i \sum_j f_j \sin 2\pi (hx_j + ky_j + \ell z_j) \quad (6)$$

which can be written  $F(hk\ell) = A + iB$

$$A = \sum_j f_j \cos 2\pi (hx_j + ky_j + \ell z_j) \quad B = \sum_j f_j \sin 2\pi (hx_j + ky_j + \ell z_j) \quad (7)$$

The magnitude of the structure factor  $|F(hk\ell)|$ , called the structure factor amplitude, is quantitatively equivalent to that number of electrons, which if scattering in phase, would show the same diffracting power as the actual set of electrons distributed throughout the unit cell, and can be evaluated as  $(A^2 + B^2)^{1/2}$  (see Figure 3). Using the above definitions of A and B, the structure factor amplitude is then expressed as a function of the coordinates of the atoms in the cell:

$$|F(hk\ell)| = \left\{ \left[ \sum_j f_j \cos 2\pi (hx_j + ky_j + \ell z_j) \right]^2 + \left[ \sum_j f_j \sin 2\pi (hx_j + ky_j + \ell z_j) \right]^2 \right\}^{1/2} \quad (8)$$

It is this equation which can be used to calculate struc-

ture factor amplitudes. Observed values of the modulus of the structure factor, which may then be compared with these calculated values, can be obtained from X-ray diffraction, because the intensity of the radiation reflected from an  $hkl$  plane is proportional to  $|F(hkl)|^2$ . There are various other factors in addition to electron density which influence the intensities, and the derivation of the values of  $|F(hkl)|^2$  from measured intensities requires correction for polarization of X-rays, for the length of time the plane is in the reflecting position (Lorentz effect) and for absorption of X-rays by the crystal. The intensities may be measured on films or by using counting methods which involve a diffractometer.

The phase of the resultant wave is

$$\alpha(hkl) = \tan^{-1}\left(\frac{B}{A}\right) \quad (9)$$

(Figure 3), but since only the amplitude of the structure factor is determined experimentally, the A and B parts are not resolved, and the value of the phase angle cannot be directly measured. This is known as the phase problem.

#### E. Electron Density as Fourier Transform of the Structure Factor

A periodic function can be represented by a Fourier series which consists of a summation of sine and

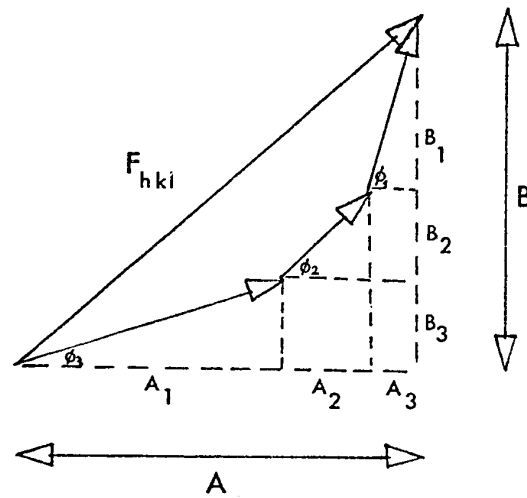


Figure 3

A and B in the Structure Factor

cosine terms. Since a crystal is periodic, its electron density can be represented by such a series. The following equation gives the three-dimensional periodic electron density at a point  $(x, y, z)$  in the unit cell, where  $mno$  are any integers:

$$\rho(xyz) = \sum_{m,n,o=-\infty}^{\infty} c_{mno} \exp(2\pi i(mx+ny+oz)) \quad (10)$$

On substitution of this expression for electron density into the structure factor expression given by equation (5),

$$F(hk\ell) = \int_V \rho(xyz) \exp(2\pi i(hx+ky+\ell z)) dV \quad (11)$$

On simplifying, it can be shown that the Fourier coefficients  $c_{mno} = \frac{1}{V} F(hk\ell)$  and  $mno$  are identical to  $hk\ell$ . Thus the three-dimensional Fourier synthesis of the electron density can be written as

$$\rho(xyz) = \frac{1}{V} \sum_{h,k,\ell=-\infty}^{\infty} F(hk\ell) \exp(-2\pi i(hx+ky+\ell z)) \quad (12)$$

F. Modifications of the Structure Factor: Friedel's Law

Calculated structure factors are modified to account for thermal vibration by introducing a temperature factor. The structure factor then becomes

$$F(hk\ell) = \sum_j f_j \exp(2\pi i(hx_j+ky_j+\ell z_j)) \exp(-B_j (\sin \theta / \lambda)^2) \quad (13)$$

where  $B_j$  is proportional to the mean square displacement of atom  $j$  from its equilibrium position. Anisotropic temperature factors can be used to account for variation with direction of the amplitude of vibration.

For a molecule with a centre of symmetry, if there is an atom at  $(x_j, y_j, z_j)$  there is an identical atom at  $(-x_j, -y_j, -z_j)$ . For atoms not related by the centre, equation (6) can then be written:

$$F(hkl) = \sum_j f_j (\cos 2\pi (hx_j + ky_j + lz_j) + \cos 2\pi (-hx_j - ky_j - lz_j)) + i \sum_j f_j (\sin 2\pi (hx_j + ky_j + lz_j) + \sin 2\pi (-hx_j - ky_j - lz_j)) \quad (14)$$

Since  $\cos(-x) = \cos(x)$  and  $\sin(-x) = -\sin(x)$ , equation (14) reduces to

$$F(hkl) = 2 \sum_j f_j \cos 2\pi (hx_j + ky_j + lz_j) \quad (15)$$

So for centrosymmetric crystals, the imaginary component has vanished, and the phase problem has been reduced to deciding the sign of  $F(hkl)$ .

If a crystal does not have a centre of symmetry,

$$F(hkl) = A(hkl) + iB(hkl); \quad F(\overline{hkl}) = A(hkl) - iB(hkl). \quad (16)$$

$$(F(\overline{hkl})) \text{ is identical to } F(-h -k -l)$$

The intensities in either case are proportional to  $A^2+B^2$ . Since the  $hkl$  and  $\overline{h}\overline{k}\overline{l}$  planes have the same intensities, the diffraction pattern has a centre of symmetry. This is Friedel's law. As a consequence of this law, it is not possible to tell from inspection of films if a crystal is centrosymmetric, but the presence of a centre can be revealed either by the structure itself once it is derived or by statistical analysis of the distribution of intensities about the mean.

An exception to Friedel's law occurs in the case of anomalous dispersion. This happens when the incident X-ray wavelength is near an absorption edge of a scattering element in the crystal. Mathematically, the result of this is to cause the atomic scattering factors for these atoms to be complex numbers.

#### G. Systematic Absences

It is now possible to discuss the assignment of the space group of a crystal from a consideration of symmetry and systematic absences. The crystal system can be assigned by a study of the symmetry expressed on the Weissenberg and rotation films. For example, if a mirror plane perpendicular to the rotation axis is seen on the oscillation film, and two mirror planes  $90^\circ$  apart on the Weissenberg 0 level film, then the crystal is said to have

mmm symmetry characteristic of the orthorhombic (or higher symmetry) crystal system. The assignment of a particular space group is often facilitated by the occurrence of systematic absences. For example, if there is a  $c$  glide plane perpendicular to the  $b$  axis, then for an atom at  $(x, y, z)$ , there is an equivalent atom at  $(x, \bar{y}, z+\frac{1}{2})$ . The contribution to the structure factor of these two atoms is

$$F(hk\ell) = (\exp(2\pi i(hx+ky+\ell z)) + \exp(2\pi i(hx-ky+\ell z+\frac{1}{2}\ell)))f \quad (17)$$

$$\begin{aligned} \text{If } k = 0, F(h0\ell) &= \exp(2\pi i(hx+\ell z))(1+\exp(2\pi i\ell/2))f \\ &= \exp(2\pi i(hx+\ell z))(1+(-1)^\ell)f \quad (18) \\ &= 0 \text{ for } \ell \text{ odd} \\ &= 2\exp(2\pi i(hx+\ell z))f \text{ for } \ell \text{ even.} \end{aligned}$$

Unless  $\ell$  is an even number,  $h0\ell$  reflections will be systematically absent. Thus the absence of  $h0\ell$  reflections for  $\ell$  odd is indicative of a  $c$  glide plane perpendicular to  $b$ . Similar derivations reveal other characteristic absences as given in Table V.

By a consideration of these absences, the space group of the crystal, if not uniquely determined, can at the very least be narrowed to two or three choices.



Table V  
Systematic Absences

<u>Symmetry Element</u>	<u>Affected Region</u>	<u>Condition for Systematic Absence</u>
2 fold screw along a	h00	$h = 2n+1$
b	0k0	$k = 2n+1$
c	00l	$l = 2n+1$
Glide Plane $\perp^r$ translation $\frac{b}{2}$	0kl	$k = 2n+1$
a translation $\frac{c}{2}$		$l = 2n+1$
Glide Plane $\perp^r$ translation $\frac{a}{2}$	h0l	$h = 2n+1$
b translation $\frac{c}{2}$		$l = 2n+1$
Glide Plane $\perp^r$ translation $\frac{a}{2}$	hk0	$h = 2n+1$
c translation $\frac{b}{2}$		$k = 2n+1$
A centred lattice		$k+l = 2n+1$
B centred lattice		$h+l = 2n+1$
C centred lattice	hk $l$	$h+k = 2n+1$
F centred lattice		not all h, k, l odd or even
I centred lattice		$h+k+l = 2n+1$

### III. Determination of Atom Positions

Atom positions within the unit cell cannot be directly inferred from the observed intensities. As previously described, only values of  $|F(hkl)|^2$  are available from intensity data, while values for  $F(hkl)$  are needed to map out the electron density and thus determine the structure. That is, the phases as well as the magnitudes of the  $F(hkl)$  must be found. There are several methods by which phase information may be extracted from the intensity data.

#### A. Patterson Synthesis

One way is by a Patterson synthesis. The Patterson function is derived by taking the product of the electron densities as expressed by equation (12) for points  $(x, y, z)$  and  $(x+u, y+v, z+w)$  and integrating over the volume of the unit cell:

$$P(u, v, w) = \int_0^1 \int_0^1 \int_0^1 \sum_{h, k, \ell=-\infty}^{\infty} F(hkl) \exp(-2\pi i (hx+ky+\ell z)) \sum_{h, k, \ell=-\infty}^{\infty} F(hkl) \exp(-2\pi i (h(x+u)+k(y+v)+\ell(z+w))) dx dy dz \quad (19)$$

This leads on simplification to

$$P(u, v, w) = \sum_{h, k, \ell=-\infty}^{\infty} |F(hkl)|^2 \cos 2\pi (hu+kv+\ell w) \quad (20)$$

The Patterson function  $P(u, v, w)$  reaches maximum

values at the points  $(u, v, w)$  which correspond to the coordinates of vectors between pairs of atoms. The Patterson function can be used to obtain a map of the vectors between atoms. There is a Patterson peak for each interatomic vector. The function has a large positive value at the origin corresponding to the vectors from each atom to itself. A crystal structure investigation usually includes the calculation of the Patterson function at a large number of points throughout the unit cell, so that those points where  $P(u, v, w)$  is large can be found. The interpretation of the Patterson function is complicated by the following:

- 1) If there are  $N$  atoms in the unit cell, there are  $(N^2 - N)/2$  peaks other than the origin which are independent. Thus, the map is crowded.
- 2) Because the atoms are not points, each Patterson peak occupies a considerable volume which causes overlap of peaks.

For these reasons, Patterson maps are most useful for molecules which contain one or more atoms which have appreciably higher atomic numbers than the others. Since the atomic scattering factors increase with the number of electrons the atoms have, the heavy atoms will contribute more to the structure factors. Because the Patterson peak heights due to these heavy atoms are proportional to the electron density at each atom, they may be easily picked out, and the heavy atom positions so obtained

used in calculations of the structure factors.

B. Direct Methods

Methods used to determine the phases of the structure factors without first deriving a set of atom parameters are called direct methods. Because the number of observations of hkl plane intensities is much larger than the number of parameters involved (three positional and either one for isotropic or six for anisotropic temperature factors per atom), the structure factors are not all independent. To derive some of the relationships between the structure factors, it is necessary to define a unitary structure factor as  $U(hkl) = F(hkl) / \sum_i f_i$ . If the structure has a centre of symmetry, this can be written:

$$U(hkl) = \sum_j n_j \cos 2\pi(hx_j + ky_j + lz_j) \tag{21}$$

where  $n_j = f_j / \sum_i f_i$ . Using Cauchy's inequality:

$$|\sum_i a_i b_i|^2 \leq (\sum_j a_j^2) (\sum_k b_k^2) \tag{22}$$

with  $a_j = (n_j)^{1/2}$  and  $b_k = (n_k)^{1/2} \cos 2\pi(hx_k + ky_k + lz_k)$ , it follows that

$$|\sum_i n_i \cos 2\pi(hx_i + ky_i + lz_i)|^2 \leq \sum_j n_j \sum_k n_k \cos^2 2\pi(hx_k + ky_k + lz_k) \tag{23}$$

Since  $\sum_j n_j = 1$  and  $\cos^2 A = (1 + \cos 2A) / 2$ , the inequality

$$U(hk\ell)^2 \leq \frac{1}{2}(1+U(2h \ 2k \ 2\ell)) \quad (24)$$

can be obtained. As an example, if  $U(130) = 0.5$  and  $U(260) = 0.6$ , then the sign of  $U(260)$  must be positive to satisfy the inequality. Another inequality for centrosymmetric structures is:

$$U^2(hk\ell) + U^2(h'k'\ell') + U^2(h+h' \ k+k' \ \ell+\ell') \leq 1 + 2U(hk\ell)U(h'k'\ell')U(h+h' \ k+k' \ \ell+\ell') \quad (25)$$

These are known as Harker-Kasper inequalities.

Thus if the signs of  $U(hk\ell)$  and  $U(h'k'\ell')$ , symbolized by  $S(hk\ell)$  and  $S(h'k'\ell')$ , respectively, are known that of  $U(h+h' \ k+k' \ \ell+\ell')$  can be deduced from equation (21) as

$$S(h+h' \ k+k' \ \ell+\ell') = S(hk\ell)S(h'k'\ell') \quad (26)$$

provided the structure factors are large. The probability that this will give the correct sign for  $F(h+h' \ k+k' \ \ell+\ell')$  increases as the magnitude of the structure factors involved increases. Once a few signs have been determined, equation (23) can be used to generate more signs and so on. The large structure factors required for this process are also those whose phases are most needed to produce a useful Fourier representation of the structure. This method was developed by D. M. Sayre<sup>3</sup>, with more recent reviews on it found in several books.<sup>4,5,6</sup>

### C. Completing the Structure

Once the phases of some of the structure factors have been determined, a Fourier map is calculated, and the atomic positions taken as the locations of the maxima of the electron density function. The atomic positions and the parameters describing thermal vibration are then refined by means of a least squares calculation, which minimizes the function  $\sum w |F_{\text{obs}}| - |F_{\text{calc}}|^2$ , with  $w$  a weighting function. The resulting parameters are those which produce the most accurate values of interatomic distances and bond angles, while at the same time give the best agreement between calculated and observed structure factor amplitudes. This agreement is usually expressed mathematically by a residual or R factor:

$$R_1 = \frac{\sum ||F_{\text{obs}}| - |F_{\text{calc}}||}{\sum |F_{\text{obs}}|} \quad (27)$$

or by the so-called weighted R factor:

$$R_2 = \left( \frac{\sum w (|F_{\text{obs}}| - |F_{\text{calc}}|)^2}{\sum w |F_{\text{obs}}|^2} \right)^{\frac{1}{2}} \quad (28)$$

with  $w$  a weighting factor.  $R_2$  is similar to a normalized standard error and more closely approximates the true statistical quality of the refinement than does  $R_1$ . It can be shown<sup>7</sup> however that both  $R_1$  and  $R_2$  become smaller

if the number of observations approaches the number of parameters, and so the proviso must be added that, provided the number of observations greatly exceeds the number of parameters, the smallness of  $R_1$ , or better  $R_2$ , is a measure of the reliability of the information given by the structure.

#### IV. Experimental

The molecules studied during the course of this research being very similar, it is natural to suppose that many of the crystallographic techniques used would also be similar. To this end, this experimental introduction will discuss some of the generally applied methods and computer programs, while the individual vagaries of the molecules will be given each in its particular chapter.

##### A. The Collection and Correction of a Set of Intensities

All data sets were collected on the manual Picker four circle diffractometer using either  $\text{CuK}_\alpha$  or  $\text{MoK}_\alpha$  X-radiation monochromated by a graphite single crystal (002 reflection). A coupled  $\omega/2\theta$  scanning technique was used with a scan rate of  $2^\circ/\text{minute}$ . Backgrounds were estimated from a linear interpolation of two stationary crystal, stationary counter measurements made at the limits of the scan. The diffractometer settings were calculated by the

program MIXG2 written by P. Shoemaker.

Accurate cell parameters were obtained from a least squares analysis of a number of high  $\sin\theta$  reflections of widely varying  $hk\ell$  values, which were accurately centred in the counter window of the diffractometer, using  $\text{CuK}_\alpha$  X-radiation ( $\lambda = 1.54051\text{\AA}$ ). A listing of DREFINE, the program used for this analysis, and a discussion of its generation and scope are given in Appendix C.

The stabilities of the crystals used throughout this study were monitored by periodically measuring a small number of reflections of varying  $\sin\theta$  throughout each data set collection. These were then available as a basis for decomposition corrections if required.

All crystals were corrected for absorption effects using W.C. Hamilton's GONO9 program. Reflections which were independent of  $\phi$  except for absorption effects (for example, the  $h00$  reflections when the crystal is mounted with a coincident with the  $\phi$  axis of the diffractometer) were measured in  $10^\circ$  intervals from  $0^\circ$  to  $180^\circ$  in  $\phi$ . Their consistency after correction for absorption gave reassurance that the absorption corrections had been applied correctly. The dimensions of all crystals were measured using a calibrated eye piece on a microscope. Generally, perpendicular distances between faces were measured.

Since the counter is non-linear above  $10^4$  counts/



second, all reflections whose peak count exceeded this were re-examined at lower values of the current. Appropriate corrections to these strong reflections were applied. At the completion of refinement, systematic errors due to secondary extinction (attenuation of primary X-ray beam by the transfer of energy to the reflected beam) were analyzed for by comparing  $F_{\text{obs}}$  and  $F_{\text{calc}}$  values. Thus any very strong, very low  $\sin\theta$  ( $<0.1$ ) data which showed  $F_{\text{obs}} \ll F_{\text{calc}}$  were rejected.

#### B. The Solution and Refinement of the Structure

The intensity data were corrected for Lorentz and polarization effects and reduced to structure factor amplitudes using the program PMMO, a local data reduction program. Standard deviations<sup>1</sup> for each observation were computed using

$$\sigma(I) = (CT + 0.25(t_c/t_b)^2(B_1 + B_2) + (pI)^2)^{1/2}$$

where CT is total integrated peak count obtained in time  $t_c$ ;  $B_1$  and  $B_2$  are background counts each obtained in time  $t_b$ ; and  $I = CT - \frac{1}{2}t_c/t_b(B_1 + B_2)$ . The p term allows for machine variability and has values around 0.03. A rejection criterion of the form  $I/\sigma(I) \leq T$  was used to eliminate unobserved reflections from the refinement. T was usually 3.0.

Unless otherwise noted, the positions of the transition metal, silicon and any other heavy atoms were

located using a Patterson map generated by the program FORDAP, written by A. Zalkin and modified by B. M. Foxman. These positions were used in a least squares refinement using the program SFLS5 written by C. T. P. Prewitt and modified by M. J. Bennett and B. M. Foxman, from which electron density difference maps were obtained again using FORDAP. From these difference maps it was possible to locate carbon, oxygen and in some cases hydrogen atoms. The atomic scattering factors of Cromer and Waber<sup>8</sup> were used for all atoms except hydrogen with anomalous dispersion corrections  $\Delta f'$  and  $\Delta f''$  as found in the International Crystallographic Tables<sup>9,10</sup> applied to silicon and heavier atoms. For hydrogen, the experimental scattering factors of Mason and Robertson<sup>11</sup> or of Stewart, Davidson and Simpson<sup>12</sup> were used.

During refinement using the program SFLS5 or SFLS5 as modified for hindered rotation by W. Hutcheon,<sup>13</sup> the function minimized in each case was  $\sum w(|F_{\text{obs}}| - |F_{\text{calc}}|)^2$  with  $w = 1/\sigma^2(F_{\text{obs}})$ . The residual factors used to measure the degree of difference between experiment and model are given by equations (27) and (28).

The introduction of anisotropic temperature factors was undertaken only if justified by electron density difference maps and by the Hamilton<sup>14</sup> statistical test (significance level 0.05).

Tables of bond lengths, bond angles and non-bonded contacts together with their estimated standard deviations were obtained from the program ORFFE2 written by W. Busing and H. A. Levy. Equations of planes and deviations from these planes were found using MGEOM by J. S. Wood. All molecular diagrams, both perspective and packing, were obtained from ORTEP written by C. K. Johnson.

CHAPTER II

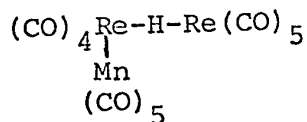
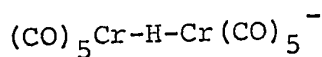
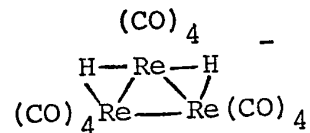
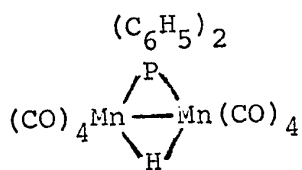
General Chemical Introduction

## GENERAL CHEMICAL INTRODUCTION

Transition metal carbonyl hydrides were first known in the 1930's when for example iron carbonyl dihydride  $\text{Fe}(\text{CO})_4\text{H}_2$  was prepared by Hieber and Leutert<sup>15</sup> and cobalt carbonyl hydride  $\text{HCo}(\text{CO})_4$  by Coleman and Blanchard,<sup>16</sup> but not until the last ten to fifteen years have these compounds been fully characterized. In 1955, a high field NMR proton absorption was assigned to the hydridic hydrogen in  $\text{HRe}(\text{C}_5\text{H}_5)_2$ <sup>17</sup> ( $\tau = 22.5$ ) and subsequently, this high field shift ( $\tau = 15-40$ ) was found to be characteristic of all hydrogen atoms bonded to transition metals. This implication of high shielding led to the concept of very short metal-hydrogen bonds, and indeed, the hydrogen was often<sup>15,16,18</sup> thought to be buried in the metal orbitals rather than being a stereochemically active ligand. (More recent interpretations of the high field NMR shift attribute it to more subtle electronic factors<sup>19,20,21</sup>). At the same time, there was indirect evidence for hydridic hydrogen occupying a stereochemically significant position in compounds such as  $\text{HPtCl}(\text{P}(\text{C}_6\text{H}_5)_2\text{C}_2\text{H}_5)_2$ <sup>22</sup>,  $\text{HPt}(\text{P}(\text{C}_2\text{H}_5)_3)_2\text{Br}$ <sup>23</sup> and  $\text{HOSr}(\text{CO})\text{P}(\text{C}_6\text{H}_5)_3$ .<sup>24</sup> Their geometries were such that a space was left that if filled by the hydrogen would complete a more or less regular geometry. In 1964 an X-ray and neutron diffraction investigation of  $\text{ReH}_9$ <sup>-25,26</sup> showed

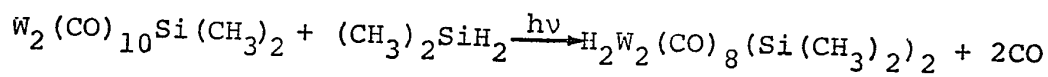
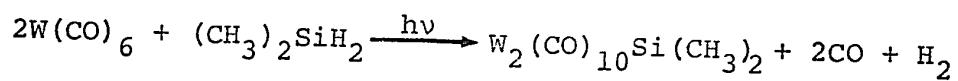
the Re-H distance to be  $1.68\overset{\circ}{\text{Å}}$ , thus locating hydridic hydrogen positively for the first time. A similar study by J. Ibers on  $\text{HMn}(\text{CO})_5$ <sup>27</sup> in 1969 also located the hydridic hydrogen conclusively and showed the hydrogen occupied a definite coordinate position with a normal covalent bond with the metal of length  $1.60\overset{\circ}{\text{Å}}$ . X-ray crystallographic evidence for the hydridic hydrogen atom locations had previously confirmed a stereo-chemically significant location for it with normal bond lengths in most cases (for example  $\text{HRh}(\text{CO})(\text{P}(\text{C}_6\text{H}_5)_3)_3$ <sup>28</sup> and  $\text{CoH}(\text{N}_2)(\text{P}(\text{C}_6\text{H}_5)_3)_3$ <sup>29</sup>). An exception does occur in  $(\text{C}_6\text{H}_5)_3\text{P}_4\text{HRh}\cdot\frac{1}{2}\text{C}_6\text{H}_6$ <sup>80</sup> where there is no obvious stereochemical position for the hydrogen.

Studies of polynuclear transition metal hydrides have suggested the hydrogen can be in a bridging position as for example in  $\text{HMnRe}_2(\text{CO})_{14}$ <sup>30</sup>,  $\text{P}(\text{C}_6\text{H}_5)_2\text{HMn}_2(\text{CO})_8$ <sup>31</sup>,  $\text{H}_2\text{Re}_3(\text{CO})_{12}$ <sup>-32</sup> and  $\text{HCr}_2(\text{CO})_{10}$ <sup>-33,34</sup>. The bridges range from bent to linear:

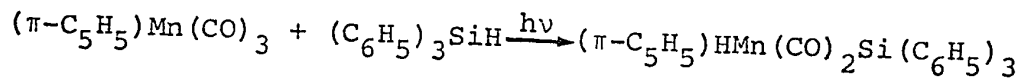


Transition metal carbonyl derivatives that contain both a hydride and a main group IV substituent other than carbon are by no means abundant, but a few examples can be found, particularly in work done in this department. A selection of such compounds together with available structural information is given in Table VI.

As can be seen from this table, there are two basic types of hydrides formed by substituted silanes and transition metal carbonyls—mononuclear and binuclear. Reactions of disubstituted silanes have resulted in binuclear hydrides as in the case of the formation of  $H_2W_2(CO)_8(Si(CH_3)_2)_2$ :<sup>35a)</sup>

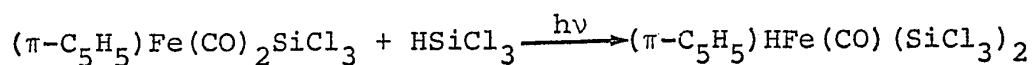
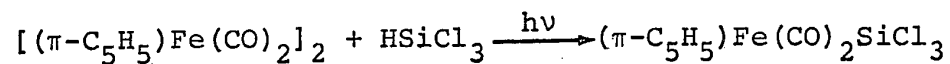


These reactions do not occur with first row transition metals; however, with these, mononuclear species may be obtained by reaction of trisubstituted silanes with transition metal carbonyls, as for example in the formation of  $(\pi-C_5H_5)HMn(CO)_2Si(C_6H_5)_3$ :<sup>35b)</sup>



By further reaction with substituted silanes, another carbonyl group can be replaced by the silane as in the forma-

tion of  $(\pi\text{-C}_5\text{H}_5)\text{HFe}(\text{CO})(\text{SiCl}_3)_2$ :<sup>36</sup>



The structures of one binuclear species,  $\text{H}_2\text{W}_2(\text{CO})_8(\text{Si}(\text{C}_2\text{H}_5)_2)_2$ , two monometal monosilicon species,  $\text{HFe}(\text{CO})_4\text{Si}(\text{C}_6\text{H}_5)_3$  and  $(\pi\text{-C}_5\text{H}_5)\text{HMn}(\text{CO})_2\text{SiCl}_2(\text{C}_6\text{H}_5)$ , and one monometal disilicon species  $(\pi\text{-C}_5\text{H}_5)\text{HFe}(\text{CO})[\text{Si}(\text{CH}_3)_2(\text{C}_6\text{H}_5)]_2$  form the main body of this thesis. These structures were undertaken to obtain structural information on compounds of these types, particularly with respect to hydrogen location, and are part of a continuing study on silyl-substituted transition metal hydrides.



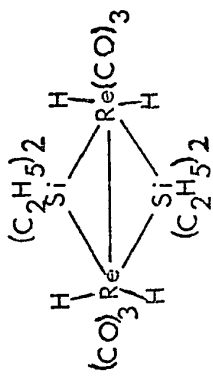
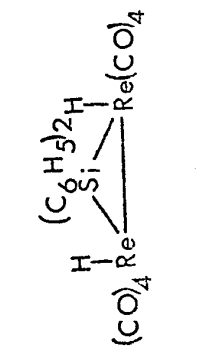
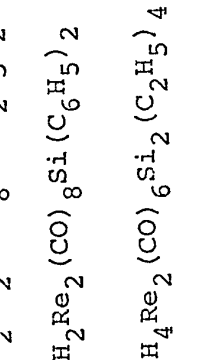
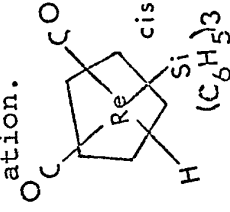
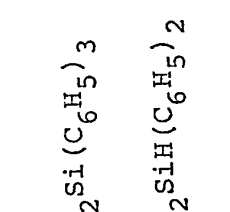
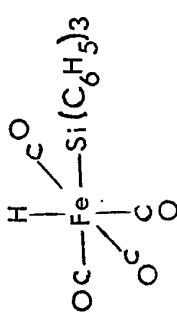
Table VI

## Transition Metal Silicon Hydrides

References	Compound	Structural Information
37	$(C_6H_6)Cr(CO)_2HSiCl_3$	
35, (a)	$H_2W_2(CO)_8Si_2(C_2H_5)_4$	
35	$H_2W_2(CO)_8Si_2(CH_3)_4$	
35, 64	$(\pi-C_5H_5)HMn(CO)_2Si(C_6H_5)_3$	
37, 87	$(\pi-C_5H_5)HMn(CO)_2SiCl_3$	Structure attempted but crystals unstable.
35	$(\pi-C_5H_5)HMn(CO)_2Si(C_6H_5)_2H$	
38, (a)	$(\pi-C_5H_5)HMn(CO)_2Si(C_6H_5)Cl_2$	
35	$H_2Re_2(CO)_7Si_2(CH_3)_4$	
35, 52	$H_2Re_2(CO)_7Si_2(C_2H_5)_4$	
35	$H_2Re_2(CO)_8Si(CH_3)_2$	

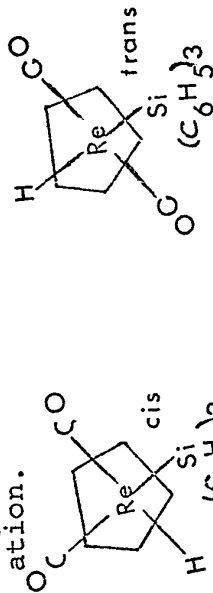
... cont'd.

Table VI - cont'd.

<u>References</u>	<u>Compound</u>	<u>Structural Information</u>
35	$H_2Re_2(CO)_8Si(C_2H_5)_2$	
35, 50	$H_2Re_2(CO)_8Si(C_6H_5)_2$	
35, 52	$H_4Re_2(CO)_6Si_2(C_2H_5)_4$	
35	$HRe_2(CO)_9SiCl_3$	
35	$HRe_2(CO)_9SiCl_2CH_3$	
35	$HRe_2(CO)_9SiCl_2C_6H_5$	
35, 72	$\begin{matrix} \text{cis} \\ \text{trans} \end{matrix} (\pi-C_5H_5)HRe(CO)_2Si(C_6H_5)_3$	
35	$\begin{matrix} \text{cis} \\ \text{trans} \end{matrix} (\pi-C_5H_5)HRe(CO)_2SiH(C_6H_5)_2$	
39, 40	$HFe(CO)_4SiH_3$	
36	$HFe(CO)_4SiCl_3$	
36, (a)	$HFe(CO)_4Si(C_6H_5)_3$	


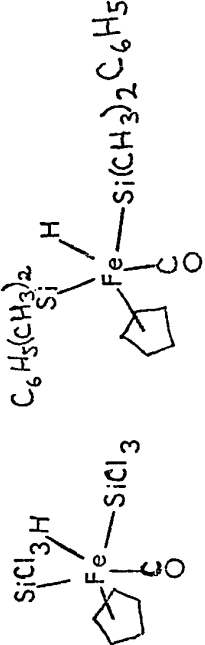
$(CO)_5Re-H-Re(CO)_4SiR_3$

Proposed structure, no suitable crystals for an X-ray determination.



Liquid.

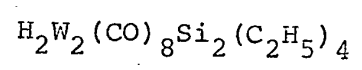
Table VI - cont'd.

<u>References</u>	<u>Compound</u>	<u>Structural Information</u>
37, 73	$(\pi\text{-C}_5\text{H}_5)\text{HFe}(\text{CO})(\text{SiCl}_3)_2$	
41, (a)	$(\pi\text{-C}_5\text{H}_5)\text{HFe}(\text{CO})(\text{Si}(\text{CH}_3)_2\text{C}_6\text{H}_5)_2$	
41	$(\pi\text{-C}_5\text{H}_5)\text{HFe}(\text{CO})(\text{Si}(\text{CH}_3)(\text{C}_6\text{H}_5)_2)_2$	
37	$(\pi\text{-C}_5\text{H}_5)\text{HCo}(\text{CO})\text{SiCl}_3$	
42	$\text{Cl}_3\text{SiHRh}(\text{CO})\text{Cl}(\text{P}(\text{C}_6\text{H}_5)_3)_2$	
43	$\text{Cl}_3\text{SiHIrCl}(\text{CO})(\text{P}(\text{C}_6\text{H}_5)_3)_2$	
43, 44	$(\text{CH}_3)_3\text{SiHIrCl}(\text{CO})(\text{P}(\text{C}_6\text{H}_5)_3)_2$	
45	$\text{Cl}_3\text{SnIrH}_2(\text{CO})(\text{P}(\text{C}_6\text{H}_5)_3)_2$	
46	$\text{Pth}(\text{SiCl}_3)((\text{C}_6\text{H}_5)_2\text{PCH}_2\text{CH}_2\text{P}(\text{C}_6\text{H}_5)_2)$	
47	$(\text{C}_6\text{H}_5)_3\text{SiPtH}(\text{P}(\text{C}_2\text{H}_5)_3)_2$	
48	$(\pi\text{-C}_5\text{H}_5)\text{HRh}(\text{CO})\text{Si}(\text{C}_6\text{H}_5)_3$	
48	$(\pi\text{-C}_5\text{H}_5)\text{HRh}(\text{CO})\text{Si}(\text{CH}_2\text{C}_6\text{H}_5)_3$	

(a) This work.

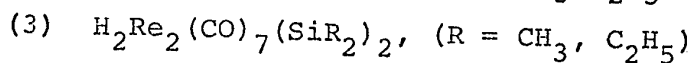
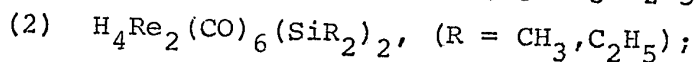
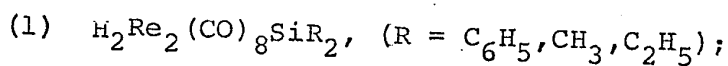
CHAPTER III

The Crystal and Molecular Structure of



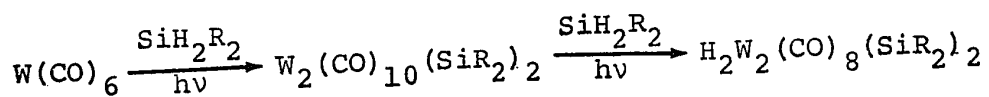
## INTRODUCTION

The reactions of disubstituted silanes with second and third row transition metal carbonyl derivatives produce an interesting series of polynuclear species containing hydridic hydrogen. The first members of the series synthesized had stoichiometries of the form

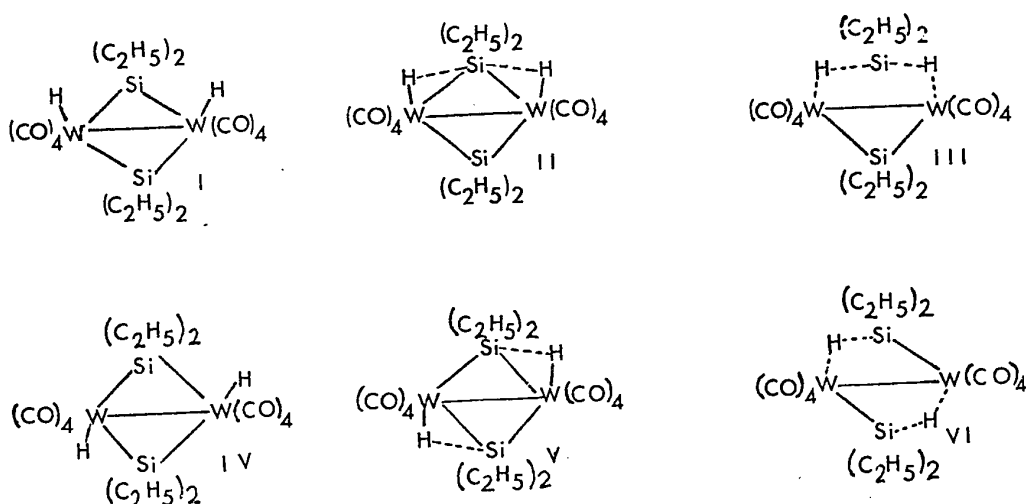


and were formed by the reaction of dirhenium decacarbonyl and the appropriate diaryl or dialkyl silane.<sup>49</sup> Both the structure of  $\text{H}_2\text{Re}_2(\text{CO})_8\text{Si}(\text{C}_6\text{H}_5)_2$ <sup>50</sup> and spectroscopic studies on the above compounds pointed to the formation of a new type of hydrogen bridge in which the hydridic hydrogen is bonded essentially in a terminal fashion to the rhenium atom but is at the same time also weakly bonded to the silicon atom. The geometry of the  $\text{Re}_2\text{Si}_2$  unit in the structures  $\text{H}_2\text{Re}_2(\text{CO})_8(\text{Si}(\text{C}_6\text{H}_5)_2)_2$ <sup>51</sup> and  $\text{H}_4\text{Re}_2(\text{CO})_6(\text{Si}(\text{C}_2\text{H}_5)_2)_2$ <sup>52</sup> is unchanged by the formation of the postulated silicon hydrogen bond, although this was not known when the research described in this chapter was begun.

With tungsten hexacarbonyl, analogous ditungsten derivatives might be expected, and indeed,  $\text{H}_2\text{W}_2(\text{CO})_8(\text{SiR}_2)_2$  is formed according to the reaction



The structure of  $\text{H}_2\text{W}_2(\text{CO})_8(\text{Si}(\text{C}_2\text{H}_5)_2)_2$  was undertaken and forms the topic for this chapter. Six structures appeared possible



These structures show the variation from pure terminal hydride, through terminal hydride with weak silicon hydrogen bond to definite insertion of the hydrogen atom into the tungsten silicon bond. Assuming there is no fast exchange, spectroscopic evidence would eliminate all cases in which both tungsten atoms were not equivalent and both hydrogen atoms were not equivalent. This compound is especially useful, since if bridging did occur, the unbridged distance is available as an internal reference.

## EXPERIMENTAL

The compound  $\text{H}_2\text{W}_2(\text{CO})_8(\text{Si}(\text{C}_2\text{H}_5)_2)_2$  was prepared by J. K. Hoyano and was recrystallized from n-hexane to obtain yellow crystals suitable for single crystal X-ray diffraction studies. Rotation,  $\text{CuK}_\alpha$  Weissenberg  $hk0, hk1, hk2$  and  $\text{MoK}_\alpha$  precession  $h0l$  photographs showed the compound to be monoclinic with systematic absences  $h0l$  for  $h+l = 2n+1$  and  $0k0$  for  $k = 2n+1$  determining the space group  $\text{P}2_1/n$ , a non-standard setting for  $\text{P}2_1/c$ . The unit cell was found to be  $a = 9.212(1)$ ,  $b = 10.131(1)$ ,  $c = 12.749(1) \text{ \AA}$ ,  $\beta = 99.07(1)^\circ$  at  $22^\circ\text{C}$  from a least squares analysis of twelve reflections of high  $\sin\theta/\lambda$ . The density was determined experimentally as  $2.04 \text{ gm/cc}$  by means of flotation using aqueous zinc iodide. It agrees only poorly with the calculated density ( $2.165 \text{ gm/cc}$ ) found for two molecules/unit cell, a molecular weight of  $766.2$  and unit cell volume  $1174.9 \text{ \AA}^3$ . Several possible reasons for the discrepancy arise: 1) defective crystals; 2) contamination by a similar but less dense compound; 3) incorporation of a small amount of solvent into the lattice. Under microscopic examination the crystals used to determine the density did not have any obvious defects, while contamination by the molybdenum analogue was ruled out by mass spectrometry. However, a solvent occupancy of perhaps 5% does appear feasible as this would adjust the calculated C,H and Si

analyses toward those actually found. (Table VII) Further evidence for solvent occurs in the mass spectrum which shows a peak at 86 a.m.u. consistent with  $C_6H_{14}^+$ . Unfortunately, this peak is also consistent with that for the  $Si(C_2H_5)_2^+$  fragment. However, the dimethyl analogue also shows an intense peak at 86 a.m.u. and in this case the only obvious source of the peak is the solvent, n-hexane.

With the crystal mounted so that  $a^*$  was coincident with the diffractometer  $\phi$  axis, intensity data were collected using  $CuK_\alpha$  radiation, a  $2\theta$  limit of  $100^\circ$  and a scan covering  $\pm 1^\circ$  in  $2\theta$  of each peak. Backgrounds were counted for 30 seconds. Eight reflections with varying  $2\theta$  values were measured periodically as standards during the data collection; these showed that decomposition which was a linearly dependent function of time and of  $\sin\theta/\lambda$  occurred. On this basis, a decomposition correction was applied, after which the standards showed variations consistent with counting statistics alone. At the end of data collection the high  $\sin\theta/\lambda$  standards had fallen to about 80% of their initial values. Of 1214 independent reflections measured, 945 were found to be above background using a criterion  $I/\sigma(I) \leq 2.0$ .<sup>53</sup>

The crystal used for data collection was of approximate dimensions  $0.15 \times 0.10 \times 0.12$  mm with crystal faces of the form  $\{100\}$  and  $\{011\}$ . An absorption correction ( $\mu = 10.90 \text{ cm}^{-1}$ ) was applied using the  $h00$ ,  $h = 2, 4$ ,



6, reflections measured in  $5^\circ$  intervals in  $\phi$  from  $\phi = 0$  to  $\phi = 180^\circ$  as a check. After correction, these data showed an internal consistency of  $\pm 1\%$  on  $|F|$ .

Table VII

% Composition of  $\text{H}_2\text{W}_2(\text{CO})_8[\text{Si}(\text{C}_2\text{H}_5)_2]_2$ 

<u>Element</u>	<u>W</u>	<u>C</u>	<u>O</u>	<u>Si</u>	<u>H</u>
Found	-	25.16%	-	7.51%	3.08%
Calculated No Solvent	47.98%	25.08	16.70%	7.33	2.89
Calculated 5% Solvent	47.71	25.42	16.61	7.29	2.97

## SOLUTION AND REFINEMENT

$P2_1/n$  is a non-standard space group whose general positions were derived as  $(x, y, z)$ ,  $(\bar{x}, \bar{y}, \bar{z})$ ,  $(\frac{1}{2}+x, \frac{1}{2}-y, \frac{1}{2}+z)$  and  $(\frac{1}{2}-x, \frac{1}{2}+y, \frac{1}{2}-z)$ . With two molecules/unit cell, the four tungsten atoms must be located at the general positions. The largest peaks on the Patterson occurring at  $(0.5, 0.33, 0.5)$ ,  $(0.21, 0.5, 0.5)$  and  $(0.3, 0.18, 0.029)$  and identified as  $(\frac{1}{2}, 2y, \frac{1}{2})$ ,  $(\frac{1}{2}-2x, \frac{1}{2}, \frac{1}{2}-2z)$  and  $(2x, 2y, 2z)$ , respectively, give the tungsten atom location  $(x, y, z)$  as  $(0.15, 0.09, 0.015)$ . The location of the silicon atom from the Patterson map was found to be  $(0.09, -0.09, -0.09)$  by a consideration of the W-Si vectors. An electron density map computed using structure factors phased by the silicon and tungsten atoms allowed the location of all but one of the remaining atoms. The C8 atom was found from an electron density difference map computed using structure factors phased on all the other atoms.

During the course of refinement, three molecular models were tested. First, with all atoms isotropic,  $R_1 = 0.11$ ,  $R_2 = 0.11$ . After corrections for decomposition and absorption, the tungsten and silicon atoms were allowed to be anisotropic with resulting residual factors  $R_1 = 0.045$  and  $R_2 = 0.059$ . Finally all atoms were allowed to vibrate anisotropically causing  $R_1 = 0.038$  and  $R_2 = 0.051$ . The

isotropic model for the decomposition correction could introduce a systematic error into the data that would influence the anisotropic temperature factors. The anisotropic refinement did not change the fractional coordinates significantly, but it was essential to attempt the computation of corrections for thermal motion.<sup>54</sup>

With the completion of the refinement, the standard deviation of an observation of unit weight was 1.27. (Defined by  $\sigma = \Sigma \omega (|F_{\text{obs}}| - |F_{\text{calc}}|)^2 / (m - n)$  with  $m$  the total number of observations and  $n$  the number of rejected observations.) The largest shift in any parameter was less than one of an estimated standard deviation as obtained from the final least squares cycle. Final electron density maps computed using 1) all data; 2) data limited by  $\sin\theta/\lambda$  0.3 showed no direct evidence for hydrogen atom locations. The all data difference map showed densities ranging from -0.41 to 0.68  $e \text{ \AA}^{-3}$ .

Table VIII lists the observed and calculated structure factor amplitudes:  $10|F_{\text{obs}}|$  and  $10|F_{\text{calc}}|$  both in absolute units of electrons. The final positional parameters and anisotropic temperature factors for all atoms are given in Table IX. The estimated standard deviations were obtained from the inverse matrix of the final least squares cycle.

Table VIII

Observed and Calculated Structure Factor  
Amplitudes for  $\text{H}_2\text{W}_2(\text{CO})_8\text{Si}_2(\text{C}_2\text{H}_5)_4$



Table IX  
Final Coordinates and Thermal Parameters (a)

Atom	X	Y	Z	$\beta_{11}$ (b)	$\beta_{22}$	$\beta_{33}$	$\beta_{12}$	$\beta_{13}$	$\beta_{23}$	$\frac{\sigma^2}{B(A)} (c)$
W	0.14320(6)	0.08287(7)	0.00860(5)	152.3(11)	211.6(12)	118.5(7)	7.8(9)	26.0(6)	17.5(7)	7.098
Si	0.0938(5)	-0.1341(5)	-0.0971(4)	188.9(65)	264.1(73)	130.6(40)	10.9(57)	43.5(41)	-15.7(45)	8.410
C1	0.229(2)	-0.021(2)	0.132(1)	255(31)	201(23)	139(17)	31(22)	70(18)	12(16)	8.354
C2	0.058(2)	0.195(2)	-0.115(1)	202(25)	195(24)	145(16)	19(20)	48(16)	7(16)	7.923
C3	0.298(2)	0.220(2)	0.054(1)	216(30)	257(32)	147(17)	4(23)	4(19)	-16(19)	9.182
C4	0.308(2)	0.030(2)	-0.071(2)	146(24)	262(28)	183(19)	-20(21)	48(18)	25(18)	9.042
C5	0.101(3)	-0.151(3)	-0.245(2)	388(54)	466(55)	211(30)	5(44)	57(30)	-1(31)	15.121
C6	0.010(3)	-0.082(3)	-0.304(2)	485(56)	511(60)	225(32)	200(49)	99(36)	83(32)	16.923
C7	0.212(2)	-0.278(2)	-0.042(2)	237(30)	249(30)	294(28)	66(26)	60(24)	-72(24)	12.272
C8	0.139(3)	-0.413(2)	-0.076(2)	449(60)	325(41)	275(33)	83(40)	67(33)	-36(30)	15.236
O1	0.292(1)	-0.080(1)	0.206(1)	246(20)	314(21)	150(12)	49(17)	40(12)	33(13)	10.176
O2	0.008(1)	0.265(1)	-0.184(1)	348(25)	254(19)	160(12)	-1(18)	7(14)	55(12)	10.914
O3	0.381(1)	0.299(1)	0.078(1)	293(25)	308(24)	191(15)	-91(19)	36(15)	-20(14)	11.576
O4	0.401(1)	0.004(1)	-0.115(1)	189(19)	355(23)	185(13)	12(17)	79(13)	1(14)	10.676

(a) Standard deviations in parentheses refer to last digit quoted.

(b) Anisotropic thermal parameters  $\times 10^4$  defined by  $\exp[-(\beta_{11}h^2 + \beta_{22}k^2 + \beta_{33}l^2 + 2\beta_{12}hk + 2\beta_{13}hl + 2\beta_{23}kl)]$ .

(c) Equivalent isotropic thermal parameter.

## RESULTS

The molecular geometry and numbering system used are shown in Figure 4, while the atoms in the plane of the heavy atom core are shown in Figure 5. The molecular packing viewed down a,b,c respectively are shown in Figure 6, 7, 8. These drawings were all made using the program ORTEP. Tables X and XI give the bond lengths and bond angles respectively. Some intramolecular contacts are listed in Table XII while Table XIII gives the intermolecular contacts. These results and the estimated standard deviations associated with them were calculated using the program ORFFE2. MGEOM was used to calculate the least squares planes and the distances of selected atoms from these planes as given in Table XIV.



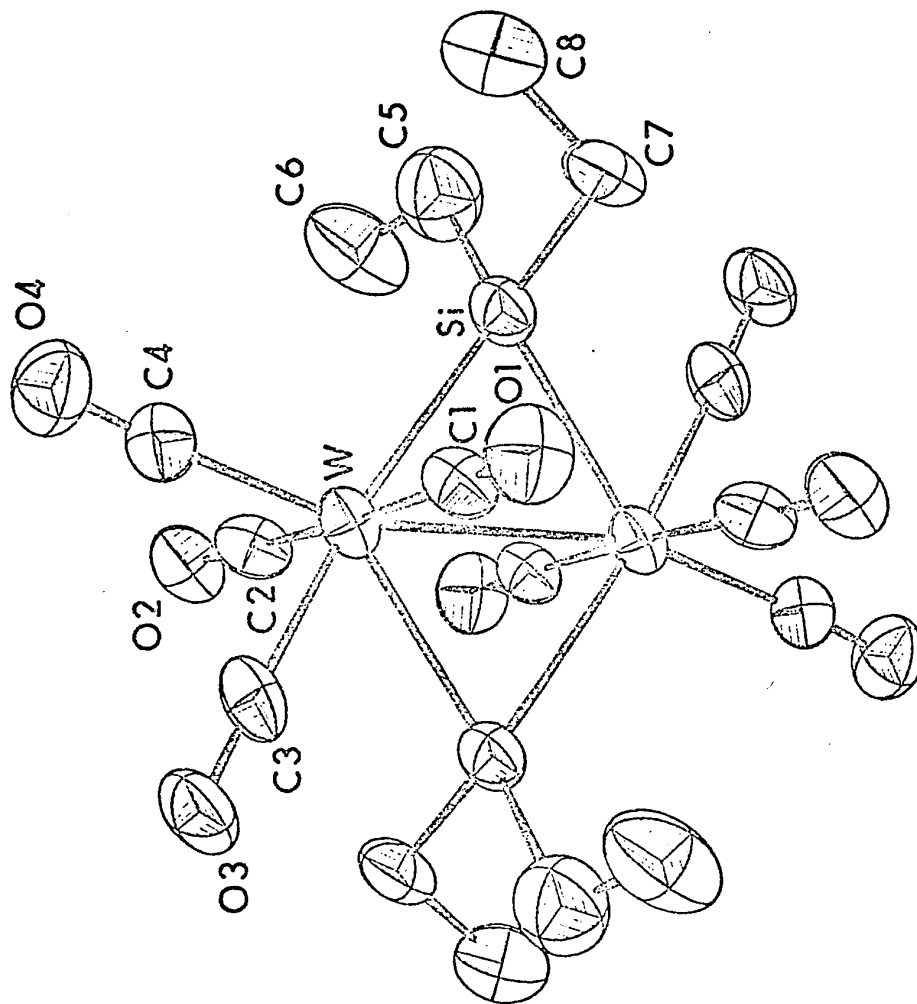


Figure 4

Perspective View of  $\text{H}_2\text{W}_2(\text{CO})_8[\text{Si}(\text{C}_2\text{H}_5)_2]_2$

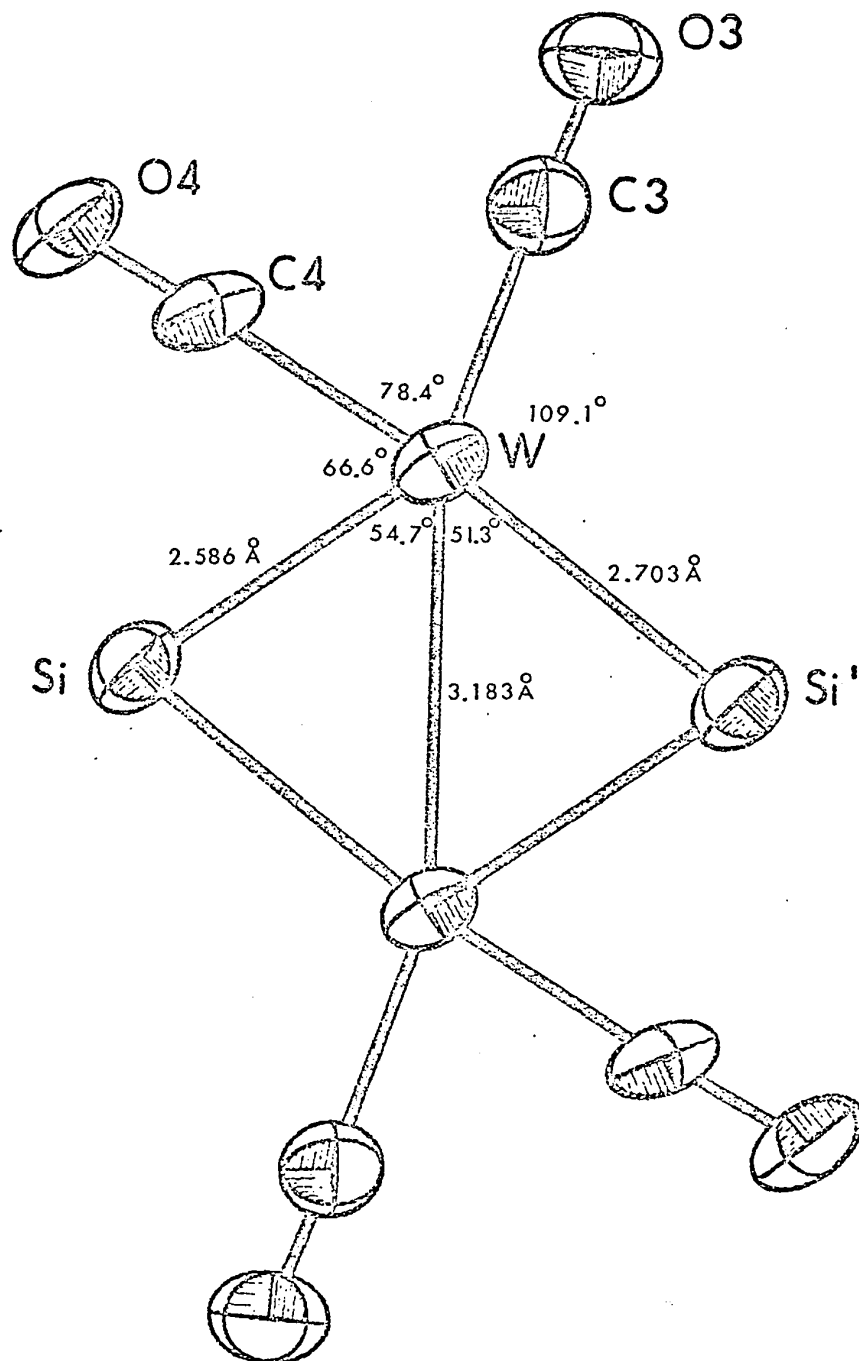


Figure 5

 $W_2Si_2$  Structural Fragment

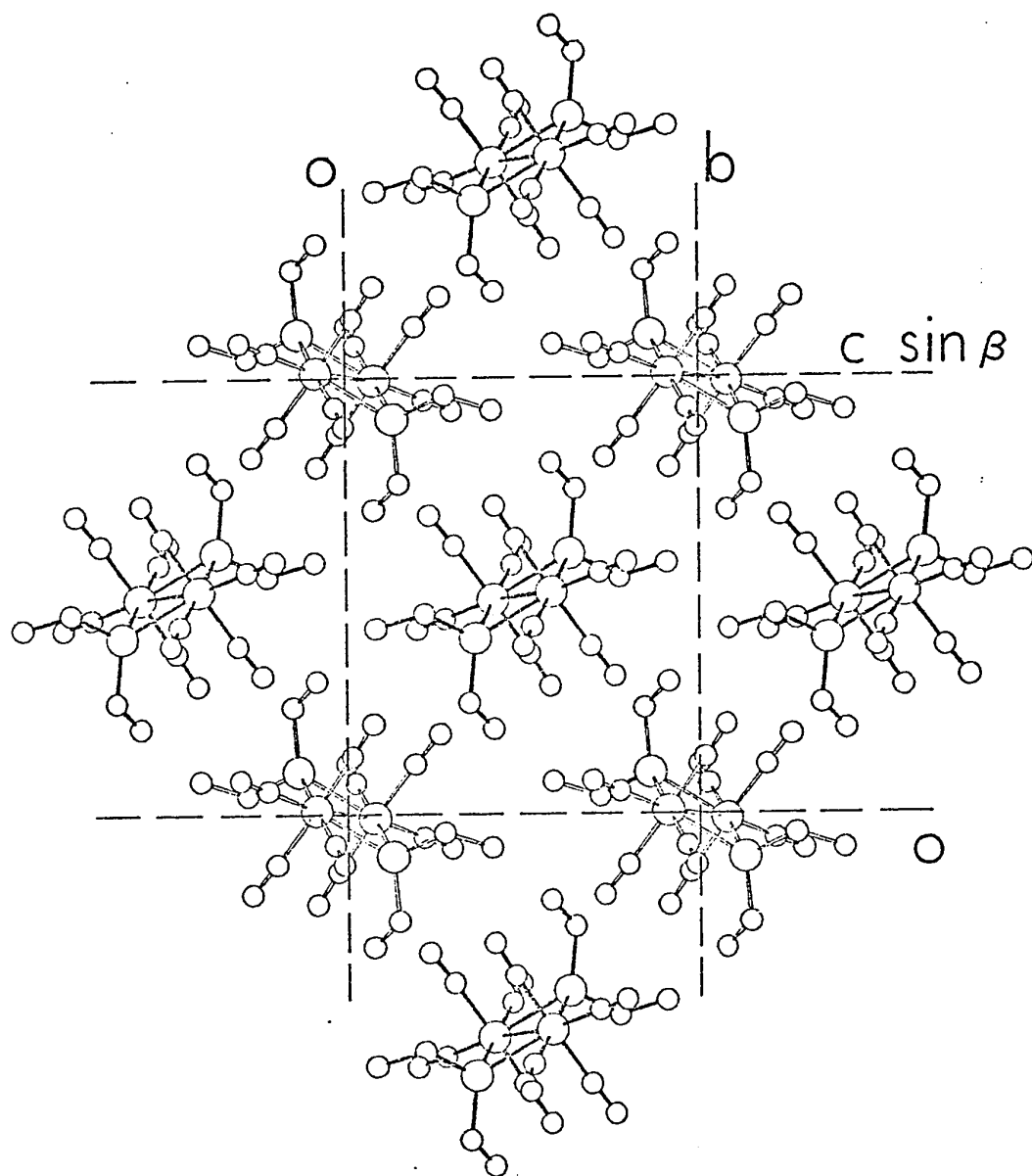


Figure 6

Packing of  $\text{H}_2\text{W}_2(\text{CO})_8[\text{Si}(\text{C}_2\text{H}_5)_2]_2$  down the  $a$  axis

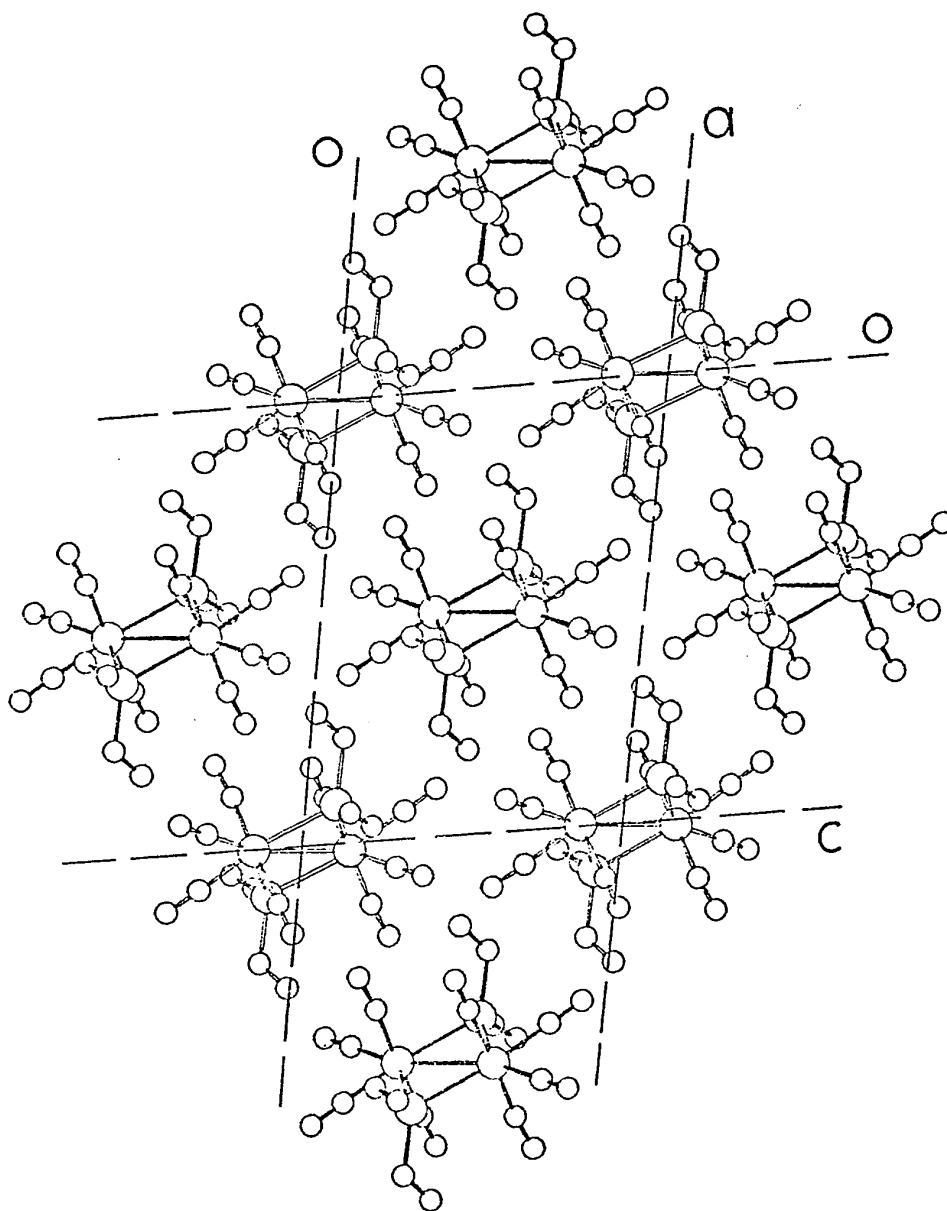


Figure 7

Packing of  $H_2W_2(CO)_8[Si(C_2H_5)_2]_2$  down the b Axis

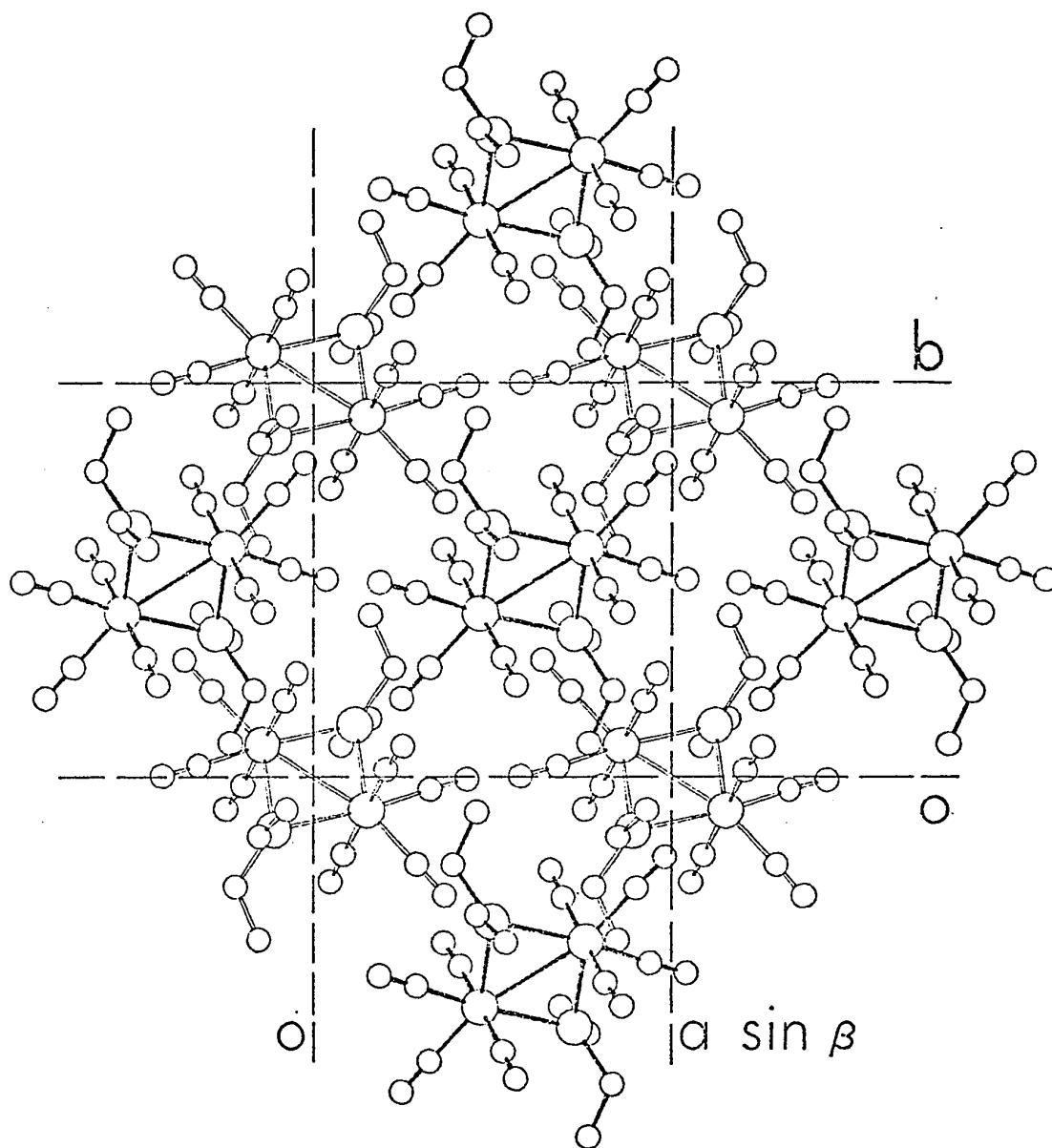


Figure 8

Packing of  $\text{H}_2\text{W}_2(\text{CO})_6[\text{Si}(\text{C}_2\text{H}_5)_2]_2$  down the  $c$  Axis

Table X  
Bond Lengths<sup>(a)</sup>

Atoms	Uncorrected Distance (Å)	Corrected Distance (Å) <sup>(b)</sup>	Corrected Distance (Å) <sup>(c)</sup>
W-W' <sup>(d)</sup>	3.183(1)	-	-
W-Si	2.586(5)	2.595(5)	2.654(5)
W-Si'	2.703(4)	2.712(4)	2.785(4)
W-C1	1.94(2)	1.95(2)	2.04(2)
W-C2	2.01(2)	2.02(2)	2.11(2)
W-C3	1.98(2)	2.00(2)	2.09(2)
W-C4	1.99(2)	2.00(2)	2.10(2)
Si-C5	1.90(3)	1.95(3)	2.07(2)
Si-C7	1.89(2)	1.93(2)	2.03(2)
C1-O1	1.19(2)	1.22(2)	1.40(1)
C2-O2	1.16(2)	1.22(2)	1.38(1)
C3-O3	1.11(2)	1.16(2)	1.37(1)
C4-O4	1.13(2)	1.17(2)	1.39(1)
C5-C6	1.25(3)	1.30(3)	1.60(2)
C7-C8	1.55(2)	1.56(3)	1.78(2)

(a) Standard deviations in parentheses refer to last digit quoted.

(b) Correction for thermal motion: second atom assumed to ride on first atom.

(c) Correction for thermal motion: atoms assumed to move independently.

(d) Primed atoms related by an inversion centre.

Table XI  
Intramolecular Angles<sup>(a)</sup>

<u>Atoms</u>	<u>Angle</u>	<u>Atoms</u>	<u>Angle</u>
W'-W-Si <sup>(b)</sup>	54.70 (10)	C2-W-C4	90.2 (6)
W'-W-Si	41.33 (10)	C3-W-C4	78.4 (7)
Si-W-Si'	106.03 (12)	W-Si-W'	73.97 (12)
Si-W-Cl	88.9 (5)	W-Si-C5	123.8 (9)
Si-W-C2	93.0 (4)	W-Si-C7	114.3 (6)
Si-W-C3	144.8 (5)	C5-Si-C7	101.0 (11)
Si-W-C4	66.6 (5)	W-Cl-01	173.6 (14)
Si'-W-C3	109.1 (5)	W-C2-02	177.1 (14)
Cl-W-C2	177.1 (6)	W-C3-03	178.8 (17)
Cl-W-C3	89.0 (7)	W-C4-04	177.3 (16)
Cl-W-C4	92.5 (7)	Si-C5-C6	115.1 (24)
C2-W-C3	90.6 (7)	Si-C7-C8	112.2 (14)

(a) Standard deviations in parentheses refer to last digit quoted.

(b) Primed atoms related by an inversion centre.

Table XII

## Non-Bonded Intramolecular Contacts

<u>Atoms</u>	<u>Distance<sup>(a)</sup></u> <u>(Å)</u>
Si C <sub>1</sub>	3.20(2)
Si C <sub>4</sub>	2.55(2)
Si C <sub>2</sub>	3.36(2)
Si C <sub>1</sub> '	3.33(2)
Si C <sub>4</sub> '	3.29(2)
C <sub>1</sub> C <sub>2</sub>	2.84(3)
C <sub>1</sub> C <sub>3</sub>	2.74(3)
C <sub>1</sub> C <sub>2</sub> '	3.16(2)
C <sub>4</sub> C <sub>3</sub>	2.51(3)
C <sub>2</sub> C <sub>4</sub>	2.83(2)
C <sub>3</sub> C <sub>2</sub>	2.84(2)
C <sub>5</sub> C <sub>7</sub>	2.93(3)

(a) Standard deviations in parentheses refer to last digit quoted.



Table XIII

Intermolecular Contacts Less Than 4.0Å

Atoms	Distance (Å)	Symmetry (a)	Atoms	Distance (Å)	Symmetry
C1 01	3.44(2)	1	01 C6	3.98(3)	6
C3 04	3.57(2)	1	03 C8	3.99(3)	8
C4 04	3.30(2)	1	02 03	3.15(2)	4
C4 C4	3.76(3)	1	02 C3	3.59(2)	4
C5 01	3.92(3)	2	02 C8	3.67(3)	8
C5 02	3.95(3)	3	02 01	3.90(2)	4
C5 04	3.92(3)	3	04 04	3.20(2)	1
C6 03	3.36(3)	4	04 C1	3.44(2)	1
C6 03	3.96(3)	3	04 03	3.66(2)	1
C7 03	3.85(2)	1	04 02	3.72(2)	3
01 03	3.61(2)	5	C4 C8	3.99(3)	7
01 04	3.30(2)	1	C8 C8	3.87(5)	9
01 C3	3.87(2)	5			
01 C8	3.89(3)	6			

(a) Symmetry position of molecule to which second atom named belongs.  
 The positions are: (1)  $\bar{x}+1 \bar{y} \bar{z}$ ; (2)  $x-\frac{1}{2} y-\frac{1}{2} z-\frac{1}{2}$ ; (3)  $\bar{x}+\frac{1}{2} y-\frac{1}{2} z-\frac{1}{2}$ ;  
 (4)  $x-\frac{1}{2} \bar{y}+\frac{1}{2} z-\frac{1}{2}$ ; (5)  $\bar{x}+\frac{1}{2} y-\frac{1}{2} z+\frac{1}{2}$ ; (6)  $x+\frac{1}{2} \bar{y}-\frac{1}{2} z+\frac{1}{2}$  (7)  $\bar{x}-\frac{1}{2} y+\frac{1}{2} z-\frac{1}{2}$ ;  
 (8)  $x \bar{y}+1 z$ ; (9)  $\bar{x} \bar{y}-1 z$ .

(b) Standard deviations in parentheses refer to last digit quoted.

Table XIV

## Selected Least Squares Planes

Atoms Defining Plane (a)	Equation of Plane (b) (c)	Deviations
W	+0.262X-0.526Y+0.809Z=0	W 0.0000 Si +0.0001 C3 +0.091 03 +0.064 C4 -0.099 04 -0.166
W	+0.269X-0.536Y+0.800Z=0	W +0.0002 Si +0.033 C3 +0.081 03 +0.048 C4 -0.073 04 -0.124
W	-0.450X+0.640Y+0.0623Z=0	W +0.0006 C1 +0.065 01 +0.070 C2 +0.035 02 +0.079

(a) and equivalent atoms related by  $\bar{1}$ .

(b) referred to Cartesian coordinate system with X, Y, Z axes defined by the directions of a, b and c\* respectively.

(c) computed using MGEOM, a molecular geometry program by John S. Wood.

## DISCUSSION

As Table IX shows, all atoms have abnormally high temperature factors. These are consistent with a lattice containing a small number of sites which are vacant, or occupied by smaller molecules, viz. n-hexane.

A metal-metal bond between the tungsten atoms is evidenced by the tungsten-tungsten distance of 3.18 Å and by the acute bridging angle (74°) at the silicon atom.<sup>55</sup> The tungsten-carbon (carbonyl) distances range from 1.94 to 2.01 Å with an average of 1.98 Å which agrees with those (1.96 Å average) observed in other tungsten carbonyl derivatives whose structures are known (( $\pi$ -C<sub>5</sub>H<sub>5</sub>)W(CO)<sub>3</sub>( $\sigma$ -C<sub>6</sub>H<sub>5</sub>) 1.96 Å;<sup>56</sup> ( $\pi$ -C<sub>5</sub>H<sub>5</sub>)W(CO)<sub>3</sub>AuP(C<sub>6</sub>H<sub>5</sub>)<sub>3</sub> 1.97(5) Å;<sup>57</sup> bipy (CO)<sub>3</sub>BrWGeBr<sub>3</sub><sup>58</sup> 1.91(6) Å; (C<sub>4</sub>H<sub>10</sub>S<sub>2</sub>)(CO)<sub>3</sub>ClWSnCH<sub>3</sub>Cl<sub>2</sub> 1.96(4) Å<sup>59</sup>). The carbon-oxygen distances in the carbonyl groups are normal with a range of 1.11 to 1.19 Å, average 1.15 Å. These groups are very nearly linear the  $\widehat{WCO}$  angles averaging 176.7°.

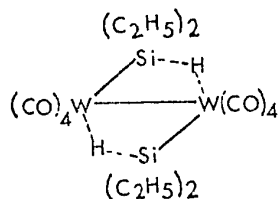
The geometry of the diethyl silicon group shows no unusual features. The two independent silicon-carbon distances show good internal agreement and the average, using the model for thermal motion correction, is 1.94 Å, the value that would be predicted on the basis of covalent radii.<sup>60a)</sup> The carbon-carbon distances in the ethyl groups show a significant difference which can be resolved by

using the independent atom model for C5C6 and the uncorrected model for C7C8 (see Table X).

The most interesting and important aspect of this structure involves the central  $W_2Si_2$  core. This cluster is planar with four of the eight carbonyl groups lying approximately in this plane as shown in Figure 5, while the remaining carbonyl groups are approximately perpendicular to the plane. There are two distinct tungsten-silicon bonds of 2.596(6) and 2.703(4) Å, and despite the high thermal parameters, it would be impossible for such a variation in bond length to occur in a central, relatively rigid group as is the  $W_2Si_2$  unit. However, the significant difference in bond length can be considered as evidence for direct insertion of a hydrogen atom into the longer tungsten-silicon bond. While the actual difference of 0.107 Å is not as large as the 0.4 Å that can be estimated<sup>61,30</sup> for linear M-M and M-H-M systems, it is consistent with a non-linear W-H-Si and would be analogous to the proposed bent Re-H-Re two electron system in  $Re_3H_2(CO)_{12}$ .<sup>32</sup> The angular distribution of ligands as shown in Figure 5 further supports the non-linear insertion of the hydrogen with  $\widehat{SiWC4}$  66.6° and  $\widehat{Si'WC3}$  109.1°, Si'W being the long bond. Predictions of the expected value for a normal tungsten-silicon bond are uncertain due to uncertainties in the value for the covalent radius of tungsten: values

of 1.30<sup>60b)</sup> and 1.62 Å<sup>62</sup> are acceptable (if it is assumed that molybdenum and tungsten have identical covalent radii). Coupled with 1.17 Å as the covalent radius for silicon, the predicted values for W-Si are 2.47 and 2.79 Å respectively and both tungsten-silicon distances lie within this range. If the calculated value of 2.79 Å is considered the most appropriate with this type of molecule, then both bonding systems are shorter than expected. It is possible to invoke direct silicon-tungsten  $\pi$  bonding over both the shorter and longer tungsten-silicon distances on purely geometric grounds resulting in an increase in the tungsten-silicon bond order. The presence of  $\pi$  bonding is supported by Graham's semi-quantitative treatment of infrared data<sup>63</sup> which suggests that  $\pi$  bonding does play an important part in transition metal-silicon bonding.

The bonding of the central unit may be described as:



a metal-metal bond, two tungsten-silicon  $\sigma$  bonds with some  $\pi$  bond character and two bent three-centre two-electron tungsten-hydrogen-silicon bonds (the two electrons being supplied by the silicon and hydrogen atoms). This view

allows the effective atomic number rule to be applied to the tungsten atoms: each tungsten atom needs twelve electrons to reach an inert gas configuration, eight come from the carbonyl groups, one from the metal-metal bond, one from the sigma W-Si bond and two from the bent 3-centre 2-electron bond with hydrogen-silicon. The tungsten coordination can be discussed in terms of a pentagonal bipyramid. The two axial bonds are then to the carbonyl groups C101 and C202 and the five equatorial sites correspond to the other two carbonyl groups, the tungsten-silicon bond, the tungsten-tungsten bond and the 3-centre 2-electron W-H-Si bond.

As described in the introduction to this chapter, the rhenium compounds which appeared analogous to this tungsten compound have no alteration in the geometry of the central  $\text{Re}_2\text{Si}_2$  cluster. That is, they show neither a shift of substituents to accommodate the hydrogen which can be thought to occupy a stereochemical position, nor a change in the rhenium silicon bond length. Conversely as has been seen, in the tungsten compound there is direct insertion of the hydrogen into the tungsten-silicon bond producing a lengthening of the bond and a shift of other substituents to allow for the hydrogen (VI). The latter is most likely the only true hydrogen-bridged transition metal bond that has been investigated in this series. The dirhenium sys-

tems,  $H_2Re_2(CO)_8SiR_2$ , ( $R = C_6H_5, CH_3, C_2H_5$ );  $H_4Re_2(CO)_6(SiR_2)_2$ , ( $R = CH_3, C_2H_5$ ); and  $H_2Re_2(CO)_3(SiR_2)_2$ , ( $R = CH_3, C_2H_5$ ) probably contain only terminally bound hydrogen although structures II and V are possible. However, as later chapters will show, weak Si-H bridges appear only in sterically crowded situations not found in the rhenium compounds, but present in this tungsten system where one more carbonyl has to be accommodated.

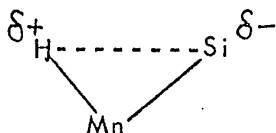
## CHAPTER 4

The Crystal and Molecular Structure of  $\text{HFe}(\text{CO})_4\text{Si}(\text{C}_6\text{H}_5)_3$



## INTRODUCTION

The crystal structure of  $(\pi\text{-C}_5\text{H}_5)\text{HMn}(\text{CO})_2\text{Si}(\text{C}_6\text{H}_5)_3$  determined by W. Hutcheon<sup>64</sup> showed the hydridic hydrogen to have a weak interaction with the silicon atom at a distance  $1.76(4) \text{ \AA}$  from it (compared with the Si-H bonding distance of  $1.48 \text{ \AA}$  in  $\text{SiH}_4$ <sup>65</sup>). This compound did not show an Mn-H stretch in the infrared, but its trichlorosilyl analogue, which was too unstable for an X-ray structure, did. Interpreting this difference in infrared activity as indicative of different hydrogen behavior, Hutcheon proposed the following explanation for these two compounds: In the triphenylsilyl compound, close contact between silicon and hydrogen is favored by a slight negative charge on the silicon atom,



while in the trichlorosilyl compound (and in  $(\pi\text{-C}_5\text{H}_5)\text{HFe}(\text{CO})(\text{SiCl}_3)_2$ <sup>73</sup>), the chlorine substituents cause the silicon to be slightly positive, thereby destabilizing the weak hydrogen bond. In this view, then, non-interacting hydrogens are expected to give rise to bands in the infrared. Although such bands were obscured by the carbonyl stretches in the case of  $\text{HFe}(\text{CO})_4\text{Si}(\text{C}_6\text{H}_5)_3$ , it has the same triphenylsilyl substituent as  $(\pi\text{-C}_5\text{H}_5)\text{HMn}(\text{CO})_2\text{Si}(\text{C}_6\text{H}_5)_3$  and would

be expected to have the same weak silicon-hydrogen interaction as the manganese prototype, thus confirming the electrostatic rationale of Hutcheon. Deuterium substitution studies on both compounds which might be expected to produce a characteristic M-D stretch around  $1300\text{ cm}^{-1}$ , and which perhaps would have shown differences between these compounds, were unfortunately not carried out. The structure of  $\text{HFe}(\text{CO})_4\text{Si}(\text{C}_6\text{H}_5)_3$  forms the topic for this chapter.

## EXPERIMENTAL

The compound hydrido-triphenyl-silyl-tetracarbonyl iron ( $\text{HFe}(\text{CO})_4\text{Si}(\text{C}_6\text{H}_5)_3$ ) forms colorless prismatic crystals which decompose with the formation of a black coating. Rotation and Weissenberg photographs disclosed a triclinic cell. The unit cell dimensions were obtained from a least squares refinement of  $2\theta$  values of thirteen reflections from crystal VIII, as described in Appendix C. The cell dimensions are  $a = 10.062(1) \text{ \AA}$ ,  $b = 10.377(1) \text{ \AA}$ ,  $c = 10.800(6) \text{ \AA}$ ,  $\alpha = 90.96(3)^\circ$ ,  $\beta = 111.43(1)^\circ$ ,  $\gamma = 98.55(1)^\circ$ . The density was determined by flotation using aqueous potassium iodide to be 1.37 gm/cc which agrees well with the calculated density (1.374 gm/cc) obtained for two molecules per unit cell, a molecular weight of 428.3 and unit cell volume of  $1034.9 \text{ \AA}^3$ .

All crystals were mounted with  $a^*$  coincident with the  $\phi$  axis of the diffractometer and the intensity data within the  $1 \text{ \AA}$  sphere were collected using  $\text{MoK}_\alpha$  radiation. The peak scan  $2\theta$  range was  $1.4^\circ$  with backgrounds counted for twenty seconds.

Because of the severe decomposition problem, eight crystals were used during the data collection. Each crystal was prepared for X-ray crystallography by washing off the black coating with ethanol to leave a well-formed col-

orless crystal, mounting the crystal on a thin glass fibre, coating it with shellac, and covering the fibre and crystal by a glass capillary which had been flushed with dried argon. It was possible by these means to use each crystal for from 4 to 20 hours (see Table XV). No crystal was used after the intensities as measured by a set of eight standard reflections fell below 80% of the initial intensity. Decomposition corrections were applied to each crystal by a least squares analysis of the standard reflections. The decomposition was found to vary with  $\sin\theta/\lambda$ , with time irradiated, and with absolute time. Consequently, a correction that was linear in  $\sin\theta/\lambda$  and time was applied to each collection time period.

Each crystal used (except VIII) had faces of the form {010}, {100} and {012}; their dimensions are given in Table XV. Absorption corrections ( $\mu = 8.34 \text{ cm}^{-1}$ ) were applied to the decomposition corrected data. The consistency of these corrections was tested using data from the  $h00$ ,  $h = 3, 5, 9$ , reflections measured from  $\phi = 0^\circ$  to  $\phi = 180^\circ$  in  $10^\circ$  intervals and corrected for decomposition. The internal consistency of each data set was within the limits of counting statistics as was tested by substituting values for  $\sigma(F)$ , the standard deviation in  $F$ , obtained from corrected  $\phi$  scan data, and average values for counts into the equation

Table XV

Crystal	No. Reflections Collected (a)	Crystal Information			Crystal Dimensions $\times 10^3$ cm		
		Time Irradiated (Hr)	(b)	010(c)	100(c)	012(c)	012(c)
I	316	13.5		15	14.5	12	12
II	324	12.5		13	18.2	11	9
III	528	20.0		18	20	17	16
IV	413 (d)	15.25		23	22	18	19
V	396	15.5		17	20	16	14
VI	105	3.75		15	18	11	12
VII	98	4.0		9	10	7	8
VIII	151	7.0		-(e)	13	19	24

(a) Includes unobserved reflections.

(b) Does not include irradiation time before collection was begun.

(c) And centrosymmetrically related face. Perpendicular distances between face edges are given.

(d) 151 of these reflections were recollected using crystal VIII.

(e) This pair of faces not found on crystal VIII which was prepared and used much later than the previous seven.

$$\sigma(F) = \frac{1}{2} \frac{1}{\sqrt{LP}} \sqrt{\frac{N_T + N_{bg_1} + N_{bg_2} + (pN_{pk})^2}{N_{pk}}}$$

where LP are Lorentz-polarization factors,  $N_T$  is the total peak count,  $N_{bg_1}$  and  $N_{bg_2}$  are background counts and  $N_{pk} = N_T - N_{bg_1} - N_{bg_2}$ . Solving the equation for p, the machine constant, gave effectively zero,<sup>1</sup> implying good internal consistency.

After decomposition corrections and absorption corrections had been applied, the first seven of the individual data sets were merged into one set by using data collected on the seventh crystal, which included four randomly selected reflections collected with each of the first six crystals. A least squares fit was used and after all corrections, the standards as measured for each of the seven crystals were consistent with each other to an average of 4% (range 3.2 to 4.5%). Twenty-two reflections were corrected for nonlinearity of the counter.

Of 2180 independent reflections measured, 1567 were estimated to be significantly above background using a criterion  $I/\sigma(I) \leq 3.0$ .<sup>53</sup>

The eighth crystal was used to obtain data for the determination of accurate cell constants and for correcting three regions of data, each of which contained an inordinate number of unobserved reflections and in which  $F_{obs} \ll F_{calc}$  for most observed planes. The 151 reflections

so collected contained 133 observed datum using the above criteria, increasing the total number of reflections to 1612. The significant data were corrected for absorption and decomposition and merged with the previous data set using the standard reflections. This data was collected and merged with the preceding data after refinement was essentially complete.

## SOLUTION AND REFINEMENT

A Patterson map was calculated using the uncorrected data set with the expectation of finding the two iron and two silicon atoms contained in the unit cell. The space group  $P\bar{1}$  was assumed. The vector list, its multiplicities, and relative weights are given in Table XVI. Upon examination of the Patterson map, four possible solutions as given in Table XVII were apparent, with the second being chosen as the most probable since it alone gave both a good Fe-Si distance (2.3 Å) and had a peak corresponding to  $(2x_{Si} \ 2y_{Si} \ 2z_{Si})$ . A least squares refinement using structure factors phased on the second solution gave  $R_1 = 0.24$  and  $R_2 = 0.31$ , but an electron density map did not reveal the positions of any of the remaining atoms. At this point, corrections were made for the decomposition, but again the observed Fourier map did not locate any atoms other than the input iron and silicon. Since the space group could be  $P1$  rather than  $P\bar{1}$ , the data was tested statistically for the presence of a centre using the program FAME written by R. Dewar and A. Stone. The distribution found, as well as that expected for centro- and non-centrosymmetric structures, is given in Table XVIII and clearly confirms the choice of  $P\bar{1}$  as the space group. At this point, it was decided to use direct methods to solve the structure. With the original data set and using the pro-



Table XVI  
Patterson Vectors

	<u>Vector</u>			<u>Multiplicity</u>	<u>Relative Weight</u>
$2x_{\text{Fe}}$	$2y_{\text{Fe}}$	$2z_{\text{Fe}}$		1	676
$2\bar{x}_{\text{Fe}}$	$2\bar{y}_{\text{Fe}}$	$2\bar{z}_{\text{Fe}}$		1	676
$x_{\text{Fe}} + x_{\text{Si}}$	$y_{\text{Fe}} + y_{\text{Si}}$	$z_{\text{Fe}} + z_{\text{Si}}$		2	728
$x_{\text{Fe}} + \bar{x}_{\text{Si}}$	$y_{\text{Fe}} + \bar{y}_{\text{Si}}$	$z_{\text{Fe}} + \bar{z}_{\text{Si}}$		2	728
$\bar{x}_{\text{Fe}} + x_{\text{Si}}$	$\bar{y}_{\text{Fe}} + y_{\text{Si}}$	$\bar{z}_{\text{Fe}} + z_{\text{Si}}$		2	728
$\bar{x}_{\text{Fe}} + \bar{x}_{\text{Si}}$	$\bar{y}_{\text{Fe}} + \bar{y}_{\text{Si}}$	$\bar{z}_{\text{Fe}} + \bar{z}_{\text{Si}}$		2	728
$2x_{\text{Si}}$	$2y_{\text{Si}}$	$2z_{\text{Si}}$		1	196
$2\bar{x}_{\text{Si}}$	$2\bar{y}_{\text{Si}}$	$2\bar{z}_{\text{Si}}$		1	196

Table XVII  
Patterson Solutions

Weight	Peak	Solution 1	Solution 2	Solution 3	Solution 4
295	.112-.110-.152	$x_{Fe} + \bar{x}_{Si} \quad y_{Fe} + \bar{y}_{Si} \quad z_{Fe} + \bar{z}_{Si}$	$x_{Fe} + \bar{x}_{Si} \quad y_{Fe} + \bar{y}_{Si} \quad z_{Fe} + \bar{z}_{Si}$	$x_{Fe} + \bar{x}_{Si} \quad y_{Fe} + \bar{y}_{Si} \quad z_{Fe} + \bar{z}_{Si}$	$x_{Fe} + \bar{x}_{Si} \quad y_{Fe} + \bar{y}_{Si} \quad z_{Fe} + \bar{z}_{Si}$
288	.448+.490-.239	$x_{Fe} + x_{Si} \quad y_{Fe} + y_{Si} \quad z_{Fe} + z_{Si}$	$x_{Fe} + x_{Si} \quad y_{Fe} + y_{Si} \quad z_{Fe} + z_{Si}$	$x_{Fe} + x_{Si} \quad y_{Fe} + y_{Si} \quad z_{Fe} + z_{Si}$	$x_{Fe} + x_{Si} \quad y_{Fe} + y_{Si} \quad z_{Fe} + z_{Si}$
266	.448-.280 .399	$-2x_{Fe} \quad -2y_{Fe} \quad -2z_{Fe}$	$-2x_{Fe} \quad -2y_{Fe} \quad -2z_{Fe}$	$-2x_{Fe} \quad -2y_{Fe} \quad -2z_{Fe}$	$-2x_{Fe} \quad -2y_{Fe} \quad -2z_{Fe}$
173	.504 .340-.413	$\sim 2x_{Fe} \quad 2y_{Fe} \quad 2z_{Fe}$	$\sim 2x_{Fe} \quad 2y_{Fe} \quad 2z_{Fe}$	$\sim 2x_{Fe} \quad 2y_{Fe} \quad 2z_{Fe}$	$\sim 2x_{Fe} \quad 2y_{Fe} \quad 2z_{Fe}$
153	.504+.490 .225	$\sim \bar{x}_{Fe} + \bar{x}_{Si} \quad \bar{y}_{Fe} + \bar{y}_{Si} \quad \bar{z}_{Fe} + \bar{z}_{Si}$	$\sim \bar{x}_{Fe} + \bar{x}_{Si} \quad \bar{y}_{Fe} + \bar{y}_{Si} \quad \bar{z}_{Fe} + \bar{z}_{Si}$	$\sim \bar{x}_{Fe} + \bar{x}_{Si} \quad \bar{y}_{Fe} + \bar{y}_{Si} \quad \bar{z}_{Fe} + \bar{z}_{Si}$	$\sim \bar{x}_{Fe} + \bar{x}_{Si} \quad \bar{y}_{Fe} + \bar{y}_{Si} \quad \bar{z}_{Fe} + \bar{z}_{Si}$
148	.	.	.	.	.
101	.308-.410-.065	-	$2x_{Si} \quad 2y_{Si} \quad 2z_{Si}$	-	-
	Fe	-0.224 0.19 -0.195	0.276 0.19 -0.195	-0.224 -0.25 -0.38	0.276 -0.25 -0.38
	Si	.168 0.30 -0.044	0.168 0.30 -0.044	-0.336 -0.14 -0.23	0.168 -0.14 -0.23
	Fe-Si Distance	4.2 Å	2.3 Å	5.9 Å	2.3 Å

Table XVIII  
 Statistical Distribution of  $E(hk\ell)$ 's (a)

<u>Quantity</u>	<u>Observed</u>	<u>Theoretical Centric</u>	<u>Theoretical Acentric</u>
Average magnitude of $E(hk\ell)$ 's	0.803	0.798	0.886
Average of $E(hk\ell)^2$	1.000	1.000	1.000
Average of $ E(hk\ell)^2 - 1 $	0.967	0.968	0.736
Percent $E(hk\ell)$ 's greater than one	30.85	32.00	37.00
Percent $E(hk\ell)$ 's greater than two	5.08	5.00	1.80
Percent $E(hk\ell)$ 's greater than three	0.40	0.30	0.01

(a)  $E(hk\ell)$  values defined by the formula  $E(hk\ell)^2 = \frac{|F(hk\ell)|^2}{\epsilon \sum f_j^2}$

$\epsilon$  accounts for systematic absences in the data.

Table XIX  
Hydrogen Peak as a Function of  $\sin\theta/\lambda$

$\frac{\sin\theta/\lambda}{\text{Cut-off } \lambda^{-1}}$	Number of Terms in Unique Section	Calculated Height (b), %			Observed Height	Position			Distances	
		4.0	5.3	8.7		x	y	z	Fe-H	Si-H
0.20	130	0.15	.15	.14	0.11	+ .183	-.220	-.478	1.73	2.76
0.25	246	0.24	.23	.21	0.21	.170	-.235	-.482	1.66	2.81
0.30	408	.32	.31	.27	0.26	.173	-.235	-.468	1.54	2.68
0.35	644	.40	.37	.31	0.33	.165	-.238	-.463	1.56	2.63
0.40	926	.46	.42	.34	0.37	.171	-.242	-.465	1.51	2.67
0.45	1254	.51	.46	.36	0.36	.164	-.245	-.460	1.53	2.62
0.53 (a)	1612	.56	.50	.38	0.40	.165	-.248	-.455	1.48	2.58

(a) Full data set

$$(b) \rho_H^C = \frac{1}{2\pi} \int_0^{2\pi} \int_0^{\pi} (1 + a^2 s^2/4)^{-2} \exp(-Bs^2/16\pi^2) s^2 ds$$

$$s = 4\pi \sin\theta/\lambda \quad a = \text{Bohr's radius}$$

Evaluated using Simpson's Rule with 20 intervals.

gram FAME to choose six  $hkl$  planes of large relative intensity and interaction, and the program MAGIC also written by Dewar and Stone to assign signs to the three non-origin defining planes, the method of symbolic addition developed by Sayre<sup>3</sup> allowed the phases of the 250 relatively strongest intensities to be determined. An  $E(hkl)$  map,

$$E(hkl)^2 = \frac{|F(hkl)|^2}{\epsilon \sum f_j^2}$$

with  $\epsilon$  a measure of the systematic absences in the data, phased in this way showed the iron and silicon in the positions dictated by the fourth Patterson solution, and also located the carbonyl groups and phenyl rings. A least squares refinement with the phenyl carbon atoms as rigid bodies and all other non-hydrogen atoms as isotropic atoms gave  $R_1 = 0.100$  and  $R_2 = 0.143$  after four cycles. When corrections were made for decomposition and absorption and the data sets were merged,  $R_1 = 0.093$  and  $R_2 = 0.138$ . Next, the iron, silicon, carbonyl carbon and oxygen atoms were made anisotropic, and anomalous dispersion corrections<sup>9</sup> were applied to the silicon and iron atoms. The locations of the hydrogen atoms were determined from an electron density difference map, and the addition of the phenyl hydrogens as rigid bodies resulted in  $R_1 = 0.069$  and  $R_2 = 0.117$ . The fifth largest peak on this map,  $0.57 \text{ e}/\text{\AA}^3$  was

located at (-.471, .170, -.245) and was attributed to the hydridic hydrogen. It is of very similar density to the hydrogen peak found by Ibers<sup>29</sup> et al in the structure of  $\text{CoH}(\text{N}_2)(\text{P}(\text{C}_6\text{H}_5)_3)_3$ . When electron density difference maps limited in  $\sin\theta/\lambda$  ( $\sin\theta/\lambda \leq 0.45, 0.40, 0.35, 0.30, 0.25, 0.20$ ) were calculated, this hydridic hydrogen peak was the highest peak on each map. The heights of the peaks were less than those predicted by the calculated theoretical values of La Placa and Ibers<sup>66</sup> probably because the temperature factor used initially in the calculations (that of the iron) was too small: the hydrogen atom appears more spread out as evidenced by its large refined temperature factor. When this temperature factor is used in the calculation of the theoretical value ( $B = 8.7$  in column 3 of Table XIX), much better agreement is obtained. However, probably the best temperature factor to use would be near in value to the carbonyl carbon values which average about 5.3. Hence, these values of the integral are also included in the table. The agreement is adequate. A comparison of these calculated peak values for the hydridic hydrogen with those observed for this peak for various  $\sin\theta/\lambda$  cut-offs is given in Table XIX. The addition of the hydridic hydrogen as an isotropic atom reduced the R factors to  $R_1 = 0.067$  and  $R_2 = 0.112$ .

A strong correlation (0.9895) between two of

the angular parameters,  $E$  and  $\xi$ , for rigid body 1 was observed, and in efforts to eliminate it, the cell was redefined twice: 1)  $a_n=b_o$ ;  $b_n=c_o$ ;  $c_n=a_o$ ;  $\alpha_n=\beta_o$ ;  $\beta_n=\gamma_o$ ;  $\gamma_n=\alpha_o$ ;  $h_n=k_o$ ;  $k_n=l_o$ ;  $l_n=h_o$ ; 2)  $a_n=c_o$ ;  $b_n=a_o$ ;  $c_n=b_o$ ;  $\alpha_n=\gamma_o$ ;  $\beta_n=\alpha_o$ ;  $\gamma_n=\beta_o$ ;  $h_n=l_o$ ;  $k_n=h_o$ ;  $l_n=k_o$ . This only resulted in shifting the correlation from rigid body 1 to rigid body 3 (0.9819) to rigid body 2 (0.9888) indicating that the phenyl rings essentially define the coordinate system. Finally, refinement of each of  $E$  and  $\xi$  separately, followed by joint refinement was tried, but the correlation remained. So, the coordinate system with the greatest correlation was retained, and the value of  $E$  fixed.

The final  $R$  values after substituting the 133 observed reflections collected with the eighth crystal were  $R_1 = 0.061$  and  $R_2 = 0.083$ . At the completion of the refinement, no coordinate shifted more than  $1/3$  of a standard deviation, and the final standard deviation for an observation of unit weight was 2.432. This rather large value can be attributed in part to the rigid body constraint placed on the phenyl rings and in part to the numerous corrections to the data set. A final electron density difference map was calculated with all atoms in their refined positions; it had a maximum density of  $0.59 \text{ e}/\text{A}^3$  and a minimum of  $-0.44 \text{ e}/\text{A}^3$ .

Table XX lists the final coordinate and thermal parameters for the individual atoms while Table XXI has

the rigid body parameters. The derived parameters for the rigid bodies are given in Table XXII. The standard deviations quoted were obtained from the inverted matrix of the final least squares cycle. The observed and calculated structure factor amplitudes,  $10|F_{\text{obs}}|$  and  $10|F_{\text{calc}}|$  are given in Table XXIII.



Table XX  
Final Coordinate and Thermal Parameters (a)

Atom	X	Y	Z	$\beta_{11}$ (b)	$\beta_{22}$	$\beta_{33}$	$\beta_{12}$	$\beta_{13}$	$\beta_{23}$	$B(\text{\AA})^2$ (c)
Fe	0.2843(1)	-0.2356(1)	-0.3738(1)	115(2)	120(2)	86(2)	52(2)	12(1)	15(1)	4.03
Si	0.1704(2)	-0.1309(3)	-0.2152(2)	106(3)	101(4)	79(3)	41(3)	5(2)	16(2)	3.65
C1	0.1538(11)	-0.4012(12)	-0.3585(8)	174(16)	124(18)	77(10)	56(14)	-1(10)	4(11)	4.90
O1	0.0605(8)	-0.5051(8)	-0.3582(7)	168(11)	140(13)	150(10)	15(10)	-9(8)	19(9)	6.41
C2	0.3384(10)	-0.0684(12)	-0.4274(9)	165(14)	169(20)	119(12)	100(14)	44(11)	45(12)	5.30
O2	0.3693(8)	0.0387(9)	-0.4697(7)	263(14)	196(15)	182(11)	116(12)	97(10)	82(10)	7.74
C3	0.3651(10)	-0.3167(11)	-0.4973(9)	185(15)	143(18)	107(12)	65(13)	32(11)	11(11)	5.60
O3	0.4148(8)	-0.3655(8)	-0.5747(8)	242(13)	206(15)	189(11)	102(11)	80(10)	8(10)	8.16
C4	0.4009(10)	-0.2126(10)	-0.2392(10)	114(13)	164(18)	113(12)	63(13)	-8(10)	8(11)	4.91
O4	0.4780(7)	-0.1959(9)	-0.1552(7)	136(10)	324(19)	154(10)	102(11)	-28(8)	13(10)	7.58
H	0.160(10)	-.244(11)	-.472(9)	-	-	-	-	-	-	8.7

(a) Standard deviations in parentheses refer to last digit quoted.

(b) Anisotropic temperature factors  $\times 10^4$ , defined by  $\exp[-(\beta_{11}h^2 + \beta_{22}k^2 + \beta_{33}l^2 + 2\beta_{12}hk + 2\beta_{13}hl + 2\beta_{23}kl)]$ .

(c) Equivalent isotropic thermal parameter.

Table XXI  
Rigid Body Parameters (a)

<u>Ring</u>	<u>x</u>	<u>y</u>	<u>z</u>	<u>D</u>	<u>E</u>	<u>ξ</u>
1	-.1501(4)	-.2424(4)	-.3078(4)	4.879(4)	0.1754(b)	5.882(3)
2	.2879(4)	.2249(5)	-.1672(4)	0.044(4)	3.008(4)	5.062(4)
3	.1908(4)	-.2167(5)	.0759(4)	3.348(4)	1.685(3)	6.009(3)
4	-.1501	-.2424	-.3078	4.879	0.175	6.922
5	.2879	.2249	-.1672	0.044	3.008	6.102
6	.1908	-.2167	.0759	3.348	1.686	7.049

(a) Standard deviations in parentheses refer to last digit quoted.

(b) Parameters for which no estimated errors are given were not refined.

Table XXII

Thermal and Derived Positional Parameters  
for Rigid Bodies<sup>(a)</sup>

<u>Ring</u>	<u>Atom</u>	<u>x</u>	<u>y</u>	<u>z</u>	<u>B</u>
1 Phenyl Carbon	C11	-.0150 (4)	-.1968 (5)	-.2696 (5)	4.1 (2)
	C12	-.0554 (5)	-.1902 (5)	-.3957 (5)	5.2 (2)
	C13	-.1905 (6)	-.2357 (7)	-.4339 (4)	7.0 (3)
	C14	-.2853 (4)	-.2879 (5)	-.3460 (5)	6.8 (2)
	C15	-.2448 (5)	-.2946 (5)	-.2199 (5)	6.7 (2)
	C16	-.1097 (6)	-.2490 (7)	-.1817 (4)	4.7 (2)
2 Phenyl Carbon	C21	.2400 (6)	.0743 (5)	-.1903 (5)	3.8 (2)
	C22	.1523 (5)	.1459 (7)	-.1975 (4)	5.2 (2)
	C23	.2002 (6)	.2965 (7)	-.1743 (5)	7.1 (3)
	C24	.3358 (6)	.3754 (5)	-.1440 (6)	7.2 (3)
	C25	.4236 (5)	.3038 (7)	-.1369 (4)	6.7 (2)
	C26	.3756 (6)	.1532 (7)	-.1600 (5)	5.6 (2)
3 Phenyl Carbon	C31	.1832 (6)	-.1827 (7)	-.0484 (4)	3.4 (2)
	C32	.1596 (6)	-.3248 (6)	-.0333 (5)	5.5 (2)
	C33	.1672 (6)	-.3589 (5)	.0909 (6)	6.4 (2)
	C34	.1984 (6)	-.2506 (7)	.2002 (4)	6.0 (2)
	C35	.2219 (6)	-.1086 (6)	.1851 (5)	6.6 (2)
	C36	.2143 (6)	-.0746 (5)	.0608 (6)	5.8 (2)
4 Phenyl Hydrogen	H12	.0140	-.1524	-.4577	5.9
	H13	-.2178	-.2302	-.5249	7.6
	H14	-.3820	-.3202	-.3750	7.4
	H15	-.3142	-.3323	-.1580	6.9
	H16	-.0823	-.2545	-.0907	5.4
	5 Phenyl Hydrogen	H22	.0551	.0876	-.2193
H23		.1358	.3463	-.1797	7.6
H24		.3686	.4836	-.1275	7.6
H25		.5208	.3621	-.1150	7.7
H26		.4401	.1034	-.1546	6.5
6 Phenyl Hydrogen		H32	.1373	-.4012	-.1129
	H33	.1501	-.4615	.1000	6.8
	H34	.2035	-.2770	.2888	6.5
	H35	.2443	-.0322	.2647	7.5
	H36	.2315	.0280	.0518	6.3

(a) Standard deviations in parentheses refer to last digit quoted.

Table XXIII

Observed and Calculated Structure Factor  
Amplitudes,  $10|F_o|$  and  $10|F_c|$







## RESULTS

The molecular geometry and the numbering system used are shown in Figure 9. The molecular packing viewed down each of the axes are given in Figures 10 to 12. These drawings were made using the program ORTEP. Table XXIV gives the bond lengths while the bond angles are listed in Table XXV. In Table XXVI some non-bonding intramolecular distances are given while intermolecular contacts are listed in Table XXVII. These results and the standard deviations associated with them were calculated using the program ORFFE2.



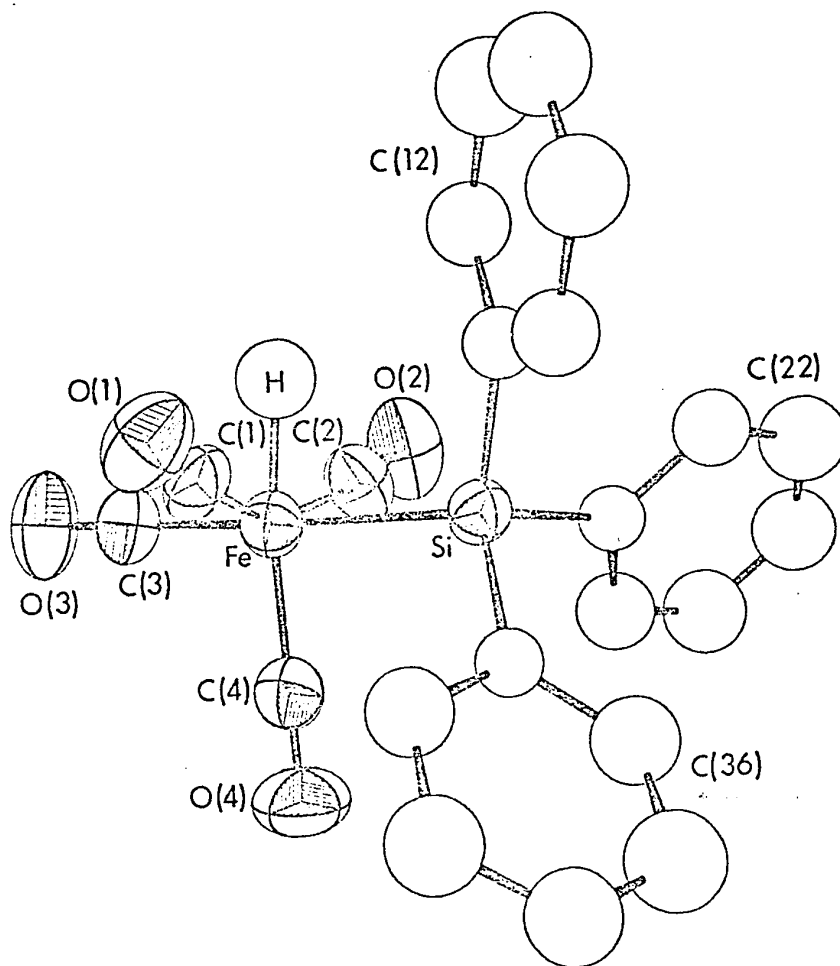


Figure 9

Perspective view of  $\text{HFe}(\text{CO})_4\text{Si}(\text{C}_6\text{H}_5)_3$ , the anisotropic atoms having 50% probability thermal ellipsoids

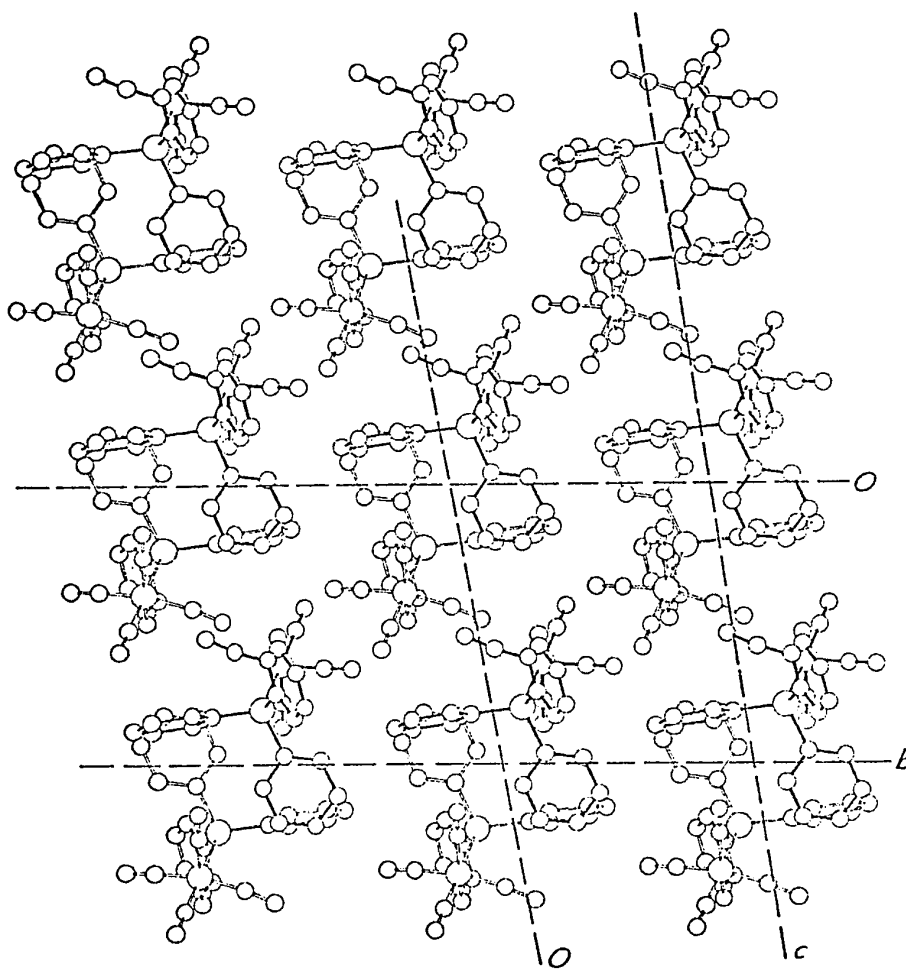


Figure 10

Packing of  $\text{HFe(CO)}_4\text{Si(C}_6\text{H}_5)_3$  down the  $a$  axis  
( $\underline{b}$  is  $b\sin\gamma$  and  $\underline{c}$  is  $c\sin\beta$ )

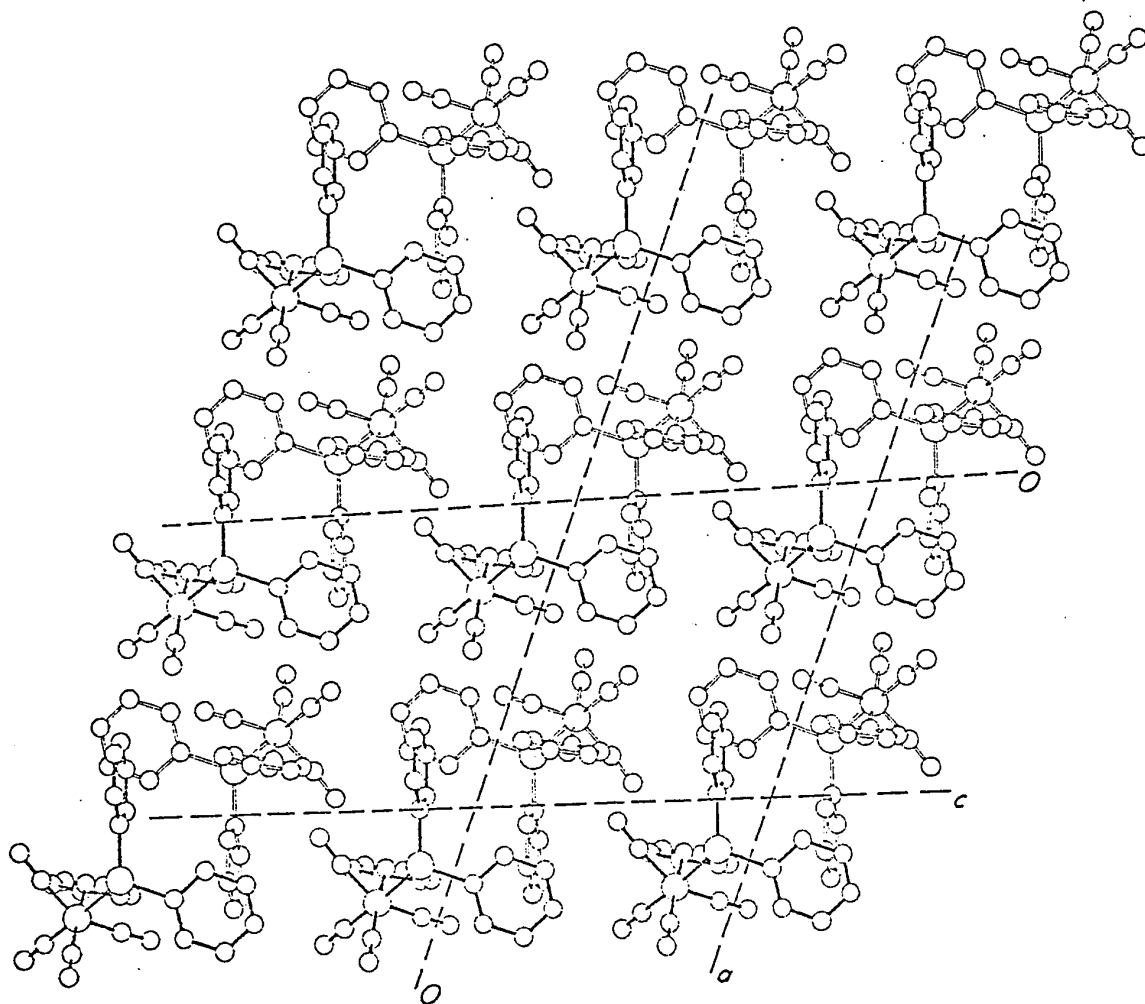


Figure 11  
Packing of  $\text{HFe}(\text{CO})_4\text{Si}(\text{C}_6\text{H}_5)_3$  down the b axis  
(a is  $a\sin\gamma$  and c is  $c\sin\alpha$ )

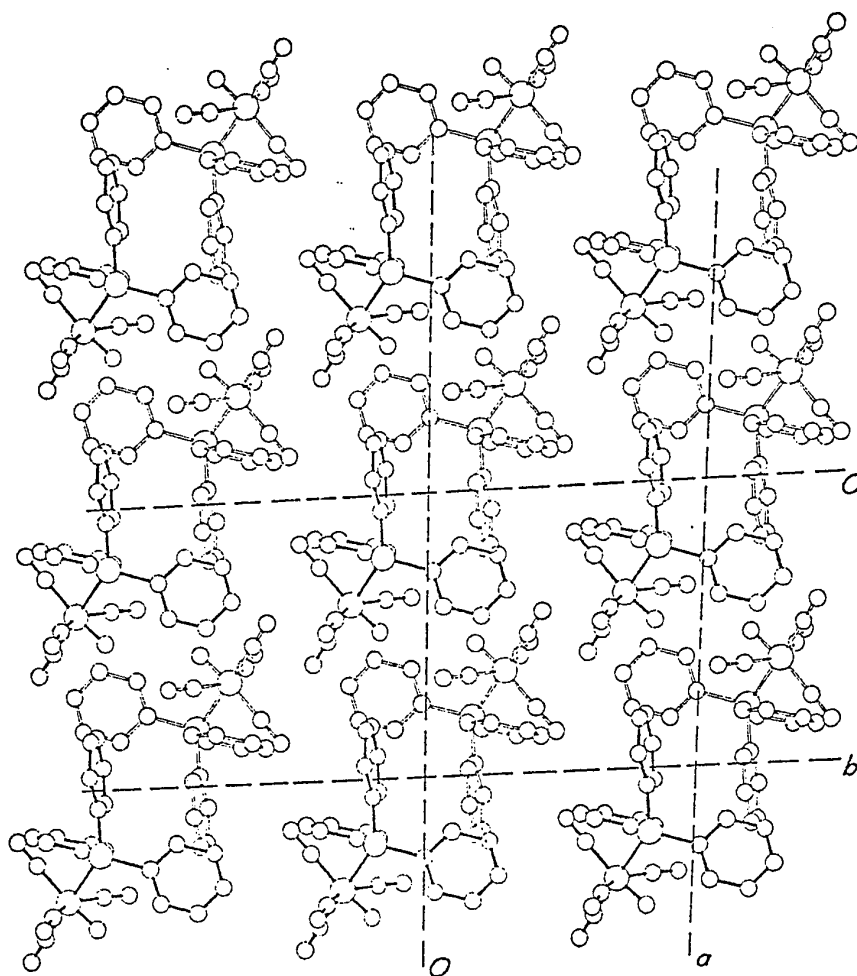


Figure 12

Packing of  $\text{HFe}(\text{CO})_4\text{Si}(\text{C}_6\text{H}_5)_3$  down the  $c$  axis  
 ( $\underline{a}$  is  $a\sin\beta$  and  $\underline{b}$  is  $b\sin\alpha$ )

Table XXIV  
 Bond Lengths (Å) in  $\text{HFe}(\text{CO})_4\text{Si}(\text{C}_6\text{H}_5)_3$

<u>Atoms</u>	<u>Length</u>	<u>Atoms</u>	<u>Length</u>
Fe-Si	2.415(3)	Si-C11	1.910(5)
Fe-C1	1.777(12)	Si-C21	1.896(5)
Fe-C2	1.747(10)	Si-C31	1.898(5)
Fe-C3	1.821(10)	C-C (Ring 1)	1.391
Fe-C4	1.795(11)	C-C (Ring 2)	1.391
C1-01	1.158(10)	C-C (Ring 3)	1.391
C2-02	1.161(10)		
C3-03	1.123(10)		
C4-04	1.144(10)		
Fe-H	1.64(10) <sup>(a)</sup>		

(a) Refined position for hydrogen.

Table XXV  
Bond Angles

<u>Atoms</u>	<u>Angle (°)</u>	<u>Atoms</u>	<u>Angle (°)</u>
Si Fe C1	83.9(3)	Fe Si C11	110.3(2)
Si Fe C2	85.6(3)	Fe Si C21	112.5(2)
Si Fe C3	178.0(4)	Fe Si C31	112.2(2)
Si Fe C4	85.6(3)	C11 Si C21	107.9(3)
Fe C1 O1	172.5(9)	C11 Si C31	107.2(3)
Fe C2 O2	175.9(10)	C21 Si C31	106.5(3)
Fe C3 O3	179.0(9)	Si C11 C12	120.3(3)
Fe C4 O4	178.1(9)	Si C21 C22	118.8(3)
Fe H Si	61(3)	Si C31 C32	121.8(3)
C1 Fe C2	149.8(4)	Si Fe H	82(3)
C1 Fe C3	95.2(4)	Si Fe H	36(2)
C1 Fe C4	102.4(4)	C1 Fe H	76(3)
C2 Fe C3	94.3(4)	C2 Fe H	75(3)
C2 Fe C4	104.9(5)	C3 Fe H	96(3)
C3 Fe C4	96.3(4)	C4 Fe H	168(3)

Table XXVI  
Some Non-Bonded Intramolecular Contacts

<u>Atoms</u>	<u>Distance (Å)</u>	<u>Atoms</u>	<u>Distance (Å)</u>
Si H	2.73(10)	C1 C3	2.658(14)
C1 H	2.10(9)	C1 C4	2.783(16)
C2 H	2.06(10)	C2 C3	2.616(14)
C3 H	2.57(9)	C2 C4	2.809(14)
C12 H	2.69(9)	C3 C4	2.694(14)
C11 H	2.96(9)	C11 C31	3.064(8)
Si C1	2.841(10)	C11 C21	3.078(8)
Si C2	2.872(9)	C21 C31	3.040(7)
Si C4	2.897(9)		

Table XXVII

Intermolecular Distances Less Than 4.0 Å Involving Non-Hydrogen Atoms

Atoms	Distance (Å)	Symmetry (a)	Atoms	Distance (Å)	Symmetry
02 03	3.220 (12)	1	01 C12	3.670 (9)	2
02 02	3.238 (14)	1	C2 02	3.69 (2)	1
02 C3	3.259 (13)	1	02 C14	3.715 (10)	4
02 C2	3.273 (11)	1	02 C35	3.750 (10)	8
03 C14	3.216 (10)	2	03 C14	3.752 (10)	6
04 C36	3.449 (10)	3	C32 C33	3.756 (11)	5
C1 01	3.499 (12)	2	01 C33	3.809 (9)	5
02 C13	3.461 (10)	4	01 C13	3.812 (10)	2
01 C34	3.588 (10)	5	C3 C14	3.839 (12)	2
03 C25	3.511 (10)	1	C3 C34	3.852 (11)	8
03 C15	3.568 (10)	2	03 C34	3.854 (10)	8
04 C26	3.507 (10)	3	03 C13	3.871 (11)	2
04 C15	3.526 (8)	6	C4 C14	3.878 (10)	6
04 C14	3.559 (9)	6	03 C26	3.961 (10)	1
04 C35	3.612 (11)	3	C1 C23	3.996 (11)	7
04 C25	3.635 (11)	3	C3 C14	3.959 (12)	6
01 C23	3.625 (9)	7			

(a) Symmetry position of molecule to which second atom named belongs.  
 The positions are: 1)  $\bar{x}+1 \bar{y} \bar{z}-1$  2)  $\bar{x} \bar{y}-1 \bar{z}-1$  3)  $\bar{x}+1 \bar{y} \bar{z}$  4)  $\bar{x} \bar{y} \bar{z}-1$   
 5)  $\bar{x} \bar{y}-1 \bar{z}$  6)  $\bar{x}+1 \bar{y} \bar{z}$  7)  $\bar{x} \bar{y}-1 \bar{z}$  8)  $\bar{x} \bar{y} \bar{z}-1$ .

(b) Standard deviations in parentheses refer to last digit quoted.



## DISCUSSION

A perspective drawing of  $\text{HFe}(\text{CO})_4\text{Si}(\text{C}_6\text{H}_5)_3$  is shown in Figure 9. The geometry around the iron atom can be described as a distorted octahedron with the six ligands being the four carbonyl groups, the hydridic hydrogen and the triphenylsilyl group. Around the silicon, the coordination is almost a regular tetrahedron. As can be seen, the hydrogen, which is at a normal covalent bond distance from the iron, is in a non-bridging position with respect to the silicon atom.

The silicon-phenyl bond lengths which average  $1.901 \text{ \AA}$  are slightly longer than those found in  $(\pi\text{-C}_5\text{H}_5)\text{-HMn}(\text{CO})_2\text{Si}(\text{C}_6\text{H}_5)_3$ <sup>64</sup> which average  $1.886 \text{ \AA}$ .

The distortion from tetrahedral symmetry is minimal with  $\text{Fe-Si-C}(\text{C}_6\text{H}_5)$  angles varying from  $110.3(2)^\circ$  to  $112.5(2)^\circ$  and  $\text{C}(\text{C}_6\text{H}_5)\text{-Si-C}(\text{C}_6\text{H}_5)$  from  $106.5(3)^\circ$  to  $107.9(3)^\circ$ . The phenyl rings were treated as rigid bodies throughout, with the hydrogen atoms given the same orientation and centre of gravity as the attached carbon atoms at a distance  $1 \text{ \AA}$  from them. As previously noted, the strong correlation between  $E$  and  $\xi$  in the rigid bodies was handled by fixing the value of  $E$  for the rigid body displaying the highest correlation. The implications of these correlations can be seen in the packing diagrams, Figures 10, 11

and 12 where a different phenyl ring is perpendicular to the plane of the page in each viewing direction, thus essentially defining the coordinate system. Under these conditions, satisfactory values of the derived atomic positions and their associated standard deviations were obtained as are shown in Table XXII.

The iron-carbon distances vary from 1.747(10) to 1.821(10) Å which are comparable to those in other iron carbonyls:  $\text{Fe}(\text{CO})_5$ ,<sup>67</sup> axial 1.797(15) Å, equatorial 1.842(15) Å;  $\text{Fe}_2(\text{CO})_9$ ,<sup>68</sup> 1.85(5) Å;  $\text{C}_{10}\text{H}_{10}\text{Fe}_2(\text{CO})_5$ ,<sup>69</sup> 1.741(8)-1.785(8) Å. The average iron-carbon distance is 1.78(3) Å, the estimated standard deviation being some three times the standard deviation for the individual atoms. Hence, it is likely that these bond lengths are significantly different from each other, and in fact they can be divided into two sets: Fe-C1, Fe-C2 which are trans to each other and Fe-C3, Fe-C4 which are trans to non-carbonyl groups, these being the longer set. This result is highly unusual: it is expected that carbonyls trans to other carbonyls will have the longest bonds, the so-called trans effect, as in such compounds as  $\text{HMn}(\text{CO})_5$ <sup>27</sup> where carbonyls trans to each other have a bond length of 1.836(5) Å and that trans to the hydrogen is 1.821(9) Å and  $\text{HRe}_2\text{Mn}(\text{CO})_{14}$ <sup>71</sup> where trans carbonyl bond lengths are 1.840(15) Å and nontrans 1.830(3) Å. An explanation for this discrepancy is not at all obvious

although the distortion from strict octahedral symmetry may have an influence: the three carbonyl groups cis to the silicon are inclined about  $5^\circ$  toward it ( $\widehat{\text{Se Fe Cl}} = 83.9(3)^\circ$ ,  $\widehat{\text{Si Fe C2}} = 85.6(3)^\circ$ ,  $\widehat{\text{Si Fe C4}} = 85.6(3)^\circ$  while the carbonyl groups trans to each other are greatly distorted toward the hydrogen atom ( $\widehat{\text{C}_1 \text{ Fe C2}} = 149.8(4)^\circ$ ). It is unfortunate that this potentially significant result has occurred with a data set that has undergone much correction, but the trend does appear to be real since other distances and angles seem to be free of obvious systematic error. A structural determination of the anion,  $\text{Fe}(\text{CO})_4^- \text{Si}(\text{C}_6\text{H}_5)_3^-$  would prove highly useful since first of all, being the conjugate base of a reasonably strong acid, it should be stable, and secondly the carbonyl angle distortions would be changed. If the same general pattern of carbon-iron distances were found, this would represent a rare and significant exception to the almost universal trans rule. (a)

The iron-silicon bond length of  $2.415(3) \text{ \AA}$  is consistent with that found in  $(\pi\text{-C}_5\text{H}_5)\text{HMn}(\text{CO})_2\text{Si}(\text{C}_6\text{H}_5)_3$ <sup>64</sup>

---

(a) More recent information seems to indicate that the carbonyl groups are exchanging with each other, that is that the molecule is fluxional, in which case the above arguments concerning the trans effect would not be meaningful.

(Mn-Si = 2.424(2) Å) if one considers the decrease in metal iron radius with increasing atomic number in going from manganese to iron. It is somewhat shorter than the single bond length of 2.51 Å predicted on the basis of covalent radii (1.17 Å<sup>60a</sup> for silicon and 1.34 Å<sup>70</sup> for iron) which may suggest some double bond character between silicon and iron.

The most interesting aspects of this crystal structure determination involve the position of the hydridic hydrogen atom. Using the most reliable position for it (as determined from an electron density difference map limited to  $\sin\theta/\lambda \leq 0.35$ ), the hydridic hydrogen atom is located 1.56 Å from the iron atom and 2.63 Å from the silicon atom. As was mentioned in the introduction, the similarity of this compound to  $(\pi\text{-C}_5\text{H}_5)\text{HMn}(\text{CO})_2\text{Si}(\text{C}_6\text{H}_5)_3$  led to the expectation of a hydrogen atom weakly bonded to silicon, an expectation which has not been realized. Hutcheon's rationalization of the hydrogen-silicon interaction was electrostatic: if the substituents on silicon were electronegative (for example chlorine) then electrostatic repulsion prevented the weak H-Si bond from forming; with electropositive substituents (phenyl, for example), the weak interaction could occur. Hence the prediction of weak hydrogen silicon interaction in this structure. But with the finding that the hydrogen is not bridged here,

a careful examination of the two structures was made which revealed a possible explanation for when hydrogen-silicon interaction will occur. The only significant difference appears to be in the highly crowded environment of the manganese structure. It is necessary for the hydrogen atom to move closer to the silicon atom in order to prevent close contact of the carbonyl carbon atoms in the manganese case (as it is,  $\widehat{\text{C Mn C}} = 88.7(3)^\circ$ ). In the iron compound, no such steric crowding occurs with the  $\widehat{\text{C Fe C}}$  angles all greater than  $90^\circ$ . So no interaction between silicon and hydrogen is required.

CHAPTER 5

The Crystal and Molecular Structure of  
 $(\pi\text{-C}_5\text{H}_5)\text{HMn}(\text{CO})_2\text{SiCl}_2(\text{C}_6\text{H}_5)$

## INTRODUCTION

Following the completion of the crystal structure determinations of  $(\pi\text{-C}_5\text{H}_5)\text{HMn}(\text{CO})_2\text{Si}(\text{C}_6\text{H}_5)_3$ <sup>64</sup> in which the hydridic hydrogen is bonded weakly to the silicon atom ( $\text{Si-H} = 1.76(4) \text{ \AA}$ ) as well as to the manganese atom, and of  $\text{HFe}(\text{CO})_4\text{Si}(\text{C}_6\text{H}_5)_3$ <sup>(a)</sup> in which the hydrogen has no interaction with the silicon atom, it was realized that the most probable cause of weak silicon hydrogen interaction was steric hindrance: in the presence of a cyclopentadienyl ring, steric crowding forces the hydrogen into closer contact with the silicon atom. A further test of this hypothesis is provided by the compound whose structure is the subject of this chapter: hydridodichlorophenylsilyl( $\pi$ -cyclopentadienyl)dicarbonyl manganese  $(\pi\text{-C}_5\text{H}_5)\text{HMn}(\text{CO})_2\text{SiCl}_2(\text{C}_6\text{H}_5)$ . It should be just as crowded as  $(\pi\text{-C}_5\text{H}_5)\text{HMn}(\text{CO})_2\text{Si}(\text{C}_6\text{H}_5)_3$  and should have the same weak silicon-hydrogen interaction in spite of the apparently unfavorable electro-negative nature of the chlorine substituents of silicon.

At the same time, the infrared data could be shown to be non-predictive for hydrogen-silicon interaction. Although  $(\pi\text{-C}_5\text{H}_5)\text{HMn}(\text{CO})_2\text{SiCl}_3$  shows a Mn-H stretch at  $1890 \text{ cm}^{-1}$  and  $(\pi\text{-C}_5\text{H}_5)\text{HMn}(\text{CO})_2\text{Si}(\text{C}_6\text{H}_5)_3$  does not (although there is a weak band in the Raman), both are expected to

---

(a) This work, Chapter 4.

have the same form of silicon-hydrogen interaction on the basis of steric crowding. As previously noted nothing can be said for  $\text{H}(\text{CO})_4\text{FeSi}(\text{C}_6\text{H}_5)_3$  where the important region is obscured by the carbonyl stretches. In  $(\pi\text{-C}_5\text{H}_5)\text{HMn}(\text{CO})_2\text{SiCl}_2(\text{C}_6\text{H}_5)$  there is a Mn-H stretch at  $1895\text{ cm}^{-1}$ . A clear-cut solution to the confusing infrared evidence could have come from a study of the deuterium substituted compounds which would have M-D stretches in the relatively empty region around  $1300\text{ cm}^{-1}$ . Unfortunately this study has not yet been carried out, so it is not possible to see if changes in metal-hydrogen stretching intensities can be correlated to changes in the silicon substituents.



## EXPERIMENTAL

Crystals of hydridodichlorophenylsilyl( $\pi$ -cyclopentadienyl)dicarbonyl manganese,  $(\pi\text{-C}_5\text{H}_5)\text{HMn}(\text{CO})_2\text{Si}(\text{C}_6\text{H}_5)\text{Cl}_2$  were supplied by A. Hart-Davis in a form suitable for X-ray diffraction work. They were prepared by ultraviolet irradiation of  $(\pi\text{-C}_5\text{H}_5)\text{Mn}(\text{CO})_3$  in the presence of excess phenyldichlorosilane and were recrystallized from pentane.<sup>38</sup> Preliminary photography did not reveal any systematic absences or symmetry other than  $\bar{1}$  thus indicating a triclinic cell which could belong to space group P1 or  $P\bar{1}$ .  $P\bar{1}$  was assumed, and this was later confirmed by an analysis of the statistical distribution of  $E(\text{hkl})$  values (Table XXIX). Precise cell constants were determined from a least squares analysis of 21 reflections (as described in Appendix C) as  $a = 10.995(1)$  Å,  $b = 8.171(1)$  Å,  $c = 8.486(1)$  Å,  $\alpha = 98.25(1)^\circ$ ,  $\beta = 98.06(1)^\circ$ ,  $\gamma = 100.26(1)^\circ$  at  $22^\circ\text{C}$  ( $K_{\alpha 1} \lambda = 1.54051$  Å). The density as determined by flotation using aqueous zinc iodide was 1.50 gm/cc which agrees well with that calculated (1.490 gm/cc) for two molecules per unit cell, a molecular weight of 353.15 and a unit cell volume of  $786.72$  Å<sup>3</sup>. The crystals were slightly sensitive to moisture, but coating with shellac and storing in a desiccator were sufficient to prevent any apparent decomposition over a period of months.

The dimensions and habit of the crystal used for data collection are shown below. The crystal was mounted with the  $a^*$  axis coincident with the  $\phi$  axis of the diffractometer, and data out to  $42^\circ$  in  $2\theta$  was collected (the limit observed on the Weissenberg films) using  $\text{MoK}_\alpha$  radiation to minimize absorption. The peak scan range was  $2^\circ$  with stationary background readings counted for twenty seconds on each side of the peak scan. Seven well distributed standard reflections measured at various times throughout the data collection indicated no decomposition of the crystal. The maximum variation was about  $\pm 3v$ ,

$$\left( v = \sqrt{\frac{\sum (I_m - I_o)^2}{m}} \right. \quad \left. \begin{array}{l} \text{where } m \text{ was the number of observations} \\ \text{of intensity and } I_o \text{ was the average of} \\ \text{these } I_m \end{array} \right)$$

with no apparent pattern in the peak height values. Absorption corrections ( $\mu = 12.9 \text{ cm}^{-1}$ ) were applied to the data with the transmission factors ranging from 0.921 to 0.935. The appropriateness of these corrections was confirmed by the agreement of the  $\phi$  scan data ( $h00$ ,  $h=2,5$ ,  $\phi = 0-180^\circ$  in  $10^\circ$  steps) after correction. Of 1524 independent reflections measured, 968 were considered to be significantly above background using a criterion  $I/\sigma(I) \leq 3.0$  with a  $p$  value of 0.03 as described in the crystallographic introduction.

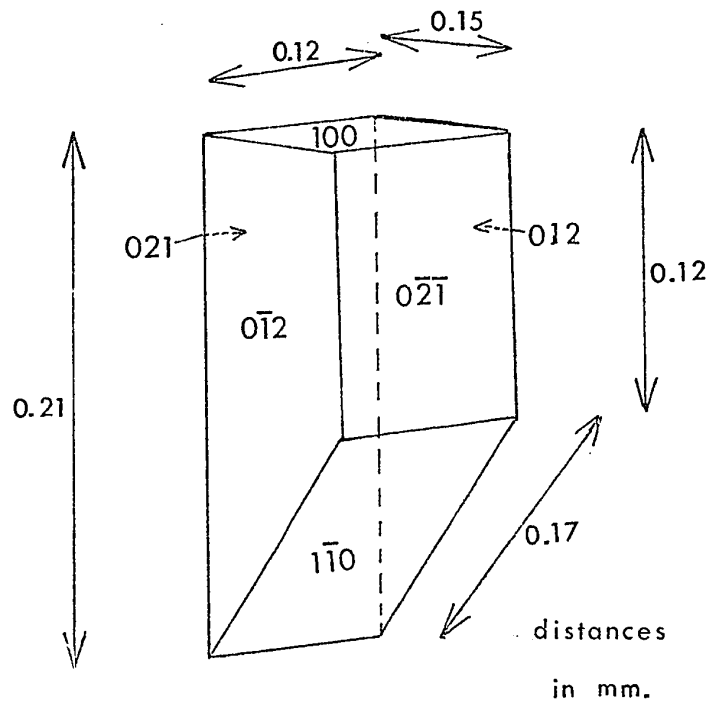


Table XXIX

Statistical Distribution of  $E(hk\ell)$ 's (a):  $(\pi-C_5H_5)HMn(CO)_2SiCl_2(C_6H_5)$ 

Quantity	Observed	Theoretical Centric	Theoretical Acentric
Average magnitude of $E(hk\ell)$ 's	0.806	0.798	0.886
Average of $E(hk\ell)^2$	1.000	1.000	1.000
Average of $ E(hk\ell)^2 - 1 $	0.933	0.968	0.736
Percent $E(hk\ell)$ 's greater than one	33.81	32.00	37.00
Percent $E(hk\ell)$ 's greater than two	4.07	5.00	1.80
Percent $E(hk\ell)$ 's greater than three	0.07	0.30	0.01

$$(a) E(hk\ell) \text{ defined by the formula } E(hk\ell)^2 = \frac{|F(hk\ell)|^2}{\epsilon \sum f_j^2}$$

where  $\epsilon$  accounts for the systematic absences in the data.

## SOLUTION AND REFINEMENT

The structure solution and refinement was straight forward with the manganese, silicon and chlorine atoms located from a Patterson map and the remaining atoms from electron density difference maps. With just the four heavy atoms in place,  $R_1 = 0.33$  and  $R_2 = 0.41$ . An electron density difference map phased on these four atoms revealed the carbonyl groups whose addition gave  $R_1 = 0.24$  and  $R_2 = 0.32$ . The remaining non-hydrogen atoms were found on a difference map phased on these eight atoms. After several cycles in which the heavy atoms were anisotropic and had anomalous dispersion corrections applied to their scattering factors ( $\Delta f'_{\text{Mn}} = 0.3$ ,  $\Delta f''_{\text{Mn}} = 0.85$ ,  $\Delta f'_{\text{Si}} = 0.10$ ,  $\Delta f''_{\text{Si}} = 0.10$ ,  $\Delta f'_{\text{Cl}} = 0.10$ ,  $\Delta f''_{\text{Cl}} = 0.20$ ),<sup>9</sup> the carbonyls were isotropic, the phenyl carbon ring was a rigid body and the cyclopentadienyl carbon ring was a hindered rotor,<sup>13</sup>  $R_1 = 0.073$  and  $R_2 = 0.084$ . The initial parameters for the rings were calculated using the program MMMR with a radius of  $1.395 \text{ \AA}$  for the rigid body and  $1.20 \text{ \AA}$  for the hindered rotor.

The hydrogen atoms were located on an electron density difference map with peak heights ranging from 0.47 to  $0.29 \text{ e/\AA}^3$ . The phenyl hydrogens were added as a rigid body having the same orientation and centre of gravity as

the phenyl carbon ring and with a C-H distance of 1 Å, while the cyclopentadienyl hydrogens were added as a hindered rotor similarly riding on the cyclopentadienyl carbon ring. The second largest peak on this map, 0.44 e/Å<sup>3</sup> (x = 0.150, y = -0.345, z = -0.307) was between the manganese and silicon atoms in a position similar to that of the hydridic hydrogen in  $(\pi\text{-C}_5\text{H}_5)\text{HMn}(\text{CO})_2\text{Si}(\text{C}_6\text{H}_5)_3$ .<sup>64</sup> After four cycles in which the positional and thermal parameters of all individual atoms and of the carbon rings and the centre of gravity parameters of the cyclopentadienyl hydrogen ring were refined,  $R_1 = 0.041$  and  $R_2 = 0.047$ . A difference map showed that the peak between the silicon and manganese atoms was the largest with a peak height of 0.49 e/Å<sup>3</sup>. It was of similar density to that found by Ibers<sup>29</sup> et al in the structure of  $\text{HCo}(\text{N}_2)(\text{P}(\text{C}_6\text{H}_5)_3)_3$ . To further check the validity of this apparent hydride peak, difference maps were calculated using various  $\sin\theta/\lambda$  data cutoffs ( $\sin\theta/\lambda \leq 0.35, \leq 0.30, \leq 0.25, \leq 0.20$ ). On each map the largest peak was the hydride, it being greater than the next largest peak by a factor of at least two. The peak positions and their heights as well as the height calculated by evaluating the integral

$$\rho_{\text{H}}^{\text{c}} = \frac{1}{2\pi} \int_0^{s_0} (1 + \frac{a^2 s^2}{4})^{-2} \exp(-Bs^2/16\pi^2) s^2 ds$$

where  $s_0$  is the  $\sin\theta$  limit,  $a$  is the Bohr radius, and  $B$  the

isotropic temperature factor as described by La Placa and Ibers,<sup>66</sup> are given in Table XXX. Subsequently, then, this hydridic hydrogen was added as an isotropic atom and allowed to refine. The final R values were  $R_1 = 0.040$  and  $R_2 = 0.044$  obtained with all non-ring, non-hydrogen atoms anisotropic, with the phenyl ring as a rigid body, the cyclopentadienyl ring as a hindered rotor and the hydridic hydrogen as an isotropic atom.

A final difference map computed with all atoms as described above showed a peak range of  $-0.29$  to  $0.34 \text{ e}/\text{\AA}^3$ . At the completion of refinement, no parameter shifted more than one half of an estimated standard deviation, and the standard deviation for an observation of unit weight was 1.259.

Table XXXI lists the observed and calculated structure factor amplitudes,  $10|F_o|$  and  $10|F_c|$  both in absolute units of electrons. The final positional and thermal parameters for the individual atoms are given in Table XXXII. Parameters for the rigid bodies and hindered rotors are found in Table XXXIII while the derived individual atom positions are to be found in Table XXXIV. The estimated standard deviations were obtained from the inverse matrix of the final least squares cycle. Slant Fourier maps were calculated through the planes of the phenyl and cyclopentadienyl rings and are shown in Figures

13 and 14 respectively.



Table XXX

Hydrogen Peak as a Function of  $\sin\theta/\lambda$ 

$\sin\theta/\lambda$ Cut Off Å <sup>-1</sup>	Number of Terms in the Unique Section	Calculated <sup>66</sup> Height (b)	Observed Height	Position			Distance (Å)	
				$\underline{x}$	$\underline{y}$	$\underline{z}$	Mn-H	Si-H
0.20	86	0.16	0.15	0.157	-0.356	-0.326	1.44	1.75
0.25	172	0.24	0.28	0.149	-0.358	-0.325	1.45	1.79
0.30	283	0.32	0.35	0.141	-0.351	-0.324	1.44	1.78
0.35	431	0.39	0.41	0.148	-0.362	-0.326	1.48	1.81
0.439 (a)	968	0.49	0.49	0.147	-0.354	-0.314	1.38	1.85

(a) Full data set.

$$(b) \rho_H^C = \frac{1}{2\pi} \int_0^S (1 + a^2 s^2/4)^{-2} \exp(-Bs^2/16\pi^2) s^2 ds$$

$$s = 4\pi \sin\theta/\lambda \quad a = \text{Bohr's Radius} \quad B = 4.25$$

Evaluated using Simpson's Rule with 20 intervals.

Table XXXI

Observed and Calculated Structure Factor Amplitudes  
 $10|F_o|$  and  $10|F_c|$

111a.

K	L	FOBS	FCAL	K	L	FOBS	FCAL	K	L	FOBS	FCAL	K	L	FOBS	FCAL	K	L	FOBS	FCAL
4	4	252	256	3	4	134	126	2	0	260	243	-1	2	60	47	-4	1	112	109
4	5	92	83	3	6	176	110	2	1	92	80	-1	3	163	181	-4	2	139	112
4	6	98	97	3	7	150	141	2	2	143	137	-1	6	162	153	-4	3	356	363
5	3	236	227	4	-4	249	262	2	3	128	114	0	-8	173	171	-3	6	301	294
5	4	93	106	4	-3	410	408	2	4	314	312	0	-6	164	181	-3	-6	165	173
5	5	198	192	4	-2	321	305	2	7	172	168	0	-5	132	123	-3	-4	157	154
6	4	90	89	4	-1	453	433	3	-8	196	204	0	-3	567	563	-3	-3	248	239
7	1	83	87	4	0	555	555	3	-8	196	188	0	-2	330	327	-3	-2	160	152
7	3	122	126	4	1	128	136	3	-4	291	286	0	-1	397	388	-3	-1	479	465
8	0	112	120	4	4	233	240	3	-3	465	480	0	0	657	653	-3	0	166	165
				4	5	214	205	3	-2	201	207	0	1	568	575	-3	1	242	239
				5	-6	185	189	3	-1	228	220	0	2	476	485	-3	3	456	459
				5	-5	155	143	3	0	565	552	0	3	495	502	-3	4	360	348
				5	-3	343	343	3	1	162	154	0	4	256	248	-3	5	110	94
				5	-2	214	230	3	3	200	201	0	6	244	252	-3	7	187	188
				5	-1	164	163	3	6	130	127	1	-8	139	156	-2	-5	104	101
				5	0	137	131	4	-7	106	83	1	-5	243	232	-2	-4	270	260
				5	1	93	84	4	-6	141	124	1	-4	131	126	-2	-3	274	271
				5	2	117	104	4	-5	89	98	1	-3	282	301	-2	-2	127	122
				5	4	134	115	4	-2	226	221	1	-2	70	62	-2	0	121	114
				6	-6	110	113	4	1	353	363	1	-1	77	61	-2	1	293	290
				6	-5	115	134	4	3	272	273	1	0	257	264	-2	2	220	218
				6	-4	94	65	4	4	346	330	1	1	625	621	-2	6	276	269
				6	-3	208	207	5	-6	140	146	1	0	270	264	-1	-8	96	96
				6	0	197	194	5	-4	185	178	1	4	512	523	-1	-7	162	169
				6	1	193	196	5	-3	274	274	1	5	131	129	-1	-5	181	187
				6	4	133	149	5	-2	132	136	1	6	81	81	-1	-4	483	490
				7	-3	140	129	5	-1	87	90	1	7	141	143	-1	-3	146	139
				7	-2	106	101	5	0	105	106	2	-6	219	213	-1	-2	821	787
				7	0	128	150	5	1	351	355	2	-7	118	121	-1	-1	74	94
				7	1	136	135	5	2	235	250	2	-6	133	127	-1	0	386	384
								5	4	117	140	2	-5	124	147	-1	2	296	289
								5	5	202	191	2	-3	244	246	-1	3	568	585
								6	-4	352	363	2	-2	303	297	-1	4	550	575
								6	-1	311	322	2	-1	523	516	-1	5	81	92
								6	1	119	116	2	0	224	226	-1	7	101	105
								6	2	95	100	2	2	290	290	0	-7	179	166
								6	4	149	141	2	3	204	216	0	-6	241	242
								7	-4	207	203	2	4	257	261	0	-4	463	467
								7	-3	194	207	2	5	178	168	0	-3	441	461
								7	0	138	157	3	-7	220	213	0	-2	120	127
												3	-5	88	106	0	0	196	197
												3	-4	703	701	0	1	757	744
												3	-3	407	388	0	2	76	69
												3	-2	165	155	0	3	197	219
												3	-1	405	405	1	-8	102	76
												3	1	419	417	1	-6	142	149
												3	2	66	69	1	-4	460	461
												3	4	241	244	1	-3	176	163
												3	6	96	93	1	-2	210	205
												4	-7	142	163	1	-1	594	590
												4	-6	287	281	1	0	266	268
												4	-4	213	212	1	1	491	482
												4	-3	410	424	1	2	74	80
												4	0	393	385	1	3	295	284
												4	1	88	92	1	4	297	297
												4	2	89	91	1	5	146	148
												4	3	247	244	2	-8	125	120
												4	5	82	80	2	-7	185	188
												5	-6	101	95	2	-6	132	144
												5	-4	230	237	2	-5	99	102
												5	-1	91	70	2	-4	388	395
												5	0	110	113	2	-3	265	260
												5	1	275	278	2	-1	255	254
												5	4	137	143	2	0	145	150
												6	-6	179	161	2	1	248	240
												6	-3	157	132	2	2	133	139
												6	-2	168	169	2	3	350	356
												6	0	162	142	2	6	208	213
												6	1	90	73	3	-8	114	123
												6	3	129	125	3	-6	173	172
												7	-4	151	197	3	-5	170	167
												7	1	243	242	3	-4	98	116
																3	-3	326	321
																3	-2	178	182
																3	0	412	415
																3	1	398	399
																3	2	209	195
																3	3	445	441
																3	4	197	207
																3	5	86	60
																4	-7	220	215
																4	-4	212	214
																4	-3	77	70
																4	-2	254	258
																4	0	132	129
																4	1	415	413
																4	4	153	145
																5	-5	176	167
																5	-4	92	93
																5	-3	164	176
																5	-2	118	117
																5	-1	82	95
																5	0	136	126
																6	-4	299	293
																6	-3	131	134
																6	-1	124	122
																6	1	87	69

K	L	FORS	FCAL	K	L	FORS	FCAL	K	L	FORS	FCAL	K	L	FORS	FCAL	K	L	FORS	FCAL
7	0	201	201	3	-3	229	225	2	-3	195	211	1	1	75	85	-5	-1	251	254
***H = 4****																			
-7	-3	101	115	3	-2	97	113	2	-1	255	259	1	2	161	154	-5	2	104	99
-7	0	143	139	3	0	280	277	2	0	545	542	1	3	105	107	-4	-5	150	145
-7	3	136	142	3	2	226	223	2	1	251	251	1	4	127	137	-4	-4	83	77
-7	4	112	125	3	3	221	226	2	5	42	95	1	5	129	129	-4	-3	171	173
-6	-4	159	156	4	-7	103	100	3	-7	261	262	2	-7	206	194	-4	0	183	152
-6	-1	337	346	4	-6	98	96	3	-6	156	159	2	-4	260	264	-4	1	105	114
-6	0	95	88	4	-4	120	126	3	-3	291	287	2	-3	173	170	-4	2	159	123
-6	2	116	125	4	-3	321	310	3	-2	267	264	2	-2	99	107	-4	3	126	120
-5	-5	144	141	4	-2	243	252	3	0	108	198	2	-1	350	375	-3	-4	120	123
-5	-3	163	173	4	-1	155	171	3	1	229	243	2	0	160	164	-3	-1	350	344
-5	-2	92	89	4	0	365	373	3	3	85	75	2	2	210	218	-3	0	113	88
-5	-1	158	139	4	1	266	263	3	4	196	190	2	4	237	235	-3	2	123	117
-5	0	105	116	4	3	148	134	4	-5	190	196	3	-4	192	186	-2	-5	125	103
-5	3	375	376	5	-5	177	163	4	-3	158	149	3	-3	383	367	-2	-4	118	126
-5	4	101	92	5	-2	179	177	4	-2	219	225	3	-1	216	229	-2	-3	310	312
-5	5	114	111	5	-1	157	163	4	-1	98	93	3	0	274	268	-2	-1	210	224
-5	6	228	232	5	0	142	138	4	0	264	270	3	3	131	126	-2	0	252	260
-4	-1	295	289	5	1	127	115	4	1	128	98	4	-6	137	135	-2	3	167	154
-4	-1	202	187	5	2	87	95	4	4	155	135	4	-3	140	125	-1	-6	119	148
-4	-1	253	263	5	3	99	74	5	-5	93	77	4	-1	121	112	-1	-3	170	163
-4	-1	297	300	6	-3	287	288	5	-4	133	137	4	0	143	143	-1	-1	232	231
-4	3	160	155	6	0	194	199	5	-3	218	191	4	1	156	160	-1	0	85	67
-4	4	348	354	**H = 5****				5	-2	120	113	4	3	111	106	-1	1	161	152
-4	7	155	143	-7	-2	172	166	5	0	95	97	5	-4	90	72	-1	3	192	176
-3	-6	109	111	-6	-4	206	207	5	2	170	191	5	-3	89	111	-1	4	267	276
-3	-5	110	114	-6	-2	202	196	6	-4	155	145	5	-2	85	82	0	-4	352	354
-3	-4	193	169	-6	-1	104	102	6	-3	161	152	5	-1	94	69	0	-3	138	141
-3	-3	318	317	-6	0	108	99	6	-1	294	296	5	0	130	160	0	-2	75	57
-3	-2	347	344	-6	1	112	103	6	0	166	161	**H = 7****				0	-1	108	93
-3	0	95	99	-6	2	83	56	**H = 6****				-6	-1	215	203	0	0	80	41
-3	1	229	215	-6	3	114	113	-7	0	130	123	-6	2	164	163	0	1	278	239
-3	2	103	112	-5	-4	194	204	-7	1	160	166	-6	3	145	144	0	2	106	109
-3	3	261	273	-5	-3	172	184	-6	-2	210	216	-5	-3	123	143	0	4	129	131
-3	4	92	85	-5	-1	282	285	-6	0	108	110	-5	-1	243	233	1	-6	124	105
-3	5	96	90	-5	0	243	246	-6	1	92	105	-5	0	352	346	1	-5	130	146
-2	-7	175	166	-5	2	200	198	-6	2	170	177	-5	1	88	115	1	-4	169	159
-2	-5	79	90	-5	3	261	276	-6	3	230	227	-5	2	164	161	1	-2	201	194
-2	-4	509	512	-5	5	93	123	-6	4	84	65	-5	3	236	230	1	-1	264	292
-2	-3	113	128	-4	-6	135	138	-5	-5	149	131	-4	-3	85	110	1	3	195	192
-2	-2	325	314	-4	-4	164	160	-5	-4	193	190	-4	-2	152	146	1	4	88	109
-2	-1	594	590	-4	-3	114	130	-5	-1	110	106	-4	-1	105	106	2	-4	286	278
-2	0	155	165	-4	-1	94	79	-5	0	228	246	-4	0	138	135	2	-3	234	247
-2	1	387	385	-4	0	369	368	-5	1	145	147	-4	1	167	157	2	-1	152	174
-2	2	274	283	-4	1	407	407	-5	2	91	93	-4	2	120	135	2	1	117	103
-2	4	210	208	-4	3	367	373	-5	3	168	168	-4	3	166	78	3	0	92	73
-2	6	91	104	-4	4	199	179	-4	-3	134	136	-4	4	100	97	3	1	94	104
-2	7	82	61	-3	-7	109	125	-4	-2	203	220	-3	-6	169	166	**H = 9****			
-1	-0	134	124	-3	-5	85	82	-4	-1	79	75	-3	-5	158	168	-5	-3	115	129
-1	-7	208	213	-3	-4	165	170	-4	0	227	224	-3	-3	131	130	-5	0	170	160
-1	-6	219	211	-3	-2	593	565	-4	2	139	125	-3	-2	126	135	-4	-1	235	229
-1	-5	120	121	-3	-1	175	170	-4	3	294	300	-3	-1	107	121	-4	1	150	158
-1	-4	261	254	-3	1	302	302	-4	4	152	148	-3	0	208	202	-4	3	109	108
-1	-3	322	332	-3	2	132	129	-3	-5	149	155	-3	3	122	127	-3	-5	144	152
-1	-2	252	245	-3	3	137	135	-3	-4	301	290	-3	4	152	140	-3	-2	205	213
-1	-1	128	133	-3	4	96	86	-3	-3	85	113	-3	5	105	120	-3	1	149	142
-1	0	435	427	-2	-5	297	289	-3	-1	81	71	-2	-4	167	164	-3	3	193	205
-1	1	190	189	-2	-4	427	402	-3	0	370	369	-2	-3	113	136	-2	-5	179	130
-1	2	86	90	-2	-3	260	255	-3	1	147	152	-2	-1	222	215	-2	-4	291	292
-1	3	375	362	-2	-2	309	317	-3	2	257	257	-2	2	280	284	-2	-1	268	250
-1	4	254	252	-2	-1	61	83	-3	5	187	189	-2	4	130	132	-2	1	107	94
-1	5	86	121	-2	0	433	433	-2	-7	131	139	-1	-7	112	92	-2	3	86	101
-1	6	227	238	-2	1	110	110	-2	-4	142	141	-1	-6	101	76	-1	-5	100	72
0	-7	237	246	-2	3	405	404	-2	-3	173	173	-1	-5	100	101	-1	-4	102	118
0	-4	499	503	-2	5	269	222	-2	-2	216	207	-1	-4	328	316	-1	-3	122	130
0	-3	253	258	-1	-7	290	295	-2	-1	421	424	-1	-3	362	358	-1	-1	101	92
0	-2	137	143	-1	-6	92	81	-2	0	518	522	-1	-2	163	118	-1	0	83	87
0	0	769	759	-1	-5	221	222	-2	1	111	108	-1	-1	290	296	-1	3	156	140
0	1	547	547	-1	-4	511	515	-2	2	357	358	-1	0	465	468	0	-4	88	104
0	2	191	191	-1	-3	97	81	-2	3	310	311	-1	3	101	105	0	-2	104	116
0	3	524	538	-1	-1	305	300	-1	-6	123	100	-1	4	211	216	0	-1	91	76
0	4	300	300	-1	1	274	275	-1	-5	90	99	-1	5	159	162	0	0	112	112
0	7	91	71	-1	2	327	342	-1	-3	319	321	0	-6	275	276	0	3	84	65
1	-5	234	224	-1	3	120	115	-1	-2	187	174	0	-1	150	165	1	-4	134	107
1	-4	119	102	-1	4	244	265	-1	-1	212	204	0	0	135	150	2	-4	177	166
1	-2	714	709	0	-7	162	153	-1	0	441	441	0	1	88	80	2	0	137	150
1	-1	122	119	0	-6	119	129	-1	1	276	290	0	2	109	195	2	1	153	147
1	0	326	345	0	-5	283	287	-1	3	190	190	0	3	138	123	3	-2	105	87
1	1	306	300	0	-3	280	281	-1	5	144	150	0	4	103	117	**H = 10****			
1	2	81	90	0	-2	232	229	-1	6	130	140	0	-4	273	269	-4	-2	121	128
1	3	313	307	0	-1	172	175	0	-7	155	146	1	-3	182	193	-4	-1	110	108
1	4	93	120	0	0	558	563	0	-4	167	170	1	-1	439	460	-4	0	146	139
2	-8	140	150	0	2	177	191	0	-3	145	130	1	0	108	118	-3	-1	122	129
2	-7	255	260	0	3	194	196	0	-2	250	253	1	1	253	256	-3	1	104	86
2	-6	133	126	0	4	82	75	0	-1	262	264	1	4	218	220	-3	2	111	96

Table XXXII  
Final Coordinate and Thermal Parameters (a)

Atom	X	Y	Z	$\beta_{11}$ (b)	$\beta_{22}$	$\beta_{33}$	$\beta_{12}$	$\beta_{13}$	$\beta_{23}$	$\frac{\sigma^2}{\text{Å}^2}$ (c)
Mn	0.2039(1)	-0.2308(1)	-0.1830(1)	95.1(15)	149.0(26)	110.2(22)	37.0(15)	29.0(13)	23.7(18)	3.60
Si	0.1969(1)	-0.2104(3)	-0.4527(2)	85.1(25)	143.3(45)	111.9(37)	25.2(27)	20.1(25)	34.2(32)	3.45
Cl1	0.017(2)	-0.2769(3)	-0.5955(2)	71.7(22)	240.0(50)	140.0(37)	24.0(26)	9.0(23)	54.4(33)	4.36
Cl2	0.2481(2)	0.0425(2)	-0.4799(2)	131.4(27)	121.6(40)	185.0(42)	28.6(26)	44.2(27)	50.7(32)	4.57
Cl	0.3632(8)	-0.1508(10)	-0.1871(9)	91(11)	162(18)	168(17)	29(11)	20(11)	14(13)	4.29
O1	0.4665(6)	-0.0962(7)	-0.1861(7)	93(7)	232(14)	217(12)	9(8)	20(8)	16(10)	5.51
C2	0.2427(7)	-0.4250(11)	-0.1434(9)	108(10)	178(19)	124(15)	28(11)	10(9)	39(14)	4.25
O2	0.2654(6)	-0.5532(8)	-0.1216(7)	177(9)	196(14)	259(14)	71(9)	13(8)	85(11)	6.51
H	0.143(5)	-0.359(8)	-0.328(7)	-	-	-	-	-	-	4.33

(a) Standard deviations in parentheses refer to last digit quoted.

(b) Anisotropic temperature factors  $\times 10^4$  defined by  $\exp[-(\beta_{11}h^2 + \beta_{22}k^2 + \beta_{33}l^2 + 2\beta_{12}hk + 2\beta_{13}hl + 2\beta_{23}kl)]$ .

(c) Equivalent isotropic thermal parameter.

Table XXXIII  
Rigid Body and Hindered Rotor Parameters

Ring	$\bar{x}$	$\bar{y}$	$\bar{z}$	$\bar{B}$	$\bar{B}_d$	$\bar{R}$	$\bar{D}$	$\bar{E}$	$\bar{E}$
Phenyl carbon	0.3667(3)	-0.4198(4)	-0.6591(4)	-	-	1.395	0.079(3)	0.735(3)	2.434(3)
Phenyl hydrogen	0.3667(a)	-0.4198	-0.6593	-	-	2.395	0.079	0.736	3.482
Cyclopenta-dienyl carbon	0.1116(4)	-0.1227(5)	-0.0660(5)	4.24(11)	1.22(6)	1.206	3.808(4)	2.373(5)	2.023(7)
Cyclopenta-dienyl hydrogen	0.124(4)	-0.133(5)	-0.074(5)	4.38	1.24	2.206	3.805	2.375	2.022

(a) Parameters for which no estimated errors are given were not refined.

Table XXXIV

Thermal and Derived Positional Parameters for  
Rigid Bodies and Hindered Rotors

Ring	Atom	$\bar{x}$	$\bar{y}$	$\bar{z}$	$\bar{B}$
1 phenyl carbon	C <sub>11</sub>	0.2975 (4)	-0.3269 (6)	-0.5689 (5)	3.18 (15)
	C <sub>12</sub>	0.2729 (4)	-0.5026 (6)	-0.5869 (4)	4.48 (18)
	C <sub>13</sub>	0.3422 (5)	-0.5956 (4)	-0.6772 (6)	5.13 (20)
	C <sub>14</sub>	0.4359 (5)	-0.5127 (6)	-0.7494 (5)	5.01 (19)
	C <sub>15</sub>	0.4605 (4)	-0.3369 (6)	-0.7314 (4)	5.39 (20)
	C <sub>16</sub>	0.3913 (5)	-0.2440 (4)	-0.6411 (6)	4.71 (18)
2 phenyl hydrogen	H <sub>12</sub>	0.206	-0.561	-0.535	5.2
	H <sub>13</sub>	0.324	-0.721	-0.690	5.8
	H <sub>14</sub>	0.485	-0.580	-0.814	5.7
	H <sub>15</sub>	0.528	-0.278	-0.784	6.0
	H <sub>16</sub>	0.409	-0.118	-0.629	5.3
3 cyclopenta- dienyl carbon	C <sub>21</sub>	0.1034 (8)	-0.2304 (8)	0.0176 (10)	
	C <sub>22</sub>	0.1988 (5)	-0.0829 (11)	0.0446 (5)	
	C <sub>23</sub>	0.1738 (7)	0.0096 (6)	-0.0812 (10)	
	C <sub>24</sub>	0.0628 (7)	-0.0808 (11)	-0.1850 (8)	
	C <sub>25</sub>	0.0193 (5)	-0.2291 (8)	-0.1249 (7)	
4 cyclopenta- dienyl hydrogen	H <sub>21</sub>	0.109 (4)	-0.330 (5)	0.079 (5)	
	H <sub>22</sub>	0.284 (4)	-0.060 (5)	0.128 (5)	
	H <sub>23</sub>	0.237 (4)	0.110 (5)	-0.101 (5)	
	H <sub>24</sub>	0.034 (4)	-0.056 (5)	-0.293 (5)	
	H <sub>25</sub>	-0.045 (4)	-0.328 (5)	-0.181 (5)	

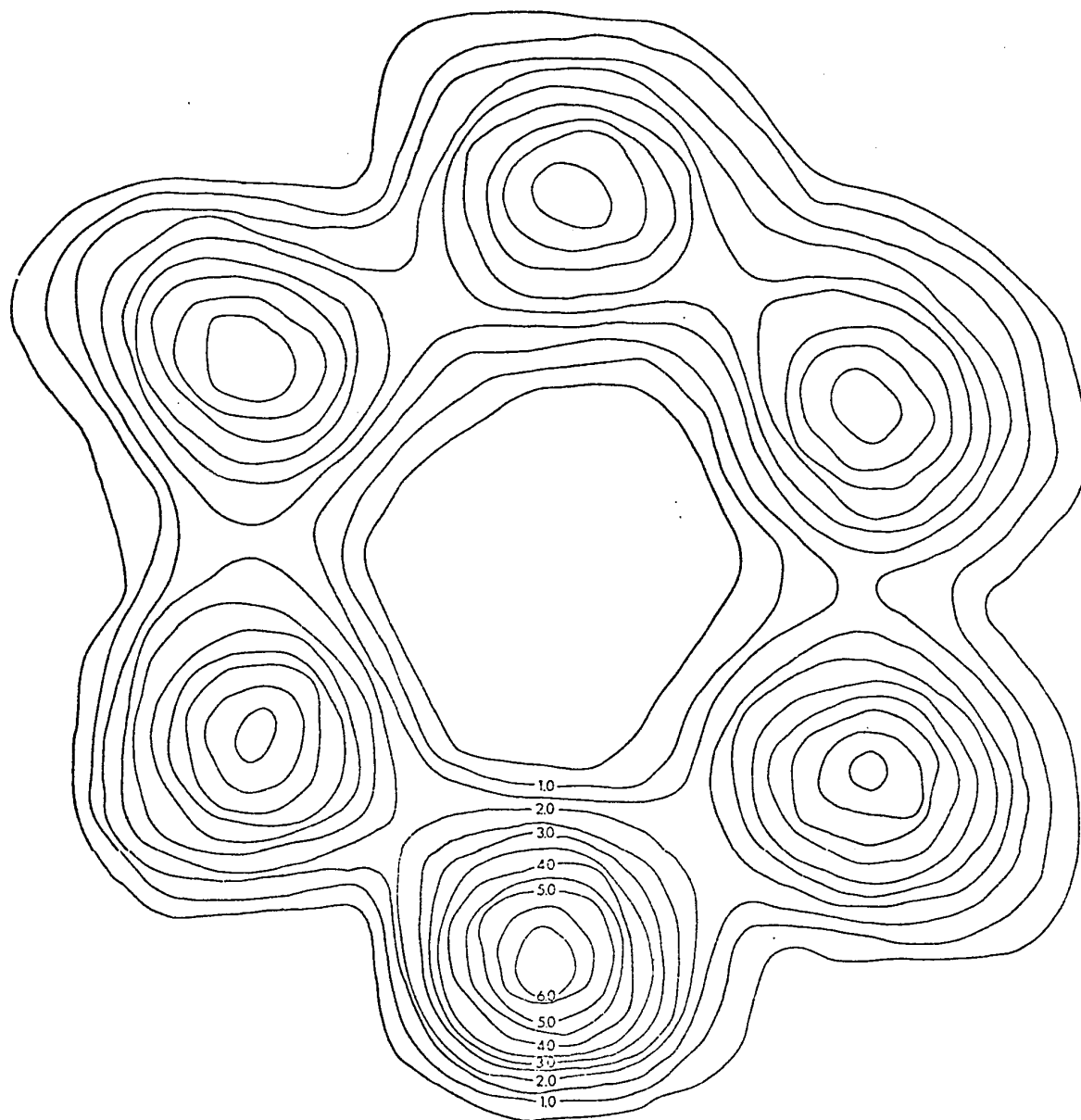


Figure 13

Slant Fourier through the Phenyl Ring Plane



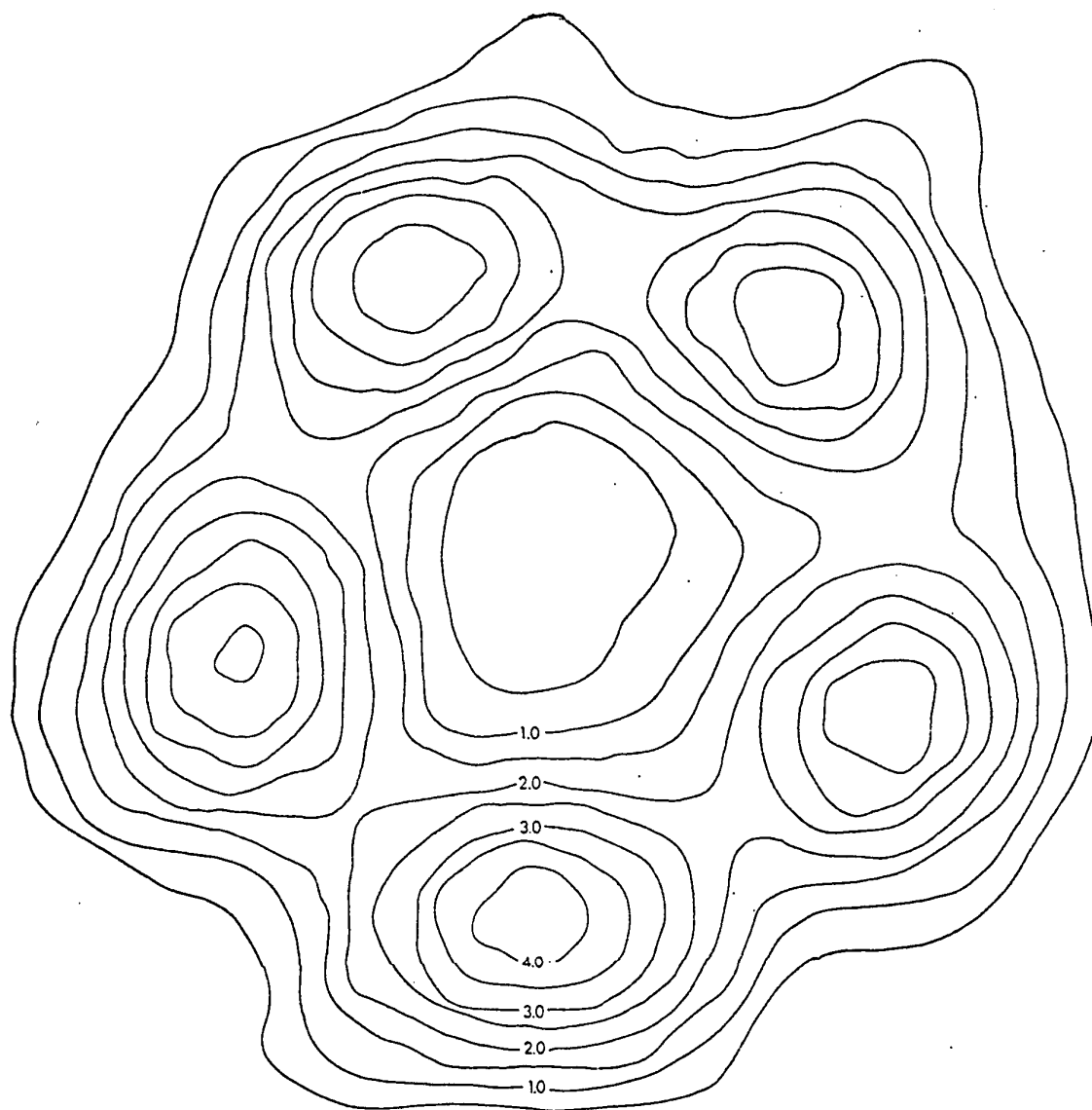


Figure 14

Slant Fourier through the Cyclopentadienyl Ring Plane

## RESULTS

The molecular geometry and the numbering system used are shown in Figure 15 while the geometry of the manganese atom is shown in Figure 16. The molecular packing viewed down the a, b, and c axes respectively is shown in Figures 17, 18, 19. The drawings were made using the program ORTEP. Table XXXV gives the bond lengths and angles within the molecule. Some intramolecular contacts are listed in Table XXXVI while Table XXXVII gives intermolecular contacts. These results and the estimated errors associated with them were calculated using the program ORFFE2.

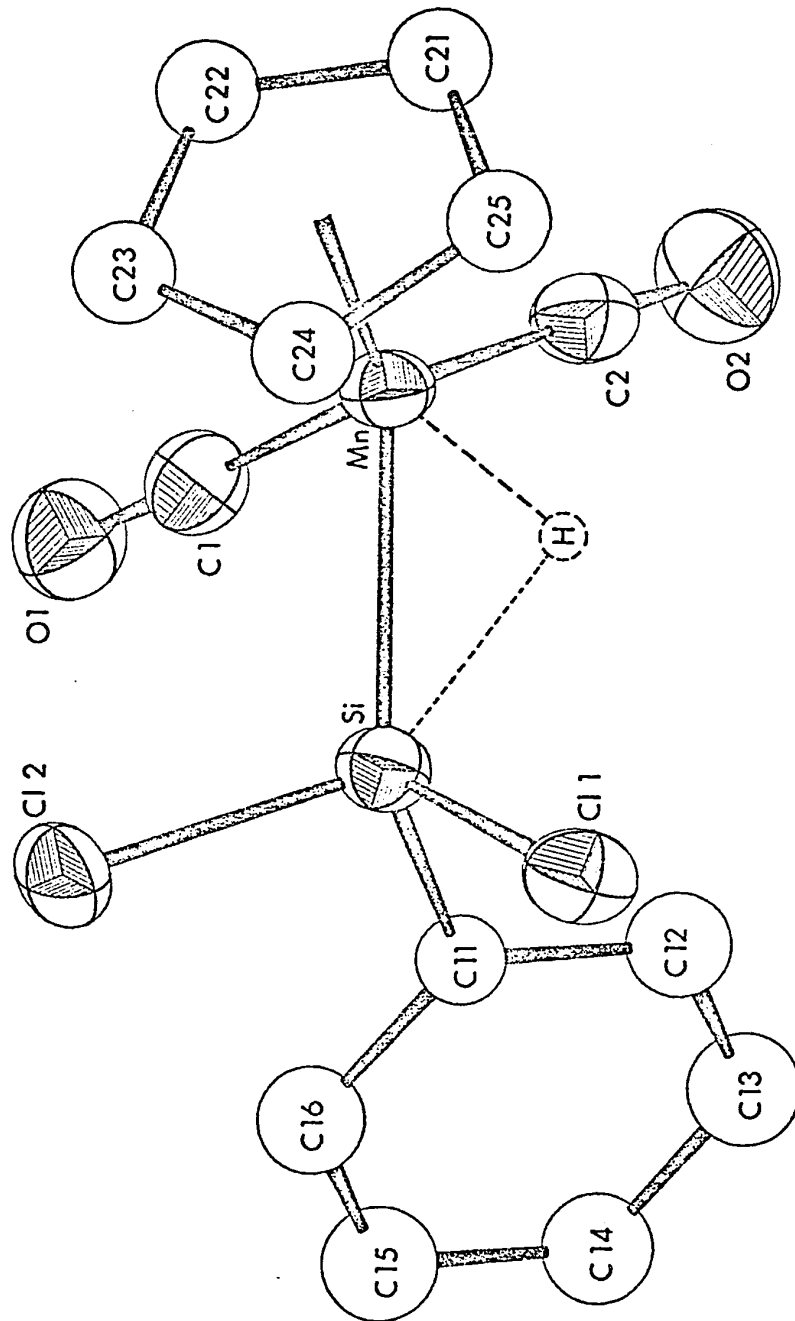


Figure 15

Perspective view of  $(\pi\text{-C}_5\text{H}_5)\text{HMn}(\text{CO})_2\text{SiCl}_2(\text{C}_6\text{H}_5)$ ,  
 the anisotropic atoms having 50% probability  
 thermal ellipsoids

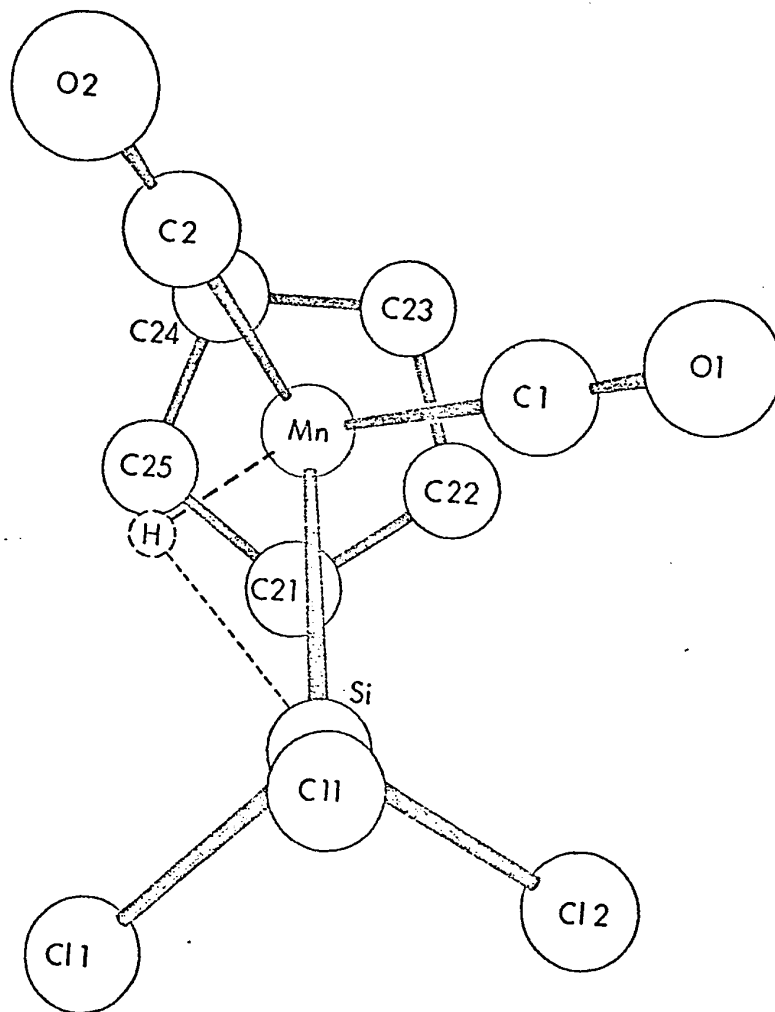


Figure 16

Geometry of the Manganese Atom Surroundings in  
 $(\pi\text{-C}_5\text{H}_5)\text{HMn}(\text{CO})_2\text{SiCl}_2(\text{C}_6\text{H}_5)$

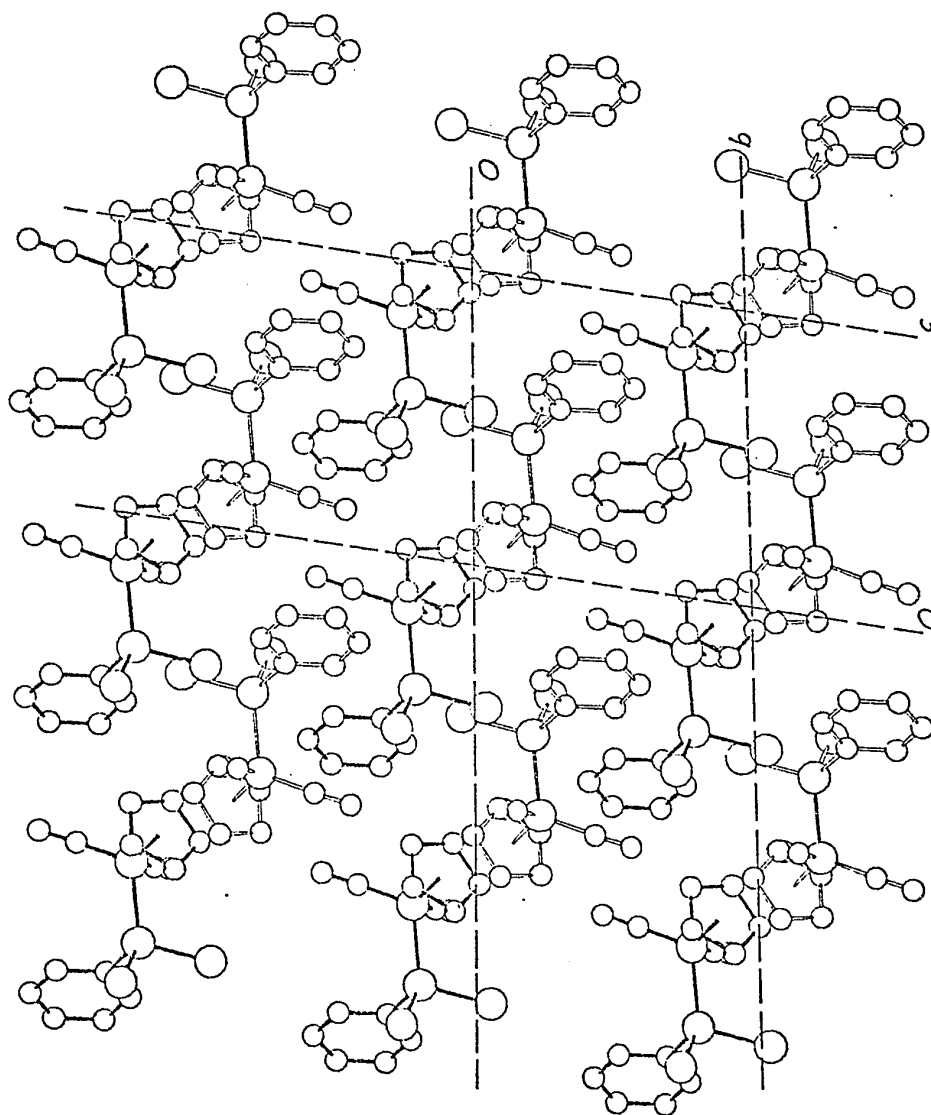


Figure 17

Packing of  $(\pi\text{-C}_5\text{H}_5)\text{HMn}(\text{CO})_2\text{SiCl}_2(\text{C}_6\text{H}_5)$   
 down the a axis  
 (b is  $b\sin\gamma$  and c is  $c\sin\beta$ )

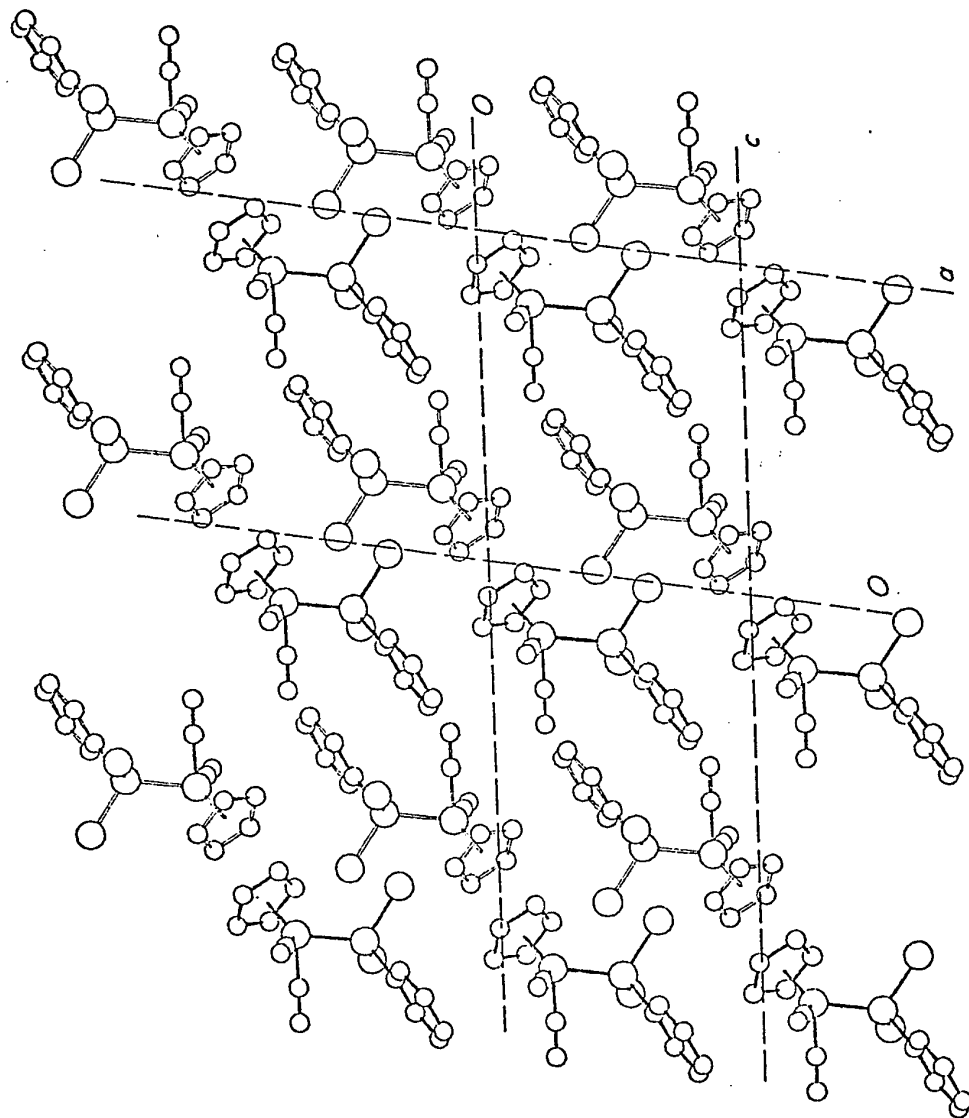


Figure 18

Packing of  $(\pi\text{-C}_5\text{H}_5)\text{HMn}(\text{CO})_2\text{SiCl}_2(\text{C}_6\text{H}_5)$

Down the  $b$  Axis

( $\underline{a}$  is  $a\sin\alpha$  and  $\underline{c}$  is  $c\sin\alpha$ )

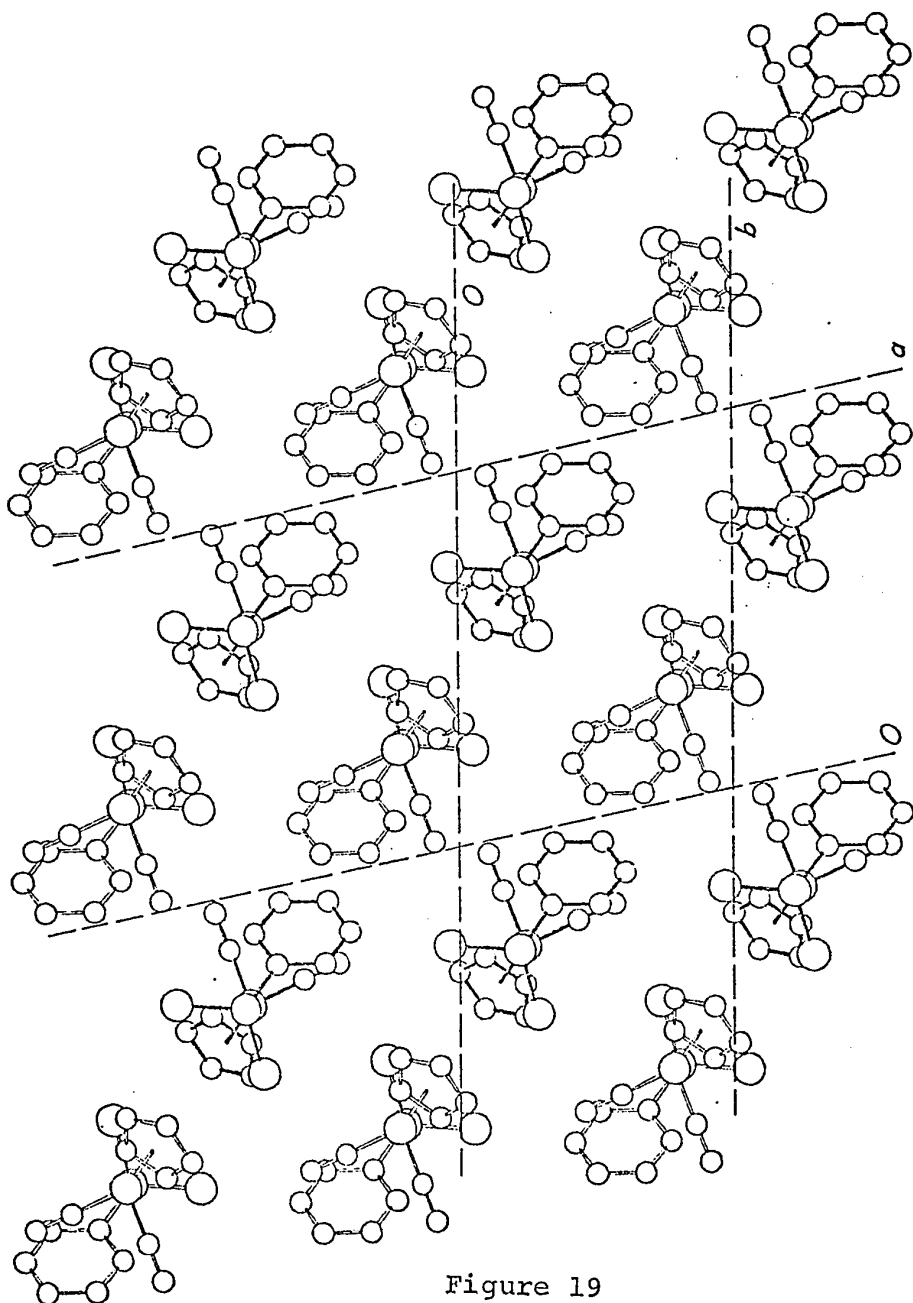


Figure 19

Packing of  $(\pi\text{-C}_5\text{H}_5)\text{HMn}(\text{CO})_2\text{SiCl}_2(\text{C}_6\text{H}_5)$   
Down the  $c$  Axis  
( $\underline{a}$  is  $a\sin\beta$  and  $\underline{b}$  is  $b\sin\alpha$ )

Table XXXVa

Bond Lengths (Å) in  $(\pi\text{-C}_5\text{H}_5)\text{HMn}(\text{CO})_2\text{Si}(\text{C}_6\text{H}_5)\text{Cl}_2$ 

<u>Atoms</u>	<u>Length</u>	<u>Atoms</u>	<u>Length</u>
Mn-Si	2.310(2) <sup>(a)</sup>	Si-Cl1	2.103(3)
Mn-Cl	1.768(10)	Si-Cl2	2.098(3)
Mn-C2	1.780(9)	Si-Cl11	1.873(4)
Mn-C <sub>p</sub>	1.774(1)	Si-H	1.79(6)
Mn-C21 <sup>(b)</sup>	2.156(6)	(C-C) <sub>phenyl</sub>	1.395
Mn-C22	2.140(6)	(C-C) <sub>C<sub>p</sub></sub>	1.418(4)
Mn-C23	2.130(6)	(C-H) <sub>phenyl</sub>	1.000
Mn-C24	2.141(6)	C21-H21 <sup>(c)</sup>	1.03(4)
Mn-C25	2.157(6)	C22-H22	1.06(4)
Mn-H	1.49(6)	C23-H23	1.03(4)
Cl-O1	1.155(9)	C24-H24	0.98(4)
C2-O2	1.153(8)	C25-H25	0.98(4)

(a) Standard deviations in parentheses refer to last digit quoted.

(b) Cyclopentadienyl atom positions derived from the hindered rotor parameters.

(c) Centre of gravity parameters of the hydrogen ring atoms only were refined.



Table XXXVb

Bond Angles ( $^{\circ}$ ) in  $(\pi\text{-C}_5\text{H}_5)\text{HMn}(\text{CO})_2\text{Si}(\text{C}_6\text{H}_5)\text{Cl}_2$ 

<u>Atoms</u>	<u>Angle</u>	<u>Atoms</u>	<u>Angle</u>
Si Mn Cl	78.8(3) <sup>(a)</sup>	Mn Si Cl1	115.4(1)
Si Mn C2	111.2(2)	Mn Si Cl2	110.6(1)
Si Mn Cp <sup>(b)</sup>	120.13(8)	Mn Si Cl1	117.8(2)
Si Mn H	51(2)	Mn Si H	40(2)
Cl Mn C2	89.5(4)	Cl1 Si Cl2	100.5(1)
Cl Mn Cp	123.5(3)	Cl1 Si Cl1	105.1(2)
Cl Mn H	112(2)	Cl1 Si H	88(2)
C2 Mn Cp	122.2(2)	Cl2 Si Cl1	105.6(2)
C2 Mn H	74(2)	Cl2 Si H	148(2)
Cp Mn H	120(2)	Cl1 Si H	101(2)
Mn H Si	89(3)	C <sub>p</sub> C21 H21	169(2)
Mn Cl O1	178.5(7)	C <sub>p</sub> C22 H22	170(2)
Mn C2 O2	178.0(7)	C <sub>p</sub> C23 H23	170(2)
		C <sub>p</sub> C24 H24	170(2)
		C <sub>p</sub> C25 H25	169(2)

(a) Standard deviations in parentheses refer to last digit quoted.

(b) C<sub>p</sub> represents the centre of gravity of the carbon ring in the cyclopentadienyl ligand.

Table XXXVI  
Some Non-Bonded Intramolecular Contacts

<u>Atoms</u>	<u>Distance (Å)</u>	<u>Atoms</u>	<u>Distance (Å)</u>
Mn C11	3.590(4) <sup>(a)</sup>	C11 C 2	3.229(3)
Mn C11	3.733(2)	C12 H16	2.720(2)
Mn C12	3.625(2)	C12 C11	3.165(4)
Si C1	2.623(9)	C1 C2	2.50(1)
Si H24	2.76(3)	C1 H	2.71(6)
Si C24	3.037(6)	C1 H23	2.81(4)
Si C2	3.389(9)	C1 C23	2.836(10)
Si C23	3.466(2)	C1 C22	2.916(10)
Si C25	3.624(7)	C2 H	1.98(6)
C11 H	2.71(6)	C2 H21	2.66(3)
C11 H24	2.88(4)	C2 C21	2.752(10)
C11 C11	3.160(5)	O2 H	2.88(6)

(a) Standard deviation in parentheses refers to last digit quoted.

Table XXXVIIa

Intermolecular Contacts Less Than 4.0 Å  
Between Non-Hydrogen Atoms

Atoms	Distance (Å)	Symmetry (a)	Atoms	Distance	Symmetry (a)
O1 O1	3.25(1)	(b)	O1 C13	3.692(7)	5
C14 O2	3.377(8)		C2 C15	3.846(9)	3
C01 O2	3.573(6)		C2 C14	3.869(9)	5
C01 C21	3.598(2)		C2 C14	3.930(9)	3
C01 C2	3.633(8)		O2 C14	3.578(8)	5
C01 C02	3.843(3)		O2 C23	3.610(6)	4
C01 C24	3.844(2)		O2 C15	3.622(8)	5
C01 C12	3.995(4)		O2 C15	3.696(8)	3
C02 C13	3.665(5)		O2 C13	3.825(8)	3
C02 C15	3.698(6)		C12 C25	3.855(5)	8
C02 C12	3.922(5)		C12 C14	3.950(8)	5
C02 C16	3.942(6)		C13 C14	3.960(10)	5
C02 C22	3.954(2)		C13 C15	3.989(8)	5
O1 C14	3.516(7)		C16 C22	3.706(5)	1
O1 C16	3.550(7)		C21 C24	3.634(0)	6
O1 C1	3.573(10)		C21 C23	3.871(0)	6
O1 C22	3.648(6)		C22 C24	3.657(0)	6
O1 C15	3.688(8)		C22 C25	3.858(0)	6
C23 C24	3.743(0)		C23 C25	3.503(0)	6
C24 C24	3.773(1)		C24 C25	3.707(1)	6

(a) Symmetry position of molecule to which second atom named belongs.

Positions are: (1)  $x \bar{y} z-1$ ; (2)  $x y+1 z$ ; (3)  $x \bar{y} z+1$ ; (4)  $x y-1 z$ ;  
(5)  $\bar{x}+1 \bar{y}-1 \bar{z}-1$ ; (6)  $x \bar{y} z$ ; (7)  $\bar{x}+1 \bar{y} z$  (8)  $x \bar{y}-1 z-1$ ; (9)  $x \bar{y} z-1$ ;  
(10)  $\bar{x}+1 \bar{y} \bar{z}-1$ .

(b) Standard deviation in parentheses refers to last digit quoted.

Table XXXVIIb

## Intermolecular Contacts Less Than 3.5 Å Involving Hydrogen Atoms

Atoms	Distance (Å)		Atoms	Distance (Å)		Symmetry (a)
	(b)	(a)		(a)	(a)	
C 1 H12	3.000 (2)	1	O1 H15	3.109 (6)	5	
C 1 H21	3.058 (2)	2	O1 H13	3.139 (6)	7	
C 1 H24	3.127 (2)	3	C2 H14	3.053 (8)	7	
C 1 H	3.181 (6)	1	O2 H23	2.742 (6)	8	
C 2 H13	2.905 (2)	4	O2 H14	2.913 (6)	7	
C 2 H15	3.209 (2)	5	O2 H15	3.007 (6)	7	
C 2 H22	3.384 (2)	2	O2 H14	3.356 (6)	9	
C 2 H12	3.432 (2)	4	C11 H21	3.359 (5)	10	
C 2 H24	3.463 (2)	3	C12 H25	2.967 (5)	1	
C1 H14	2.990 (8)	1	C13 H25	3.253 (6)	1	
O1 H22	2.726 (6)	6	C15 H22	3.458 (6)	10	
O1 H14	2.772 (6)	7	C16 H22	2.870 (5)	10	
O1 H16	2.821 (6)	5	C22 H16	3.433 (1)	9	

(a) Symmetry position of molecule to which second atom named belongs:  $(1) \bar{x} \bar{y} \bar{z}-1$   
 $\bar{z}-1$ ;  $(2) x y z-1$ ;  $(3) \bar{x} \bar{y} \bar{z}-1$ ;  $(4) x y+1 z$ ;  $(5) \bar{x}+1 \bar{y} z-1$ ;  $(6) \bar{x}+1 \bar{y} z$ ;  $(7)$   
 $\bar{x}+1 \bar{y}-1 \bar{z}-1$ ;  $(8) x y-1 z$ ;  $(9) x y z+1$ ;  $(10) x y z-1$ .

(b) Standard deviation in parentheses refers to last digit quoted.

## DISCUSSION

A drawing of the compound  $(\pi\text{-C}_5\text{H}_5)\text{HMn}(\text{CO})_2\text{SiCl}_2$  ( $\text{C}_6\text{H}_5$ ) is found in Figure 15. The geometry about the manganese atom (Figure 16) can be described as a distorted square pyramid and that of the silicon atom as a distorted tetrahedron. The molecule has a hydrogen atom cis to the silicon and close enough to interact with it ( $1.79(6) \text{ \AA}$ ).

The silicon-chlorine distances in this compound are  $2.103(3)$  and  $2.098(3) \text{ \AA}$ , the same within experimental error, but somewhat longer than those reported for similar compounds (see Table XXXVIII). For  $(\pi\text{-C}_5\text{H}_5)\text{HFe}(\text{CO})(\text{SiCl}_3)_2$ ,<sup>73</sup> the silicon chlorine bonds average  $2.052(3) \text{ \AA}$  but when corrections are made for thermal motion,<sup>54</sup> with the chlorine atoms allowed to ride on the silicon atom, the bonds are somewhat lengthened (Table XXXVIII) with the average being  $2.078(3) \text{ \AA}$ . When similar corrections are made for the thermal motion of  $(\pi\text{-C}_5\text{H}_5)\text{HMn}(\text{CO})_2(\text{SiCl}_2(\text{C}_6\text{H}_5))$  the bond length increases only slightly to  $2.112(3) \text{ \AA}$  (av). It is interesting to note that the shortest uncorrected Si-Cl distance of  $2.043(4) \text{ \AA}$  for Si(1)-Cl(3) in  $(\pi\text{-C}_5\text{H}_5)\text{HFe}(\text{CO})(\text{SiCl}_3)_2$  has undergone the greatest correction for riding becoming  $2.090(5)$ . It is expected that the electropositive nature of the phenyl substituent will increase the electronegativity of the silicon atom relative to that in the trichloro compound,

thus causing the bond lengths between silicon and the chlorine atoms to be longer in the dichlorophenyl silyl compound.

There is some distortion from tetrahedral geometry about the silicon atom with the  $\widehat{\text{MnSiCl}}$  angles being  $115.4(1)^\circ$ ,  $110.6(1)^\circ$  and the  $\widehat{\text{MnSiC}}(\text{C}_6\text{H}_5)$  angle  $117.8(2)^\circ$ . The  $\widehat{\text{ClSiC}}(\text{C}_6\text{H}_5)$  angles are  $105.1(2)^\circ$  and  $105.6(2)^\circ$  and the  $\widehat{\text{ClSiCl}}$  angle is  $100.5(1)^\circ$ . The geometry of the phenyl ring was fixed as a planar rigid body having a C-C distance of  $1.395 \text{ \AA}$  and C-H distances of  $1.00 \text{ \AA}$ . The centre of gravity and orientation of the carbon ring are adopted in the hydrogen ring.

The distances of the carbon atoms of the cyclopentadienyl ring from the manganese atom range from  $2.130(1)$  to  $2.156(1) \text{ \AA}$  with the average distance being  $2.144(1) \text{ \AA}$ . These are comparable to those found in  $(\pi\text{-C}_5\text{H}_5)\text{HMn}(\text{CO})_2\text{Si}(\text{C}_6\text{H}_5)_3$ <sup>64</sup> which average  $2.140(4)$ . The manganese atom is  $1.774(1) \text{ \AA}$  from the centroid of the ring. The cyclopentadienyl ring was treated as a planar hindered rotor with C-C distance  $1.417 \text{ \AA}$  and with the orientation of the hydrogen ring identical to that of the carbon ring. The value of the barrier to rotation of the hindered rotor is  $1.22(6)$  which is quite low indicating a large amount of libration of the carbon atoms.<sup>13</sup> In fact, it corresponds to a root mean square angular displacement of about  $13^\circ$ , larger than that of similar compounds (Table XXXIX). Thus, the hin-

dered rotor model appears appropriate since it allows for this libration. As well, the values for the temperature factors of the manganese and the ring as a whole should be very similar if the assumption made in the hindered rotor approximation is true: that is, that most of the motion of the ring is in the plane of the ring and tangential to it. The difference, in this case  $0.64 \text{ \AA}^2$ , can be attributed to out of plane oscillations of the ring which are not allowed for in the hindered rotor approximation and/or to librations of the molecule as a whole. According to Hutcheon<sup>13</sup>, differences of  $0.6 \text{ \AA}^2$  are acceptable and although no firm rule was established, in compounds similar to this one, such differences occur (Table XXXIX). So the hindered rotation model for the cyclopentadienyl ring is particularly suitable. The centre of gravity of the hydrogen ring was allowed to refine. It moved toward the manganese atom about  $0.18 \text{ \AA}$  relative to the centroid of the carbon ring causing the ring as a whole to be umbrella shaped with about a  $10^\circ$  bend. (Centroid of carbon ring-carbon-hydrogen angles are  $169(2)$ - $170(2)^\circ$ ). This effect has been observed in an electron diffraction study of ferrocene<sup>95</sup> where the bending is about  $5^\circ$ . A simple explanation suggests that the  $\pi$  electron density cloud of the cyclopentadienyl ring is contracted on the metal side and

expanded on the other side, and that the hydrogens lying in the nodal plane between them are thus displaced toward the metal.

The carbonyl carbon atoms are 1.768(10) and 1.780(9) Å from the manganese comparable to those in other manganese carbonyls such as  $(\pi\text{-C}_5\text{H}_5)\text{Mn}(\text{CO})_3$ <sup>74</sup> (Mn-C = 1.80(2)) and  $((\pi\text{-C}_5\text{H}_4\text{CH}_3)\text{Mn}(\text{CO})_2)_2$  diars<sup>75</sup> (Mn-C = 1.77(3)). The carbonyl groups are almost colinear with the metal, the  $\widehat{\text{MnCO}}$  angles being 178.5(7)° and 178.0(7)°. The geometry around the manganese atom as shown in Figure 16 is very similar to that found in the triphenyl analogue and closely resembles a substituted  $(\pi\text{-C}_5\text{H}_5)\text{Mn}(\text{CO})_3$  (see Table XL).

The manganese-silicon distance of 2.310(2) Å is significantly shorter than the calculated single bond distance of 2.56 Å (using 1.17 Å<sup>60a</sup> for the radius of silicon and 1.39 Å<sup>60b</sup> for manganese) and suggests an increase in bond order between manganese and silicon. It is even shorter than the bond found for Mn-Si in the triphenyl analogue (2.424(2) Å)<sup>64</sup>. A discussion of the bonding characteristics of the ligands  $(\text{C}_6\text{H}_5)_3\text{Si}$  and  $\text{Cl}_2(\text{C}_6\text{H}_5)\text{Si}$  is in order at this point.  $(\text{C}_6\text{H}_5)_3\text{Si}$  can be considered as a stronger  $\pi$  acceptor than  $\text{Cl}_2(\text{C}_6\text{H}_5)\text{Si}$ , back donation from chlorine to silicon having reduced the  $\pi$  acceptor ability of silicon with respect to manganese in the latter. If this were the only factor operating in the formation of the



Mn-Si bond, the bond in the  $\text{Cl}_2(\text{C}_6\text{H}_5)\text{Si}$  compound would be longer than that in the  $(\text{C}_6\text{H}_5)_3\text{Si}$  one. That it is shorter implies that factors other than  $\pi$  acceptance are applicable. According to Graham,<sup>63</sup>  $(\text{C}_6\text{H}_5)_3\text{Si}$  is considered an inferior  $\sigma$  acceptor relative to  $\text{Cl}_2(\text{CH}_3)\text{Si}$  (and presumably by extension to  $\text{Cl}_2(\text{C}_6\text{H}_5)\text{Si}$ ). It is this characteristic (i.e. poor  $\sigma$  acceptance) which causes a longer bond to be formed in  $(\pi\text{-C}_5\text{H}_5)\text{HMn}(\text{CO})_2\text{Si}(\text{C}_6\text{H}_5)_3$ .

The peak attributed to the hydridic hydrogen lies in an otherwise empty space between the manganese and silicon atoms, and is the highest peak on all difference maps computed to search for it and the second highest peak on the difference map used to locate the phenyl and cyclopentadienyl hydrogen atoms. However, it is only  $1.49(6) \text{ \AA}$  from the manganese atom, somewhat shorter than the normal covalent bond length of  $1.60 \text{ \AA}$  as found in  $\text{HMn}(\text{CO})_5$ <sup>29</sup> by X-ray diffraction. Nonetheless, this peak did follow the calculated peak height relationship found to be characteristic of hydridic hydrogen by La Placa and Ibers,<sup>66</sup> Table XXX. Furthermore, the near identity of the geometries of this and the triphenyl analogue in which the hydrogen was located  $1.55 \text{ \AA}$  from the manganese atom supports the supposition of a hydrogen in the bridging position. It has been a general observation<sup>78,12</sup> that the interatomic distances measured by X-ray diffraction are 0.05 to

0.20 Å shorter than the internuclear distances measured by neutron diffraction probably because of a shift of the K electron toward the heavier atom on bonding. Thus, the observed shortness in this compound is in the expected direction of error. Also, the shortness could in part be attributed to anharmonicity of the stretching motion of the bond, that is, the potential function describing this motion is not a parabola but an asymmetric function--see for example Figure 22. If a spherical approximation is then used to describe an atom which may be better described by an elongated ovoid, an apparent bond shortening may occur. Owing to this minor discrepancy in the bond length, the peak is shown in Figures 15 and 16 with dotted lines, but is labelled 'H' and will subsequently be referred to as the hydridic hydrogen.

The distance from the hydridic hydrogen to the silicon is 1.79 Å which is considerably longer than the Si-H bond distance of 1.48 Å in SiH<sub>4</sub><sup>65</sup> but is much shorter than a normal intramolecular contact. Because silicon has a larger radius than carbon, it would be expected that the C...H contact would be less than that of Si...H. Since this is not the case, the C2...H distance being 1.94 Å, an interaction between silicon and hydrogen in the form of a weak bond is postulated.

It is possible to speculate on the reasons for bridging hydrogen in this and the triphenyl analogue while  $\text{HFe}(\text{CO})_4\text{Si}(\text{C}_6\text{H}_5)_3$  has a terminally bonded hydrogen. In the beginning, it was proposed that the electronegativity of the chlorine atoms prevented a significant interaction between silicon and hydrogen in the case of  $(\pi\text{-C}_5\text{H}_5)\text{-HMn}(\text{CO})_2\text{SiCl}_3$ <sup>64</sup> which was too unstable for the structure to be determined crystallographically. On this basis,  $\text{HFe}(\text{CO})_4\text{Si}(\text{C}_6\text{H}_5)_3$  was predicted to contain a bridged hydrogen, but as Chapter 4 has shown, this is incorrect. Using this criterion as well,  $(\pi\text{-C}_5\text{H}_5)\text{HMn}(\text{CO})_2\text{SiCl}_2(\text{C}_6\text{H}_5)$  would be thought to contain a terminal hydrogen, also incorrect. On examination of the differences between the iron and manganese triphenyl compounds, the most likely cause of the difference in hydridic hydrogen behavior was deemed to be the presence of the cyclopentadienyl ring which constrains the geometry of the ligands surrounding the transition metal. This constraint means that for the hydrogen to occupy a position not interacting with the silicon, the angle between the carbonyl groups would have to be less than  $90^\circ$  and significant interaction between them would occur. However, if the hydrogen atom position is distorted toward the silicon, there is room for the carbonyls to be in positions which substantially reduce their interactions.

Thus, steric hindrance forces a weak interaction between hydrogen and silicon in both the triphenyl and dichlorophenyl manganese compounds.

The infrared evidence is shown to be useless for predicting the nature of hydrogen interactions in compounds of this type, in that although the dichlorophenyl compound shows a Mn-H stretching frequency in the terminal bond region while the triphenyl analogue shows no such band, both are now known to contain hydrogen in similar environments.

Table XXXVIII

## Comparison of Silicon-Chlorine Bond Lengths

<u>Molecule</u>	<u>Atoms</u>	<u>Uncorrected Distance (Å)</u>	<u>Corrected (a) Distance (Å)</u>
$(\pi\text{-C}_5\text{H}_5)\text{HMn}(\text{CO})_2\text{Si}(\text{C}_6\text{H}_5)\text{Cl}_2$ (b)	Si-Cl1	2.103 (3) (c)	2.114 (3)
	Si-Cl2	2.098 (3)	2.109 (3)
$(\pi\text{-C}_5\text{H}_5)\text{HFe}(\text{CO})(\text{SiCl}_3)_2$ <sup>73</sup>	Si(1)-Cl(1)	2.049 (4)	2.072 (4)
	Si(1)-Cl(2)	2.060 (4)	2.075 (4)
	Si(1)-Cl(3)	2.043 (4)	2.090 (5)
	Si(2)-Cl(4)	2.049 (4)	2.070 (5)
	Si(2)-Cl(5)	2.048 (4)	2.084 (4)
	Si(2)-Cl(6)	2.061 (4)	2.075 (4)
$\text{Co}(\text{SiCl}_4)(\text{CO})_4$ <sup>76</sup>	Si-Cl (av.)	2.035	-
$\text{RhHCl}(\text{SiCl}_3)(\text{P}(\text{C}_6\text{H}_5)_3)_2$ <sup>77</sup>	Si-Cl (av.)	2.054 (6)	-

(a) Correction for thermal motion: second atom assumed to ride on first atom.

(b) This work.

(c) Standard deviations in parentheses refer to last digit quoted.

Table XXXIX  
Comparison of Hindered Rotors

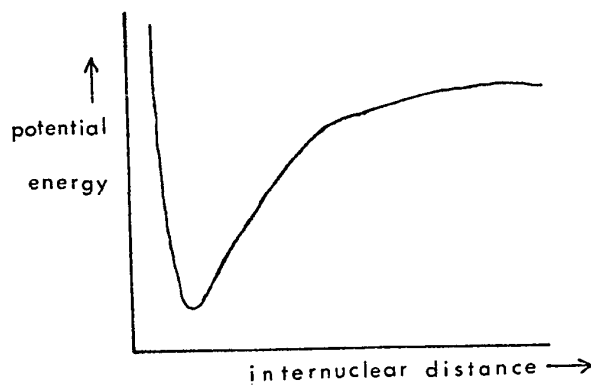
Compound	Barrier BD	RMS Displacement	Manganese Isotropic Temp. Factor $\frac{\circ}{\text{A}}^2$	Ring Isotropic Temperature Factor $\frac{\circ}{\text{A}}^2$	Temperature Factor Difference $\frac{\circ}{\text{A}}^2$
$(\pi\text{-C}_5\text{H}_5)_2\text{Mn}(\text{CO})_3$ <sup>87</sup>	1.50	12.0°	3.18	3.64(17)	0.46
$(\pi\text{-C}_5\text{H}_5)_2\text{HMn}(\text{CO})_2\text{Si}(\text{C}_6\text{H}_5)_3$ <sup>87</sup>	3.36	7.2°	3.23	3.91	0.68
$(\pi\text{-C}_5\text{H}_5)_2\text{HMn}(\text{CO})_2\text{SiCl}_2(\text{C}_6\text{H}_5)$ (a), <sup>87</sup>	1.22	12.8°	3.60	4.24	0.64

(a) This chapter.

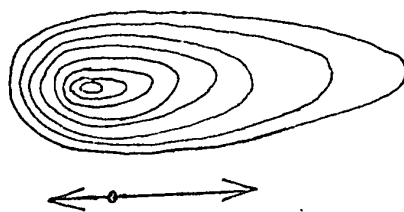
Table XL  
Comparison of Cyclopentadienyl Manganese Carbonyl Compounds

Molecule	$\overline{\text{HMnC}}$	$\overline{\text{CMnC}}$	$\overline{\text{CMnSi}}$	$\overline{\text{HMnSi}}$	$\overline{\text{HMnC}}$	$\overline{\text{CMnC}}$	$\overline{\text{SiMnC}}$
$(\pi\text{-C}_5\text{H}_5)\text{Mn}(\text{CO})_3$ <sup>74</sup>	--	91 91 94	--	--	--	124.0 123.3 123.7	--
$(\pi\text{-C}_5\text{H}_5)\text{HMn}(\text{CO})_2\text{Si}(\text{C}_6\text{H}_5)_3$ <sup>64</sup>	77.0 (1) 109.0 (2)	88.7 (3)	--	46 (2)	122.0 (1)	122.6 (2) 123.7 (2)	118.0 (1)
$(\pi\text{-C}_5\text{H}_5)\text{HMn}(\text{CO})_2\text{SiCl}_2(\text{C}_6\text{H}_5)$ (a)	74 (2) 112 (2)	89.5 (4)	78.8 (3) 111.2 (2)	51 (2)	120 (2)	122.2 (2)	120.13 (8)

(a) This chapter.



a)



b)

Figure 20<sup>78</sup>

a) Typical anharmonic potential function.

b) Scattering density distribution corresponding to the anharmonic stretching vibration described in a).



Chapter 6

The Crystal and Molecular Structure of  
 $(\pi\text{-C}_5\text{H}_5)\text{HFe}(\text{CO})[\text{Si}(\text{CH}_3)_2\text{C}_6\text{H}_5]_2$

## INTRODUCTION

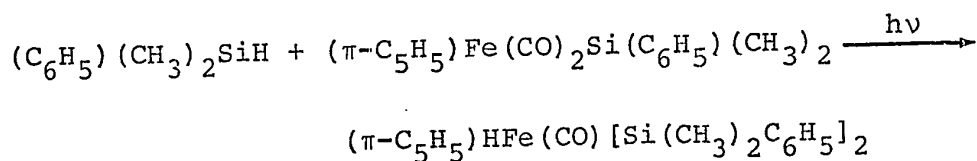
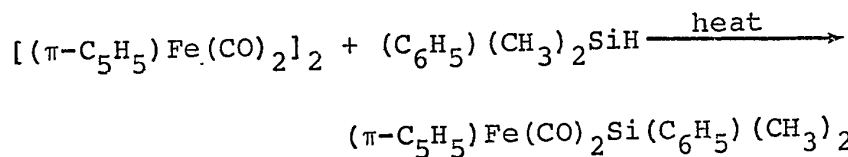
The crystal structure of hydrido bis(trichlorosilyl)carbonyl- $\pi$ -cyclopentadienyl iron,  $(\pi\text{-C}_5\text{H}_5)\text{HFe}(\text{CO})(\text{SiCl}_3)_2$ , by L. Manojlović-Muir, K. Muir and J. A. Ibers<sup>73</sup> failed to locate the hydridic hydrogen mainly because the compound unfortunately crystallized in a non-centrosymmetric space group. When the compound hydrido bis(phenyldimethylsilyl)carbonyl- $\pi$ -cyclopentadienyl iron,  $(\pi\text{-C}_5\text{H}_5)\text{HFe}(\text{CO})[\text{Si}(\text{CH}_3)_2\text{C}_6\text{H}_5]_2$ , which differed from the aforementioned compound only in the silicon ligands, became available and revealed, on preliminary investigations by A. Faust,<sup>79</sup> a centrosymmetric orthorhombic space group, it was hoped that the hydridic hydrogen could be found. It was thought that the electronegativity arguments, refuted by the structure of  $(\pi\text{-C}_5\text{H}_5)\text{HMn}(\text{CO})_2\text{SiCl}_2(\text{C}_6\text{H}_5)$ ,<sup>(a)</sup> might possibly need to be revived in a revised form: for situations not sterically hindered, the relative electronegativity of the silicon atom caused by its ligands determines whether it interacts with the hydridic hydrogen atom. In addition, it is possible to compare the geometry of this compound with the mono-silicon ones, particularly  $(\pi\text{-C}_5\text{H}_5)\text{HMn}(\text{CO})_2\text{SiCl}_2(\text{C}_6\text{H}_5)$ , by the formal replacement of a carbonyl moiety in the latter with a silicon group. For these reasons, this structural determination was undertaken.

---

(a) Chapter 5.

## EXPERIMENTAL

The compound, hydrido bis(phenyldimethylsilyl) carbonyl- $\pi$ -cyclopentadienyl iron,  $(\pi\text{-C}_5\text{H}_5)\text{HFe}(\text{CO})[\text{Si}(\text{CH}_3)_2\text{C}_6\text{H}_5]_2$ , was obtained in a form suitable for X-ray crystallographic studies from E. Wood. The crystals were prepared according to the following reaction sequence:<sup>41</sup>



The crystals formed can be recrystallized from pentane.

Preliminary photography established the crystal class as orthorhombic or higher with a mirror plane perpendicular to the axis of rotation seen in an oscillation photograph and two mirror lines  $90^\circ$  apart seen in the Weissenberg zero level photograph. The space group was uniquely determined as  $\text{Pbca}$  (#61  $D_{2h}^{15}$ ) when systematic absences  $0k\ell$ ,  $k = 2n+1$ ,  $h0\ell$ ,  $\ell = 2n+1$ ; and  $hk0$ ,  $h = 2n+1$  were observed. Precise cell constants were determined from a least squares analysis of eight reflections, accur-

ately centred on the Picker manual diffractometer as previously described (Appendix C) as  $a = 19.028(3)$ ,  $b = 13.320(2)$  and  $c = 17.316(2)$  Å at 25°C ( $\text{CuK}_{\alpha_1}$   $\lambda = 1.54051$  Å).

The density was determined as  $1.27^{(3)}$  gm/cc at 22°C by flotation using aqueous zinc iodide and this agrees favorably with that calculated (1.277 gm/cc) for eight molecules per unit cell, molecular weight of 420.48 and a unit cell volume of  $4371.75$  Å<sup>3</sup>. The golden yellow crystals appeared to be stable in air so no special handling precautions were required.

The box-like crystal used for data collection had as crystal faces the sets of planes {210} and {001} and dimensions 0.140 x 0.152 x 0.206 mm. It was mounted with the  $c$  (and  $c^*$ ) axis coincident with the  $\phi$  axis of the diffractometer, and data to 45° in  $2\theta$  was collected using  $\text{MoK}_{\alpha}$  radiation. Each plane was scanned for one minute by moving one degree on either side of its centre, and backgrounds were estimated by stationary counts for 20 seconds at the limits of the scan. Throughout the data collection eight reflections of well distributed  $2\theta$  values were monitored. These did not show any decomposition of the crystal, the maximum variation observed being less than  $\pm 3\sigma$  where  $\sigma$  is defined as in Chapter 1, with no apparent pattern in the peak height values.  $00l$ ,  $l = 4, 6,$

10 data were collected at  $10^\circ$  intervals in  $\phi$  from  $0^\circ$  to  $180^\circ$  in order to judge the correctness of the absorption corrections.  $\mu$  was  $8.73 \text{ cm}^{-1}$  and the transmission factors for the data set varied from 0.866 to 0.912.

Of 2876 reflections measured, 1180 were considered to be above background using a criterion  $I/\sigma(I) \leq 3.0$ <sup>53</sup> and 1395 were above background if the criterion is lowered to  $I/\sigma(I) \leq 2.0$ .

Table XLI

Patterson Vectors for  $(\pi-C_5H_5)HFe(CO)(SiC_6H_5(CH_3)_2)_2$

Multiplicity	Vector	Relative Weight	Multiplicity	Vector	Relative Weight
4	$k \pm 2x_{Fe}$	2704	2	$-x_{Fe} \pm x_{Si}$	728
4	0	2704	2	$x_{Fe} \pm x_{Si}$	728
4	k	2704	2	$-x_{Fe} \pm x_{Si}$	728
2	$k \pm 2y_{Fe}$	1352	2	$x_{Fe} \pm x_{Si}$	728
2	$\pm 2y_{Fe}$	1352	2	$x_{Fe} \pm x_{Si}$	728
2	$k \pm 2x_{Fe}$	1352	2	$-x_{Fe} \pm x_{Si}$	728
2	$\pm 2x_{Fe}$	1352	2	$k \pm x_{Fe} \pm x_{Si}$	728
2	k	1352	2	$k - x_{Fe} \pm x_{Si}$	728
2	$k \pm 2x_{Fe}$	1352	2	$k \pm x_{Fe} \pm x_{Si}$	728
2	$\pm 2x_{Fe}$	1352	2	$k - x_{Fe} \pm x_{Si}$	728
2	$k \pm 2y_{Fe}$	676	2	$k - x_{Fe} \pm x_{Si}$	728
2	$\pm 2y_{Fe}$	676	2	$k \pm x_{Fe} \pm x_{Si}$	728
1	$\pm 2x_{Fe}$	676	2	$k - x_{Fe} \pm x_{Si}$	728
1	$\pm 2x_{Fe}$	676	2	$k \pm x_{Fe} \pm x_{Si}$	728
1	$\pm 2x_{Fe}$	676	2	$k - x_{Fe} \pm x_{Si}$	728
1	$\pm 2x_{Fe}$	676	2	$k \pm x_{Fe} \pm x_{Si}$	728
2	$x_{Fe} \pm x_{Si}$	728	2	$k - x_{Fe} \pm x_{Si}$	728
2	$-x_{Fe} \pm x_{Si}$	728	2	$k \pm x_{Fe} \pm x_{Si}$	728
2	$-x_{Fe} \pm x_{Si}$	728	2	$k - x_{Fe} \pm x_{Si}$	728
2	$-x_{Fe} \pm x_{Si}$	728	2	$k \pm x_{Fe} \pm x_{Si}$	728
2	$x_{Fe} \pm x_{Si}$	728	2	$k - x_{Fe} \pm x_{Si}$	728
2	$x_{Fe} \pm x_{Si}$	728	2	$k \pm x_{Fe} \pm x_{Si}$	728
2	$x_{Fe} \pm x_{Si}$	728	2	$k - x_{Fe} \pm x_{Si}$	728
2	$x_{Fe} \pm x_{Si}$	728	2	$k \pm x_{Fe} \pm x_{Si}$	728
2	$-x_{Fe} \pm x_{Si}$	728	2	$k - x_{Fe} \pm x_{Si}$	728

(a) Plus and minus signs applied in pairs: ( $k \pm 2y_{Fe} \pm 2z_{Fe}$ ) corresponds to ( $k \pm 2y_{Fe} \pm 2z_{Fe}$ ) and ( $k \pm 2y_{Fe} - 2z_{Fe}$ ).

(b) Si stands for either of the two silicon atoms.

Table XLIIa

Patterson Solutions

Assignment and Solution for Iron

<u>Peak Number</u>	<u>Relative Weight</u>	<u>Position</u>	<u>origin</u>	<u>origin</u>	<u>origin</u>	<u>origin</u>
1	999	0 0 0	as 1	as 1	as 1	as 1
2	667	0 0 $\frac{1}{2}$	(0 $\frac{1}{2}$ +2y <sub>Fe</sub> $\frac{1}{2}$ ) + (0 $\frac{1}{2}$ -2y <sub>Fe</sub> $\frac{1}{2}$ )	as 1	as 1	as 3
3	373	$\frac{1}{2}$ 0 0.170	( $\frac{1}{2}$ 0 $\frac{1}{2}$ -2z <sub>Fe</sub> ) or ( $\frac{1}{2}$ 0 $\frac{1}{2}$ +2z <sub>Fe</sub> )	as 1	( $\frac{1}{2}$ $\frac{1}{2}$ +2y <sub>Fe</sub> 2z <sub>Fe</sub> ) + ( $\frac{1}{2}$ $\frac{1}{2}$ -2y <sub>Fe</sub> 2z <sub>Fe</sub> )	as 3
4	357	$\frac{1}{2}$ 0 0.323	( $\frac{1}{2}$ $\frac{1}{2}$ +2y <sub>Fe</sub> 2z <sub>Fe</sub> ) + ( $\frac{1}{2}$ $\frac{1}{2}$ -2y <sub>Fe</sub> 2z <sub>Fe</sub> )	as 1	( $\frac{1}{2}$ 0 $\frac{1}{2}$ +2z <sub>Fe</sub> ) of ( $\frac{1}{2}$ 0 $\frac{1}{2}$ -2z <sub>Fe</sub> )	as 3
5	293	0.224 $\frac{1}{2}$ 0	--	( $\frac{1}{2}$ +2x <sub>Fe</sub> $\frac{1}{2}$ 0) or ( $\frac{1}{2}$ -2x <sub>Fe</sub> $\frac{1}{2}$ 0)	--	as 2
6	269	0.336 $\frac{1}{2}$ 0	( $\frac{1}{2}$ +2x <sub>Fe</sub> $\frac{1}{2}$ 0) or ( $\frac{1}{2}$ -2x <sub>Fe</sub> $\frac{1}{2}$ 0)	--	as 1	--
7	240	0.224 $\frac{1}{2}$ $\frac{1}{2}$	--	( $\frac{1}{2}$ +2x <sub>Fe</sub> 2y <sub>Fe</sub> $\frac{1}{2}$ ) + ( $\frac{1}{2}$ +2x <sub>Fe</sub> 2y <sub>Fe</sub> $\frac{1}{2}$ )	--	as 2
11	152	0.160 $\frac{1}{2}$ 0.323	(2x <sub>Fe</sub> 2y <sub>Fe</sub> 2z <sub>Fe</sub> ) + (2x <sub>Fe</sub> 2y <sub>Fe</sub> 2z <sub>Fe</sub> )	--	as 1	--
13	131	0.160 $\frac{1}{2}$ 0.170	2x <sub>Fe</sub> $\frac{1}{2}$ $\frac{1}{2}$ -2z <sub>Fe</sub>	--	as 1	--
14	126	0.272 $\frac{1}{2}$ 0.323	--	(2x <sub>Fe</sub> 2y <sub>Fe</sub> 2z <sub>Fe</sub> ) + (2x <sub>Fe</sub> 2y <sub>Fe</sub> 2z <sub>Fe</sub> )	--	as 2
Solutions						
		x <sub>Fe</sub> = ±0.082 y <sub>Fe</sub> = ±0.25 z <sub>Fe</sub> = ±0.165	x <sub>Fe</sub> = ±0.138 y <sub>Fe</sub> = ±0.25 z <sub>Fe</sub> = ±0.165	x <sub>Fe</sub> = ±0.082 y <sub>Fe</sub> = ±0.25 z <sub>Fe</sub> = ±0.085	x <sub>Fe</sub> = ±0.138 y <sub>Fe</sub> = ±0.25 z <sub>Fe</sub> = ±0.085	145.

Table XLIIb

Patterson Solutions for Silicon Atoms using Fe (0.138, 0.25, 0.165)

Peak No.	Relative Weight	Position	Assignment	Solution	Fe-Si	Angle
6	269	0.336 $\frac{1}{2}$ 0	$(\frac{1}{2}x-Fe^{-x}Si1 \frac{1}{2}-YFe+YSil \ zSi^{-z}Fe)$ $+(\frac{1}{2}x-Fe^{-x}Si1 \frac{1}{2}+YFe-YSil \ zFe^{-z}Si)$	Si1 x .018 y .25 z .165	2.3	--
8	239	0.336 $\frac{1}{2}$ $\frac{1}{2}$	$(\frac{1}{2}x-Fe^{-x}Si1 \ YFe+YSil \ \frac{1}{2}-zSi1^{+z}Fe)$ $+(\frac{1}{2}x-Fe^{-x}Si1 \ -YFe-YSil \ \frac{1}{2}+zSi1^{-z}Fe)$	Si2 x .185 y .304 z .287	2.3	111.46
9	217	0.128 0 0	$(xFe^{-x}Si1 \ YFe-YSil \ zFe^{-z}Si1) +$ $(xFe^{-x}Si1 \ YSi1-YFe \ zSi1^{-z}Fe)$			
10	206	0.128 0 $\frac{1}{2}$	$(xFe^{-x}Si1 \ \frac{1}{2}-YFe-YSil \ \frac{1}{2}-zFe^{+z}Si1)$ $+(xFe^{-x}Si1 \ \frac{1}{2}+YFe+YSil \ \frac{1}{2}+zFe^{-z}Si1)$			
11	152	0.160 $\frac{1}{2}$ 0.323	$(xFe^{+x}Si1 \ YFe+YSil \ zFe^{+z}Si1)$			
13	131	0.160 $\frac{1}{2}$ 0.170	$(xFe^{+x}Si1 \ \frac{1}{2}+YFe-YSil \ \frac{1}{2}-zFe^{-z}Si1)$			
15	112	0.384 0 0.170	$(\frac{1}{2}x-Fe^{+x}Si1 \ YFe-YSil \ \frac{1}{2}-zFe^{-z}Si1)$			
16	98	0.288 $\frac{1}{2}$ 0.170	$(2xFe \ \frac{1}{2} \ \frac{1}{2}-2zFe)$			
18	92	0.368 0 0.323	$(\frac{1}{2}x-Fe^{+x}Si1 \ \frac{1}{2}-YSi1-YFe \ zFe^{+z}Si1)$			
19	90	0.464 0.046 0.459	$(\frac{1}{2}x-Fe^{-x}Si2 \ \frac{1}{2}+YFe+YSi2 \ zFe^{+z}Si2)$			
22	77	0.176 0.460 0.119	$(\frac{1}{2}x-Fe^{-x}Si2 \ \frac{1}{2}+YFe-YSi2 \ zSi2^{-z}Fe)$			
23	73	0.048 0.046 0.119	$(xSi2^{-x}Fe \ -YFe+YSi2 \ zSi2^{-z}Fe)$			



## SOLUTION AND REFINEMENT

With eight molecules in the unit cell occupying the eight general positions for space group Pbc<sub>a</sub> [(x y z), ( $\bar{x}$   $\bar{y}$   $\bar{z}$ ), ( $\frac{1}{2}+x$   $\frac{1}{2}-y$   $\bar{z}$ ), ( $\frac{1}{2}-x$   $\frac{1}{2}+y$  z), ( $\frac{1}{2}-x$   $\bar{y}$   $\frac{1}{2}+z$ ), ( $\frac{1}{2}+x$  y  $\frac{1}{2}-z$ ), ( $\bar{x}$   $\frac{1}{2}+y$   $\frac{1}{2}-z$ ), (x  $\frac{1}{2}-y$   $\frac{1}{2}+z$ )] and three heavy atoms per molecule (iron, silicon, silicon), it was expected that the solution to these heavy atom positions could be obtained from a Patterson map in a routine, if somewhat difficult manner. To this end, a table of expected iron-iron and iron-silicon vectors was prepared and a Patterson map calculated. The vector types, their multiplicity and relative weights are given in Table XLI. The identification of the peaks in the Patterson was complicated by the fact that the first non-special position peak was located in nineteenth position in the peak listing. Some of the Patterson peaks together with their relative weights and the assignments to iron vectors attempted for them as well as the indicated solutions for the iron positions are given in Table XLIIa. These solutions for the iron atom were used in the assignment of iron-silicon vectors to the Patterson peaks in order to obtain positions for the silicon atoms. Constraints placed on these proposed positions were that the iron-silicon distance be about 2.3 Å and the  $\overset{\circ}{\text{Si}} \widehat{\text{Fe}} \text{Si}$  be obtuse. Using these criteria, several pos-

sible Si1 and Si2 positions were obtained, in much the same manner as that illustrated in Table XLIIb which uses the second solution for the iron atom. None of the attempted solutions led to an R factor below 0.35 nor yielded an observational electron density map on which any of the other atoms could be found.

At this point, it was decided to try direct methods. The choice of phasing planes was made difficult because there were no planes with  $\ell$  odd in the largest two hundred  $E(hk\ell)$  values. This appeared to be the result of the speciality of the iron and one of the silicon positions which were shown by the Patterson vectors to have the same  $y$  and  $z$  coordinates. It was necessary to separate the data into  $\ell$  odd and  $\ell$  even planes in order to get the beginning set of planes given in Table XLIII from the program FAME. The  $\ell$  odd data was processed by leaving out the contribution to the  $E(hk\ell)$  values of the iron and one silicon atom per molecule, and as a result, the  $E(hk\ell)$  values given for the  $\ell$  odd planes in Table XLIII are much larger than they would be if calculated using the full molecule. The interactions of the  $\ell$  odd planes were few and this fact was borne in mind

during the use of the program MAGIC from which signs were assigned to the non-origin defining planes and phases determined for 200 intensities (not the strongest since there were no  $l$  odd data in the strongest 200) by the method of symbolic addition. From an  $E(hk\ell)$  map calculated using these 200 reflections, the locations for the iron and the silicon atoms were determined as in Table XLIV. With these atoms in position, several electron density maps revealed the location of the carbonyl group, the ring carbons and the methyl carbons. With all non-ring atoms isotropic, the phenyl groups as rigid bodies and the cyclopentadienyl ring as a hindered rotor, several cycles of refinement led to  $R_1 = 0.192$  and  $R_2 = 0.250$ , with  $R_1$  and  $R_2$  as defined in Chapter 1, which did not show signs of being decreased. An analysis of the R values for each  $hk\ell$  level revealed that those with  $l$  even had a composite value of  $R_1 = 0.092$  while those with  $l$  odd had a value of  $R_1 = 0.571$  over the first six levels. By considering the specific expression for the A term of the structure factor for the space group  $Pbca$ ,

$$A = 8 \cos 2\pi \left( hx - \frac{h-k}{4} \right) \cos 2\pi \left( ky - \frac{k-l}{4} \right) \cos 2\pi \left( lz - \frac{l-h}{4} \right) \quad 81$$

it was seen that movement of all atoms by  $1/4$  in  $z$  would change only the  $l$  odd data leaving the  $l$  even data un-

Table XLIII

Planes Used for Phasing in Direct Methods

<u>Sign</u>	<u>Plane</u>	<u>E(hkl)</u>
+	2 1 6 <sup>(a)</sup>	2.885
-	7 1 2	3.152
+	8 4 7 <sup>(a),(b)</sup>	2.692
+	9 2 4 <sup>(a)</sup>	3.462
+	1 2 3 <sup>(b)</sup>	3.342

(a) origin defining

(b) E(hkl) values for these odd &amp; planes are not on the same scale as for the other planes. (See text.)

Table XLIV

<u>Atom</u>	<u>Direct Methods Indicated Position</u>	<u>True Position</u>
Fe	(.36 .25 .33)	(.36 .25 .58)
Si1	(.48 .25 .33)	(.48 .25 .58)
Si2	(.31 .30 .22)	(.31 .30 .47)

touched. This change was implemented with a marked lowering of the R values ( $R_1 = 0.086$  and  $R_2 = 0.093$  after two cycles) and a dramatic decrease in the composite & odd data ( $R_1 = 0.143$ ). (The data cut off was  $3\sigma$  with  $\sigma$  defined as in Chapter 4).

The true solution is present in the Patterson map, as, of course, it must be. The Patterson y values for the heavy atoms given in the sample in Table XLII are the same as those in the true solution. The z value for iron in the true solution corresponds to solutions 3 and 4 in Table XLIIa if 1.0 is added onto the vector positions used in determining it. For example, an interpretation of peak 3 as  $(\frac{1}{2} 0 1.170)$  gives the true solution. Similarly for the x position of iron: if 1.0 is added to peak 5 and the vector assignment of solutions 2 and 4 followed, the true solution results.

From this point on, the refinement proceeded routinely. Throughout, the phenyl ring carbon atoms were treated as rigid bodies and the cyclopentadienyl carbons as a hindered rotor. Electron density difference maps showed that all other non-hydrogen atoms had some anisotropy and anisotropic temperature factors were subsequently introduced but initially only for iron and silicon atoms. Anomalous dispersion factors were applied to the iron and silicon atoms. At this stage using data with a rejection

criterion of  $2\sigma$ ,  $R_1 = 0.088$ ,  $R_2 = 0.098$ . Next, all hydrogen atoms were found on a difference map with peak heights from 0.39 to 0.59 electrons/ $\text{\AA}^3$ . The phenyl ring hydrogen atoms were placed in rigid bodies riding on the phenyl carbon atoms at a distance  $1 \text{\AA}$  from the latter, while the cyclopentadienyl hydrogen atoms were set in a hindered rotor riding analogously on the cyclopentadienyl carbon atoms. The methyl hydrogen atoms were first introduced as rigid bodies with an idealized radius of  $0.9455 \text{\AA}$  and, when their positions became stabilized, were allowed to be hindered rotors. The positions and orientations of all of these hydrogen rings were allowed to refine, but attempts at temperature factor refinement or of refinement of the barriers in the hindered rotors resulted in meaningless values with unacceptable errors. Thus, the temperature factors of the rigid body hydrogens were set at those of the attached carbon +0.5 while the temperature factor and barrier to rotation for the cyclopentadienyl hydrogen ring was taken to be that of the carbon cyclopentadienyl ring. The methyl hindered rotors were given temperature factors equal to the isotropic temperature factors for the carbon atoms to which they are attached and arbitrary barriers of 2.0. With the introduction of the hydrogen atoms, and with all non-ring atoms now anisotropic, the R values were  $R_1 = 0.059$  and  $R_2 = 0.061$  after several refinement

Table XLV  
Hydrogen Peak as a Function of  $\sin\theta/\lambda$

$\frac{\sin\theta/\lambda - 1}{\text{Cutoff } \text{\AA}}$	# Terms in Unique Section	Calculated Height(b)	Observed Height	Position	Fe-H $\frac{\text{\AA}}{\text{\AA}}$	Si1-H $\frac{\text{\AA}}{\text{\AA}}$	Si2-H $\frac{\text{\AA}}{\text{\AA}}$
0.20	125	0.16	0.15	.376 .232 .507	1.39	2.48	1.63
0.25	228	0.25	0.29	.390 .234 .514	1.36	2.19	1.86
0.30	370	0.33	0.38	.391 .235 .512	1.40	2.19	1.86
0.35	542	0.41	0.51	.388 .237 .519	1.26	2.17	1.86
0.51(a)	1180	0.57	0.68	.382 .239 .514	1.30	2.31	1.72
Refined position	--	--	--	.386(3) .235(6) .517(4)	1.28(9)(c)	2.22(8)	1.81(9)

(a) Full data set.

$$(b) \rho_H^C = \frac{1}{2r} \int_0^s O(1 + a^2 s^2/4)^{-2} \exp(-Bs^2/16\pi^2) s^2 ds^{66}$$

$$s = 4\pi \sin\theta/\lambda \quad a = \text{Bohr's Radius} \quad B = 3.6$$

Evaluated using Simpson's Rule with 20 intervals.

(c) Standard deviations as obtained from ORFFE.

cycles and using  $3\sigma$  again as the data cut off.

A difference map computed at this time showed that the largest peak, which had been the tenth largest ( $0.50 \text{ e}/\text{\AA}^3$ ) in the hydrogen atom locating map, was found at  $(0.388, 0.237, 0.519)$ . This peak of height  $0.68 \text{ e}/\text{\AA}^3$ , believed to be the hydridic hydrogen peak, was found on maps limited in  $\sin\theta/\lambda$  ( $\sin\theta/\lambda \leq 0.35, 0.30, 0.25, 0.20$ ). The results of these maps are summarized in Table XLV, where they are compared to theoretical values predicted by La Placa and Ibers.<sup>66</sup> (See Chapters 4 and 5 for detailed description.)

The addition of this peak as an isotropic hydrogen atom led to a position for it of  $(0.386, 0.235, 0.517)$ , after least squares refinement with a fixed temperature factor 0.5 greater than the isotropic temperature factor for the iron atom. The final R values were  $R_1 = 0.055$  and  $R_2 = 0.058$ . An analysis of  $hk\ell_{\text{odd}}$  and  $hk\ell_{\text{even}}$  data showed  $R_1 = 0.079$  for  $\ell$  odd and  $R_1 = 0.050$  for  $\ell$  even.

Throughout, the form factors of Cromer<sup>8</sup> were used for the non-hydrogen atoms and those of Stewart, Davison and Simpson<sup>12</sup> for the hydrogen atoms. The final standard deviation for an observation of unit weight was 1.111. A final difference map computed with all atoms in their refined positions showed a maximum of  $0.39 \text{ e}/\text{\AA}^3$  and a minimum of  $-0.33 \text{ e}/\text{\AA}^3$ .



Table XLVI lists the observed and calculated structure factor amplitudes  $10|F_o|$  and  $10|F_c|$  both in absolute units of electrons. The final positional and thermal parameters for the individual atoms are given in Table XLVII. Parameters for the rigid bodies and hindered rotors are found in Table XLVIII while the derived individual atom positions are found in Table XLIXa and XLIXb. The estimated standard deviations were obtained from the inverse matrix of the final least squares cycle.

## Table XLVI

Observed and Calculated Structure Factor Amplitudes  
 $10|F_o|$  and  $10|F_c|$

Table with 20 columns (M, K, FONS, FCAL, H, K, FONS, FCAL, M, K, FONS, FCAL, M, K, FONS, FCAL, H, K, FONS, FCAL) and multiple rows of numerical data. The table includes various headers and sub-headers, and contains a large amount of numerical information.

H	K	F015	FCAL	H	K	F015	FCAL	H	K	F015	FCAL	H	K	F015	FCAL	H	K	F015	FCAL	H	K	F015	FCAL	H	K	F015	FCAL
10	1	747	644	7	7	375	344	1	14	417	410	15	6	240	272	4	8	342	351	1	7	170	244	6	8	450	424
17	1	724	245	2	8	264	254	1	11	415	411	2	7	431	432	8	8	381	370	2	6	255	334	2	6	639	650
16	1	214	205	4	8	252	203	7	11	515	522	6	7	255	334	2	6	255	334	2	6	255	334	2	6	255	334
14	3	446	942	8	8	480	436	9	11	340	266	7	7	701	745	8	1	4	52	0	10	662	694	0	10	662	694
0	4	1317	1350	14	8	280	253	1	12	256	235	11	7	444	451	6	10	488	414	11	7	444	451	6	10	488	414
4	4	427	647	0	12	351	106	1	1	271	292	0	8	705	691	3	4	269	253	1	5	274	310	1	5	274	310
6	4	751	824	2	13	308	256	5	1	314	244	1	8	304	321	3	4	269	253	1	5	274	310	1	5	274	310
12	4	560	551	0	0	1362	1324	7	1	393	422	3	5	423	417	5	8	489	495	1	5	274	310	1	5	274	310
12	4	420	384	1	0	1535	1514	12	1	241	148	5	8	489	495	6	8	387	376	0	8	248	248	0	8	248	248
14	4	549	541	2	0	592	598	7	2	196	227	6	8	387	376	0	8	248	248	1	0	747	714	1	0	747	714
18	4	525	520	3	0	571	540	3	2	290	353	8	9	293	313	3	0	291	313	3	0	291	313	3	0	291	313
1	5	571	577	5	0	1400	1368	4	2	232	195	9	8	482	738	3	0	291	313	3	0	291	313	3	0	291	313
2	5	1155	1140	6	0	686	750	7	2	327	371	1	9	420	425	5	0	468	484	6	0	329	308	6	0	329	308
6	5	423	422	7	0	894	898	8	2	216	187	2	9	414	424	6	0	329	308	6	0	329	308	6	0	329	308
7	5	263	149	9	0	1084	1020	13	2	324	260	7	9	505	497	8	0	470	424	8	0	470	424	8	0	470	424
8	5	1241	1241	13	0	265	193	3	3	417	424	10	9	274	240	9	0	858	805	10	9	274	240	9	0	858	805
10	5	756	758	15	0	406	364	5	3	220	216	11	9	467	495	10	0	319	312	11	1	259	272	11	1	259	272
16	5	864	829	17	0	507	542	6	3	216	226	3	10	279	238	3	1	244	263	3	1	244	263	3	1	244	263
0	6	1334	1330	1	1	1602	1669	0	3	247	245	3	10	279	238	3	1	244	263	3	1	244	263	3	1	244	263
1	6	252	256	2	1	422	448	1	4	245	320	6	10	264	267	6	1	309	290	6	1	309	290	6	1	309	290
2	6	285	289	3	1	802	843	5	4	249	305	8	10	264	267	6	1	309	290	6	1	309	290	6	1	309	290
4	6	814	867	4	1	655	588	6	4	264	301	9	10	614	606	7	1	767	751	7	1	767	751	7	1	767	751
4	6	927	974	5	1	507	501	8	4	285	355	2	11	306	216	8	1	279	168	8	1	279	168	8	1	279	168
6	6	740	775	6	1	416	352	10	4	292	225	7	11	252	361	10	1	318	350	10	1	318	350	10	1	318	350
10	6	534	483	7	1	1357	1357	14	4	249	233	0	12	332	329	11	1	519	493	11	1	519	493	11	1	519	493
14	6	457	437	8	1	307	315	2	5	443	451	5	1	345	345	1	2	421	447	12	1	278	271	12	1	278	271
1	7	245	254	9	1	448	485	4	5	443	451	5	1	345	345	1	2	421	447	12	1	278	271	12	1	278	271
2	7	1134	1146	15	1	508	425	5	5	219	216	6	1	289	274	3	2	340	352	13	2	340	352	13	2	340	352
3	7	359	330	0	2	763	761	6	5	416	449	12	1	273	247	4	2	240	270	14	2	240	270	14	2	240	270
4	7	282	221	1	2	1062	1130	8	5	259	258	0	2	321	351	5	2	262	270	15	2	262	270	15	2	262	270
5	7	214	210	2	2	326	376	2	6	332	315	7	2	348	345	8	2	429	389	16	2	429	389	16	2	429	389
6	7	395	426	3	2	220	296	6	6	256	358	8	2	348	345	8	2	429	389	16	2	429	389	16	2	429	389
8	7	990	1045	4	2	525	846	9	6	260	242	9	2	293	354	10	2	319	313	17	2	319	313	17	2	319	313
10	7	549	538	5	2	856	846	1	7	232	231	12	2	301	284	1	3	505	487	18	2	319	313	18	2	319	313
16	7	565	590	6	2	571	589	4	7	289	314	15	2	246	84	2	3	230	229	19	2	319	313	19	2	319	313
0	8	1266	1270	7	2	430	490	6	7	363	385	3	3	233	248	6	3	409	408	20	2	319	313	20	2	319	313
4	8	566	565	8	2	331	381	4	8	317	359	5	3	494	485	7	3	502	541	21	2	319	313	21	2	319	313
5	8	367	364	9	2	911	856	5	8	253	252	6	3	275	244	8	3	254	248	22	2	319	313	22	2	319	313
6	8	760	792	14	2	313	210	4	10	248	223	0	4	370	412	9	3	242	184	23	2	319	313	23	2	319	313
8	8	556	672	15	2	317	344	6	10	242	144	1	4	256	307	10	3	244	214	24	2	319	313	24	2	319	313
10	8	321	350	17	2	553	573	0	10	242	144	1	4	256	307	10	3	244	214	25	2	319	313	25	2	319	313
14	8	353	379	1	3	1305	1349	0	10	1564	1593	4	5	328	319	1	4	308	284	26	2	319	313	26	2	319	313
15	8	311	328	2	3	746	741	1	3	1731	1621	5	5	293	274	3	4	362	394	27	2	319	313	27	2	319	313
2	9	874	854	3	3	267	299	3	0	364	354	0	6	294	327	8	4	264	298	28	2	319	313	28	2	319	313
5	9	287	286	4	3	283	255	4	0	545	568	1	6	375	347	9	4	647	608	29	2	319	313	29	2	319	313
6	9	268	257	6	3	231	249	5	0	392	304	3	6	255	273	1	5	488	502	30	2	319	313	30	2	319	313
8	9	618	650	7	3	1047	1068	6	5	573	553	5	6	285	306	7	5	488	502	31	2	319	313	31	2	319	313
10	9	613	628	8	3	526	510	8	0	708	744	8	6	287	327	0	6	358	309	32	2	319	313	32	2	319	313
11	9	339	243	10	3	307	312	9	0	916	811	3	7	481	491	1	6	413	419	33	2	319	313	33	2	319	313
0	10	929	909	11	3	376	354	9	0	916	811	3	7	481	491	1	6	413	419	34	2	319	313	34	2	319	313
4	10	294	182	12	3	235	172	17	0	262	272	4	7	335	346	3	6	333	369	35	2	319	313	35	2	319	313
6	10	414	392	15	3	378	391	14	0	410	461	4	7	335	346	3	6	333	369	36	2	319	313	36	2	319	313
8	10	505	534	16	3	294	249	17	0	438	432	0	0	760	762	1	7	455	414	37	2	319	313	37	2	319	313
9	10	270	311	0	4	617	642	1	1	756	812	2	0	319	244	2	7	270	329	38	2	319	313	38	2	319	313
2	11	484	485	1	4	628	650	1	1	756	812	2	0	319	244	2	7	270	329	39	2	319	313	39	2	319	313
8	11	468	487	3	4	836	857	5	1	362	321	4	0	678	694	4	7	259	223	40	2	319	313	40	2	319	313
10	11	462	356	4	4	485	453	6	1	375	367	6	0	342	297	7	7	500	520	41	2	319	313	41	2	319	313
10	12	782	770	5	4	1106	1145	7	1	948	947	8	0	952	948	0	8	305	295	42	2	319	313	42	2	319	313
6	12	467	372	6	4	589	606	8	1	551	527	9	0	410	457	1	8	446	444	43	2	319	313	43	2	319	313
2	13	488	493	8	4	380	376	10	1	623	607	10	0	350	340	5	8										

Table XLVII  
Final Coordinate and Thermal Parameters (a)

Atom	X	Y	Z	$\beta_{11}$ (b)	$\beta_{22}$	$\beta_{33}$	$\beta_{12}$	$\beta_{13}$	$\beta_{23}$	$B(\text{\AA}^2)$ (c)
Fe	0.3600(1)	0.2474(2)	0.5846(1)	20.3(4)	46.8(9)	26.9(6)	-3.1(10)	0.4(6)	-5.4(11)	3.15
Si1	0.4828(1)	0.2470(3)	0.5879(2)	20.6(8)	46.4(18)	29.5(11)	-4.4(20)	-4.4(10)	-1.7(22)	3.26
Si2	0.3157(2)	0.2992(3)	0.4648(2)	21.8(11)	55.1(23)	32.9(14)	7.1(15)	-4.5(12)	-2.2(17)	3.66
C1	0.3670(7)	0.3741(11)	0.5974(7)	27(4)	76(11)	31(6)	4(6)	-1(5)	1(7)	4.41
O	0.3715(5)	0.4606(7)	0.6086(6)	49(4)	42(6)	68(6)	4(4)	-8(4)	-10(5)	6.09
C4	0.5272(7)	0.3507(11)	0.5323(9)	28(5)	70(11)	39(7)	2(6)	-7(5)	5(8)	4.54
C5	0.5196(7)	0.1256(11)	0.5513(9)	24(5)	57(10)	45(7)	9(6)	10(5)	-5(7)	4.30
C6	0.3744(9)	0.3841(11)	0.4066(9)	53(7)	61(11)	45(8)	5(7)	-11(7)	20(8)	5.87
C7	0.2317(8)	0.3708(13)	0.4817(10)	34.7(6)	120(16)	56(8)	33(8)	-13(6)	-14(9)	6.78
H										3.6

(a) Standard deviations in parentheses refer to last digit quoted.

(b) Anisotropic temperature factors  $\times 10^4$ , defined by  $\exp[-(\beta_{11}h^2 + \beta_{22}k^2 + \beta_{33}l^2 + 2\beta_{12}hk + 2\beta_{13}hl + 2\beta_{23}kl)]$ .

(c) Equivalent isotropic thermal parameter.

Table XLVIII  
Rigid Body and Hindered Rotor Parameters

Ring	$\underline{x}$	$\underline{y}$	$\underline{z}$	$\underline{B}$	$\underline{Bd}$	$\underline{R}$	$\underline{D}$	$\underline{E}$	$\underline{\xi}$
Phenyl C11-C16	0.5412(3) (a)	0.2751(4)	0.7668(3)	--	--	1.395 (b)	2.866(6)	1.971(5)	0.122(5)
Phenyl C21-C26	0.2806(3)	0.1178(4)	0.3410(3)	--	--	1.395	5.590(5)	2.795(7)	1.996(6)
Phenyl H12-H16	0.537(3)	0.271(4)	0.763(3)	--	--	2.395	2.94(3)	1.98(3)	1.17(2)
Phenyl H22-H26	0.289(2)	0.123(4)	0.334(3)	--	--	2.395	5.64(3)	2.73(3)	3.02(3)
Cyclopentadienyl C31-C35	0.3147(3)	0.1606(4)	0.6383(4)	3.84(17)	2.89(43)	1.209(5)	2.402(6)	2.394(9)	3.901(9)
Cyclopentadienyl H31-H35	0.316(2)	0.161(4)	0.642(3)	3.92	3.0	2.205	2.40(3)	2.32(4)	3.85(4)
Methyl H41-H43	0.533(4)	0.373(6)	0.520(4)	4.56	2.0	0.9455	5.44(11)	2.21(16)	5.89(16)
Methyl H51-H53	0.524(4)	0.102(6)	0.541(4)	4.22	2.0	0.9455	0.93(10)	2.35(18)	4.68(17)
Methyl H61-H63	0.374(4)	0.401(6)	0.387(5)	5.94	2.0	0.9455	5.54(12)	2.20(16)	6.57(16)
Methyl H71-H73	0.216(4)	0.390(6)	0.483(5)	6.93	2.0	0.9455	3.78(14)	1.74(16)	5.99(15)

(a) Standard deviations in parentheses refer to last digit quoted.

(b) Parameters for which no estimated errors are given were not refined.

Table XLIXa

## Thermal and Derived Positional Parameters for Rigid Bodies

Ring	Atom	$\bar{x}$	$\bar{y}$	$\bar{z}$	$\bar{B}$
1 Phenyl Carbon	C11	0.5150 (5) (a)	0.2628 (7)	0.6921 (4)	3.40 (24)
	C12	0.5469 (5)	0.1823 (5)	0.7299 (6)	5.17 (33)
	C13	0.5730 (5)	0.1945 (6)	0.8046 (5)	6.76 (39)
	C14	0.5673 (5)	0.2873 (7)	0.8414 (4)	5.47 (33)
	C15	0.5355 (5)	0.3678 (5)	0.8036 (6)	5.51 (36)
	C16	0.5094 (5)	0.3556 (6)	0.7289 (5)	4.49 (30)
2 Phenyl Carbon	C21	0.2945 (6)	0.1912 (6)	0.3964 (5)	3.20 (24)
	C22	0.3476 (4)	0.1258 (7)	0.3730 (4)	3.93 (30)
	C23	0.3337 (4)	0.0524 (6)	0.3176 (4)	5.33 (34)
	C24	0.2666 (6)	0.0444 (6)	0.2856 (5)	4.87 (32)
	C25	0.2135 (4)	0.1099 (7)	0.3090 (4)	5.48 (35)
	C26	0.2275 (4)	0.1833 (6)	0.3644 (4)	5.16 (34)
3 Phenyl Hydrogen	H12	0.538 (5)	0.109 (4)	0.704 (4)	5.7
	H13	0.585 (5)	0.131 (4)	0.831 (4)	7.3
	H14	0.584 (5)	0.293 (5)	0.890 (3)	5.9
	H15	0.535 (5)	0.434 (4)	0.822 (4)	6.1
	H16	0.488 (5)	0.412 (4)	0.695 (4)	5.0
	4 Phenyl Hydrogen	H22	0.400 (3)	0.140 (5)	0.398 (4)
H23		0.382 (3)	0.007 (5)	0.307 (4)	5.9
H24		0.270 (4)	-0.009 (5)	0.243 (5)	5.5
H25		0.178 (3)	0.107 (5)	0.271 (4)	6.0
H26		0.196 (3)	0.239 (5)	0.362 (4)	5.6

(a) Standard deviations in parentheses refer to last digit quoted.

Table XLIXb  
Derived Parameters for Hindered Rotors

<u>Ring</u>	<u>Atom</u>	<u>x</u>	<u>y</u>	<u>z</u>
5 Cyclopentadienyl Carbon	C31	0.3285 (8)	0.2068 (7)	0.6965 (7)
	C32	0.2684 (5)	0.2211 (6)	0.6490 (6)
	C33	0.2724 (8)	0.1518 (2)	0.5868 (5)
	C34	0.3349 (6)	0.0946 (6)	0.5958 (7)
	C35	0.3696 (7)	0.1286 (7)	0.6636 (4)
6 Cyclopentadienyl Hydrogen	H31	0.338 (6)	0.240 (5)	0.751 (5)
	H32	0.232 (4)	0.273 (5)	0.660 (5)
	H33	0.242 (7)	0.151 (6)	0.544 (4)
	H34	0.353 (5)	0.042 (5)	0.564 (6)
	H35	0.413 (6)	0.097 (6)	0.692 (3)
7 Methyl Hydrogen	H41	0.517 (8)	0.355 (9)	0.471 (8)
	H42	0.508 (7)	0.420 (8)	0.550 (10)
	H43	0.575 (5)	0.344 (9)	0.541 (6)
8 Methyl Hydrogen	H51	0.497 (8)	0.059 (8)	0.573 (10)
	H52	0.507 (13)	0.122 (9)	0.492 (9)
	H53	0.569 (11)	0.124 (9)	0.558 (5)
9 Methyl Hydrogen	H61	0.339 (6)	0.416 (10)	0.351 (5)
	H62	0.377 (9)	0.438 (9)	0.434 (10)
	H63	0.407 (7)	0.350 (8)	0.376 (9)
10 Methyl Hydrogen	H71	0.216 (9)	0.406 (10)	0.430 (6)
	H72	0.189 (7)	0.335 (8)	0.501 (11)
	H73	0.242 (8)	0.430 (10)	0.518 (8)



## RESULTS

The molecular geometry and the numbering system used are shown in Figure 21 while the geometry of the iron atom is shown in Figure 22. The drawings were made using the program ORTEP. Table Ia gives the bond lengths while in Ib the bond angles are listed. In Table LI some intramolecular distances are given with various models for thermal motion considered. Intramolecular contacts are given in Table LII and intermolecular contacts in Table LIIIa and LIIIb. These results and the standard deviations associated with them were calculated using the program ORFFE2.

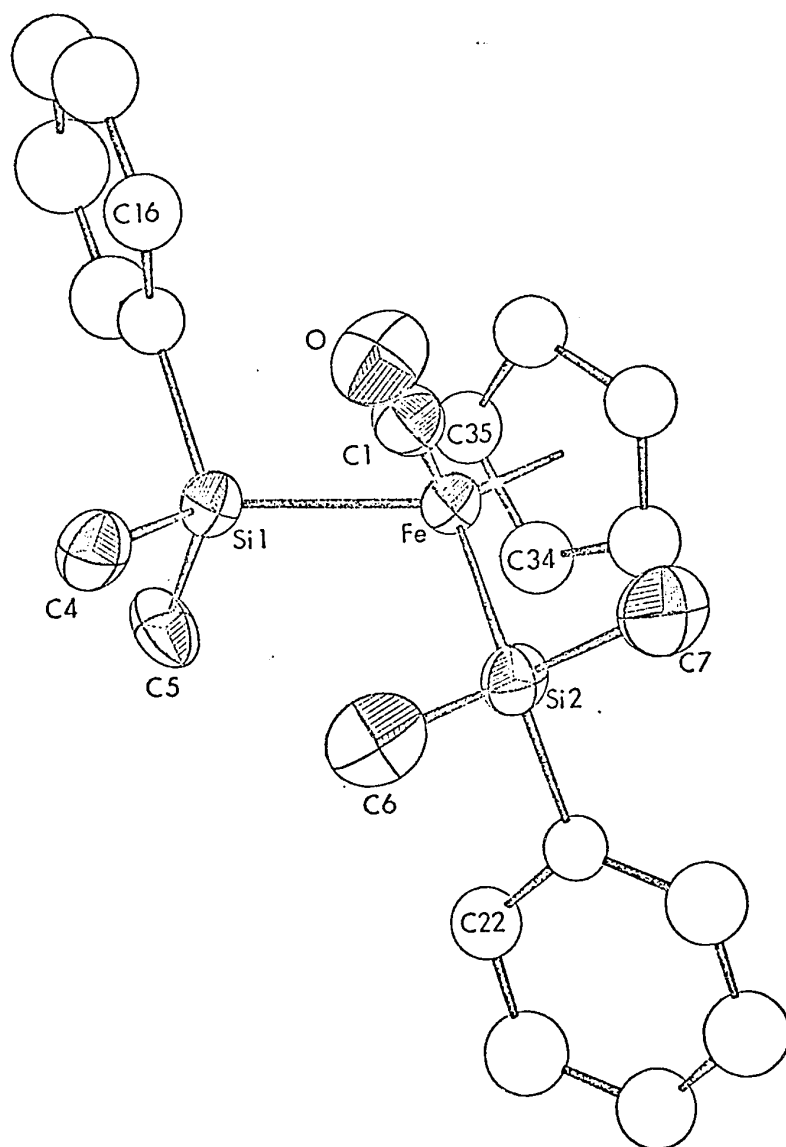


Figure 21

Perspective View of  $(\pi\text{-C}_5\text{H}_5)\text{HFe}(\text{CO})[\text{Si}(\text{CH}_3)_2\text{C}_6\text{H}_5]_2$

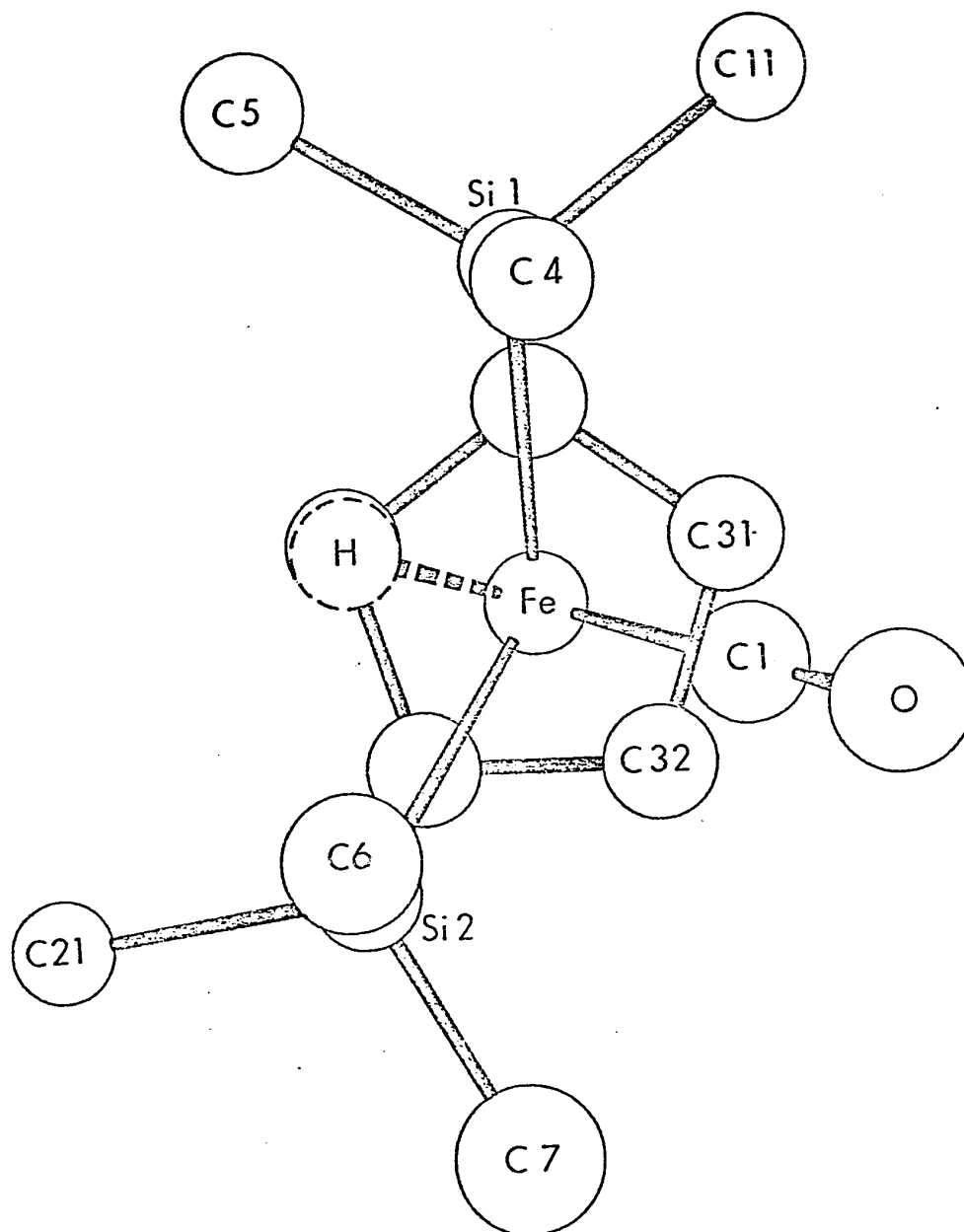


Figure 22

Geometry of the Iron Atom Surroundings

Table Ia  
Bond Lengths (Å)

<u>Atoms</u>	<u>Length</u>	<u>Atoms</u>	<u>Length</u>
Fe Si1	2.336 (3) (a)	C5 H53	0.94 (9)
Fe Si2	2.342 (4)	C6 H61	1.26 (10)
Fe Cl	1.707 (15)	C6 H62	0.86 (10)
Fe C31 (b)	2.100 (9)	C6 H63	0.93 (10)
Fe C32	2.099 (9)	C7 H71	1.06 (10)
Fe C33	2.099 (9)	C7 H72	1.00 (10)
Fe C34	2.100 (9)	C7 H73	1.02 (10)
Fe C35	2.100 (9)	C12 H12	1.09 (5)
Fe C <sub>p</sub>	1.717 (2)	C13 H13	0.99 (5)
Si1 C4	1.884 (15)	C14 H14	0.91 (5)
Si1 C5	1.873 (14)	C15 H15	0.94 (5)
Si1 C11	1.917 (7)	C16 H16	1.03 (5)
Si2 C6	1.882 (17)	C22 H22	1.10 (5)
Si2 C7	1.884 (15)	C23 H23	1.11 (5)
Si2 C21	1.907 (7)	C24 H24	1.03 (5)
Cl O	1.171 (14)	C25 H25	0.95 (5)
C C(phenyl)	1.395	C26 H26	0.96 (5)
C C(C <sub>p</sub> )	1.421 (6)	C31 H31	1.06 (5)
C4 H41 (c)	1.09 (9)	C32 H32	1.00 (5)
C4 H42	1.04 (9)	C33 H33	0.94 (5)
C4 H43	0.92 (9)	C34 H34	0.96 (5)
C5 H51	1.05 (9)	C35 H35	1.04 (5)
C5 H52	1.06 (9)		

(a) Standard deviations in parentheses refer to last digit quoted.

(b) Phenyl and cyclopentadienyl atom positions derived from rigid body and hindered rotor parameters, respectively.

(c) Centre of gravity and ring orientation parameters of hydrogen ring atoms only were refined.

Table Lb  
Bond Angles (°)

<u>Atoms</u>	<u>Angle</u>	<u>Atoms</u>	<u>Angle</u>
Si1 Fe Si2	112.49(15)	Fe Si2 C7	108.5(5)
Si1 Fe Cl	85.5(5)	Fe Si2 C21	113.8(3)
Si1 Fe C <sub>p</sub>	119.17(14)	Fe Cl O	177.9(12)
Si2 Fe Cl	81.4(4)	C4 Si1 C5	107.0(6)
Si2 Fe C <sub>p</sub>	119.82(12)	C4 Si1 Cl1	104.8(5)
Cl Fe C <sub>p</sub>	129.4(5)	C5 Si1 Cl1	107.0(6)
Fe Si1 C4	115.8(5)	C6 Si2 C7	106.4(8)
Fe Si1 C5	111.6(5)	C6 Si2 C21	104.2(6)
Fe Si1 Cl1	107.0(6)	C7 Si2 C21	107.4(6)
Fe Si2 C6	116.0(5)		

Table LI  
 Intramolecular Distances with Corrections  
 for Thermal Motion

<u>Atoms</u>	<u>Uncorrected Distance (Å)</u>	<u>Corrected<sup>(a)</sup> Distance (Å)</u>	<u>Corrected<sup>(b)</sup> Distance (Å)</u>
Fe Si1	2.336(3) <sup>(c)</sup>	2.336(3)	2.372(3)
Fe Si2	2.342(4)	2.346(4)	2.379(4)
Fe Cl	1.707(15)	1.712(14)	1.760(14)
Cl O	1.171(14)	1.212(14)	1.296(13)
Si1 C4	1.884(15)	1.891(15)	1.936(15)
Si1 C5	1.873(14)	1.886(14)	1.928(14)
Si1 Cl1	1.917(7)	-	-
Si2 C6	1.882(17)	1.900(16)	1.943(16)
Si2 C7	1.884(15)	1.914(15)	1.969(15)
Si2 C21	1.907(7)	-	-

(a) Correction for thermal motion: second atom assumed to ride on first atom.

(b) Correction for thermal motion: atoms assumed to move independently.

(c) Standard deviation in parentheses refer to last digit quoted.

Table LII  
Some Non-Bonded Intramolecular Contacts

<u>Atoms</u>	<u>Distance (Å)</u>	<u>Atoms</u>	<u>Distance (Å)</u>
Si1 C1	2.782(14)	Si1 C35	3.00(8)
Si2 C1	2.685(14)	C1 H73	2.84(13)
O H16	2.76(7)	C1 C31	2.91(2)
C5 H12	2.68(8)	C1 C32	2.91(2)
C6 C21	2.991(17)	O H16	2.75(7)
Si1 H16	2.88(9)	C12 H35	2.87(7)
Si2 C33	3.00(1)		

Table LIIIa  
 Intermolecular Contacts Less Than 4.0 Å Between Non-Hydrogen Atoms

Atoms	Distance (Å)	Symmetry (a)	Atoms	Distance (Å)	Symmetry (a)
O C13	3.617(11)	4	C24 C31	3.840(13)	7
O C24	3.659(13)	2	C25 C31	3.814(13)	7
O C23	3.695(13)	2	C1 C24	3.931(16)	7
C25 C32	3.720(13)	7	C7 C23	3.933(19)	1
C26 C31	3.781(13)	7	C12 C23	3.950(9)	1
C21 C31	3.775(12)	7	C14 C5	3.922(17)	8
C7 C34	3.794(18)	1	C15 C25	3.920(11)	2
O C33	3.759(13)	1	C6 C31	3.933(19)	5
C15 C22	3.772(12)	2	C14 C32	3.930(13)	7
C5 C5	3.86(3)	3	C24 C32	3.918(12)	6
C6 C25	3.833(17)	1	C15 C35	3.956(12)	7
C14 C4	3.858(17)	2	C16 C22	3.969(12)	2
C16 C23	3.877(12)	2	C16 C25	3.967(10)	5
C13 C32	3.820(12)	7	C15 C23	3.991(13)	2
C22 C31	3.802(12)	7	C1 C23	3.988(16)	2
C23 C31	3.834(12)	7	O C4	3.997(18)	8

(a) Symmetry position of molecule to which second atom named belongs. Positions are: (1)  $\frac{1}{2}-x \frac{1}{2}+y z$ ; (2)  $x \frac{1}{2}-y \frac{1}{2}+z$ ; (3)  $1-x -y 1-z$ ; (4)  $1-x \frac{1}{2}+y \frac{1}{2}-z$ ; (5)  $\frac{1}{2}+x \frac{1}{2}-y 1-z$ ; (6)  $\frac{1}{2}+x y \frac{1}{2}-z$ ; (7)  $x \frac{1}{2}-y 1-z$ ; (8)  $1-x 1-y 1-z$ .

(b) Standard deviation in parentheses refers to last digit quoted.



Table LIIB  
 Intermolecular Contacts Less Than 3.5 Å Between a Hydrogen Atom  
 and a Non-Hydrogen Atom

Atoms	Distance (Å)	Symmetry (a)	Atoms	Distance (Å)	Symmetry (a)
O H13	2.63(5) <sup>(b)</sup>	8	C13 H32	3.26(7)	5
C12 H23	2.94(5)	7	C6 H31	3.24(8)	6
C21 H31	2.80(6)	6	C5 H51	3.28(12)	7
C22 H31	2.77(5)	6	C23 H12	3.27(8)	7
C23 H71	2.91(12)	9	H14 C5	3.23(7)	2
C23 H31	2.99(6)	6	H14 C4	3.30(7)	2
C24 H61	2.86(10)	9	C5 H72	3.39(14)	4
C25 H61	2.85(12)	9	C15 H52	3.31(9)	2
H73 C34	2.96(14)	1	C15 H23	3.37(7)	2
O H24	3.09(8)	2	C15 H51	3.39(9)	8
C25 H32	3.03(7)	6	C16 H23	3.32(7)	2
C15 H22	3.05(8)	8	C22 H71	3.31(6)	9
C15 H25	3.01(5)	4	C24 H32	3.32(7)	6
C26 H31	3.05(7)	6	C26 H43	3.36(9)	10
C7 H53	3.18(10)	10	C31 H24	3.33(6)	3
C13 H41	3.13(10)	2	C32 H24	3.34(5)	3
C14 H32	3.14(6)	5	C35 H61	3.35(12)	2
C14 H25	3.19(6)	4	C35 H24	3.39(6)	3
C24 H71	3.12(10)	9	C34 H24	3.44(5)	3
H15 C35	3.17(7)	8	C33 H24	3.41(5)	2
C31 H61	3.14(13)	2	O H23	3.46(7)	3
H73 C33	3.20(12)	1	C4 H62	3.40(13)	11
C25 H31	3.25(7)	6	C4 H42	3.43(12)	11
C24 H31	3.23(7)	6	C5 H52	3.42(12)	11
C16 H25	3.24(5)	4	C12 H26	3.42(6)	4
C15 H35	3.21(7)	8	C13 H23	3.42(6)	7
C14 H22	3.47(7)	2	C13 H63	3.44(11)	2

... cont'd.

Table LIIIb cont'd.

- (a) Symmetry position of molecule to which second atom named belongs. Positions are: (1)  $\frac{1}{2}-x \frac{1}{2}+y z$ ; (2)  $x \frac{1}{2}-y \frac{1}{2}+z$ ; (3)  $\frac{1}{2}-x -y \frac{1}{2}+z$ ; (4)  $+x \frac{1}{2}-y 1-z$ ; (5)  $\frac{1}{2}+x y \frac{1}{2}-z$ ; (6)  $x \frac{1}{2}-y z-\frac{1}{2}$ ; (7)  $1-x -y 1-z$ ; (8)  $1-x \frac{1}{2}+y \frac{1}{2}-z$ ; (9)  $\frac{1}{2}-x y-\frac{1}{2} z$ ; (10)  $x-\frac{1}{2} \frac{1}{2}-y 1-z$ ; (11)  $1-x 1-y 1-z$ .
- (b) Standard deviation in parentheses refers to last digit quoted.

Table IIV

## Comparison of Bond Lengths, Angles

Distance (Å) Angle (°)	( $\pi$ -C <sub>5</sub> H <sub>5</sub> )HFe(CO) [SiC <sub>6</sub> H <sub>5</sub> (CH <sub>3</sub> ) <sub>2</sub> ] <sub>2</sub> (a)	( $\pi$ -C <sub>5</sub> H <sub>5</sub> )HFe(CO) (SiCl <sub>3</sub> ) <sub>2</sub> 73	( $\pi$ -C <sub>5</sub> H <sub>5</sub> )HMn(CO) <sub>2</sub> SiCl <sub>2</sub> C <sub>6</sub> H <sub>5</sub> (a)	( $\pi$ -C <sub>5</sub> H <sub>5</sub> )HMn(CO) <sub>2</sub> Si(C <sub>6</sub> H <sub>5</sub> ) <sub>3</sub> 64
	M-Si	2.339(4)	2.252(3)	2.310(2)
M-CC <sub>P</sub>	1.717(2)	1.718	1.774(1)	Not quoted
M-Carbonyl	1.707(15)	1.758(9)	1.762(10)	1.771(7)
	--	--	1.779(10)	1.764(7)
C-O	1.171(14)	1.132(10)	1.164(9)	1.162(6)
	--	--	1.158(8)	1.168(6)
Si-Cl	--	2.052(3) (av)	2.100(3)	--
Si-C phenyl	1.912(7)	--	1.874(4)	1.886(5) (av)
CC <sub>P</sub> -M-Si	119.17(14)	119.4	120.14(8)	118.0(1)
	119.82(12)	118.1	--	--
CC <sub>P</sub> -M-C	129.4(5)	125.8	123.5(3)	122.6(2)
	--	--	122.2(2)	123.7(2)
Si-M-Si	112.49(15)	115.3(1)	--	--
Si-M-C	85.5(5)	85.1(3)	78.8(3)	Not quoted
	81.4(4)	84.4(3)	112.2(2)	Not quoted

(a) This work.

## DISCUSSION

The coordination polyhedron about the iron atom can be described as a distorted tetragonal pyramid with the centroid of the cyclopentadienyl ring at the apex, the carbonyl and dimethylphenylsilyl ligands in the basal plane with the dimethylphenylsilyl groups trans to each other. The iron atom occupies a position above this basal plane in the direction toward the cyclopentadienyl ring so that the  $\overset{\frown}{\text{CC}}_{\text{p}} \text{Fe C}$  angle is  $129^\circ$  and the  $\overset{\frown}{\text{CC}}_{\text{p}} \text{Fe Si}$  angles are  $119^\circ$  and  $120^\circ$  while the  $\overset{\frown}{\text{Si Fe Si}}$  angle is  $112^\circ$ . This leaves one position in the tetragonal pyramid trans to the carbonyl group and in the basal plane to accommodate the hydridic hydrogen. This geometry most strongly resembles that found by Ibers<sup>73</sup> et al for the trichlorosilyl analogue (see Table LIV). It also is similar to that of  $(\pi\text{-C}_5\text{H}_5)\text{MoR}(\text{CO})_3$  ( $\text{R}=\text{C}_2\text{H}_5$ ,<sup>82</sup>  $\text{C}_3\text{H}_7$ <sup>83</sup>) where the cyclopentadienyl centroid is again at the apex and the alkyl and CO groups are in the basal plane with the molybdenum displaced from the basal plane toward the ring. In addition, there is an analogy to the mono silyl compounds such as  $(\pi\text{-C}_5\text{H}_5)\text{HMn}(\text{CO})_2\text{SiX}_3$  where  $\text{X}_3 = \text{Cl}_2\text{C}_6\text{H}_5$  or  $(\text{C}_6\text{H}_5)_3$ <sup>64</sup> (see Table LIV) where a CO group has replaced one of the silicon moieties in the basal plane.

The iron-cyclopentadienyl carbon distances aver-

age  $2.100(10) \text{ \AA}$  which is comparable to that in  $(\pi\text{-C}_5\text{H}_5)\text{Fe}(\text{H})(\text{CO})\text{SiCl}_3$  ( $2.093(4) \text{ \AA}$ ) but somewhat longer than that in ferrocene ( $2.047(5) \text{ \AA}$ )<sup>(a)</sup>. This weakening of the cyclopentadienyl carbon-iron bonding can be understood in terms of replacement of one of the two cyclopentadienyl rings by strongly  $\pi$  accepting groups. The iron atom is  $1.717(2)$  from the centroid of the ring. The treatment of the ring as a planar hindered rotor appears appropriate with the overall temperature factor for the ring being  $3.84$ , or  $0.69$  above the isotropic temperature factor of the iron which is very close to the average increase of  $0.60$  observed for a variety of compounds.<sup>13</sup> The barrier to rotation can be correlated to a root mean square oscillation of about  $8^\circ$ , again indicating the suitability of the hindered rotor approximation, which considers this libration. The radius of the ring,  $1.209 \text{ \AA}$ , leads to a carbon-carbon distance of  $1.421 \text{ \AA}$  which is slightly longer than the average ( $1.404 \text{ \AA}$ ) observed in the trichlorosilyl analogue, probably because in the latter there was individual atom treatment of the ring without correction for librational motion. The hydrogen atoms, initially set to ride on the carbon atoms, were refined only in position and orientation. With the barrier and temperature factor fixed at the carbon ring values, the C-H distances ranged from  $0.94(5) \text{ \AA}$  to  $1.06(5) \text{ \AA}$ .

---

(a) This work: Appendix B.

The Fe-C-O angle of  $177.9(12)^\circ$  shows the near linearity expected while the C-O distance of  $1.171(14) \text{ \AA}$  is within the accepted range for carbonyl distances.<sup>84</sup> The distance of the carbonyl carbon to the iron atom is  $1.707(15)$ , considerably shorter than in the trichloro analogue ( $1.758(9)$ ). This can be rationalized as follows: chlorine, being an electron withdrawing substituent, leaves the silicon in the trichlorosilyl compound much more able to accept electron density from the iron than do methyl and phenyl substituents which are electropositive. Thus, the iron atom in the dimethylphenyl silyl case, being unable to donate as much electron density to the silyl groups, increases its  $\pi$  bonding with the carbonyl group resulting in shorter Fe-CO bond. Further evidence for the reduced bonding between silicon and iron is provided by the silicon-iron bond distances of  $2.336(3)$  and  $2.342(4) \text{ \AA}$ , identical within experimental error, but longer than in the trichlorosilyl compound ( $2.252(3) \text{ \AA}$ ). A prediction of the expected bond length may be obtained by summing the covalent radii for iron and silicon. The best choice for iron radius is  $1.34 \text{ \AA}$  obtained from the Fe-Fe distance of  $2.679(3) \text{ \AA}$  and the Fe-C<sub>sp<sup>3</sup></sub> distance of  $2.123(15) \text{ \AA}$  in  $\text{Fe}_2(\text{C}_2\text{H}_2)_3(\text{CO})_6$ .<sup>70</sup> Coupled with the accepted radius of  $1.17^{60a}$  for silicon, a Fe-Si single bond of  $2.51 \text{ \AA}$  can be predicted. That the bond length found is shorter than this can be interpreted as

indicative of some  $d_{\pi}-d_{\pi}$  back-bonding from the metal.

The silicon-phenyl carbon distances average to 1.912(5) Å, somewhat longer than the silicon-methyl carbon distances which average 1.879(6) Å. It is expected that the silicon-phenyl carbon distances would be shorter since  $sp^2$  hybridization is involved whereas the methyl carbons bond by  $sp^3$  hybridization.<sup>85</sup> Using a covalent radius of 0.73 for  $sp^2$  carbon and 0.772 for  $sp^3$  carbon with the covalent radius of silicon gives  $Si-C_{sp^2} = 1.90$  Å and  $Si-C_{sp^3} = 1.94$ . The reasons for the observed reversal may in part be caused by inadequate allowance for thermal motion: when the methyl carbons are allowed to ride on the silicon atoms, the average  $Si-C_{sp^3}$  bond distance is increased to 1.898(10) Å (av.), certainly moving in the right direction. Such a riding correction is not possible for  $Si-C_{sp^2}$  distances in this case since the rigid body approximation used for the phenyl groups necessitates the use of isotropic temperature factors. But if such a riding correction were done, it would increase the  $Si-C_{sp^2}$  distances and in all probability, the anomaly would remain. The angles C-Si-C average to 106.1(18)°, while four of the six Fe-Si-C angles are larger than the tetrahedral angle, giving some measure of the distortion from tetrahedral symmetry about the silicon atoms.

The phenyl hydrogen atoms were treated as rigid

bodies with the positions and orientations refined and the temperature factors fixed at 0.5 greater than the attached carbon atoms. The carbon-hydrogen bond lengths varied from 0.94 to 1.11 Å. The hindered rotor model, used to describe the methyl hydrogen atoms, seemed to be particularly appropriate, since while free rotation of the hydrogens is known for methyl groups, in this case the hydrogen atoms were not completely disordered as they were located from electron density difference maps as peaks of normal heights. Methyl groups have previously been considered as hindered rotors in the case of the antibiotic cyathin A<sub>3</sub> (C<sub>20</sub>H<sub>30</sub>O<sub>3</sub>)<sup>86</sup> and trifluoro substituted methyls in Cs[Y(HFA)<sub>4</sub>]<sup>87,88</sup> where HFA represents the hexafluoroacetyl acetate ion CF<sub>3</sub>COCHO<sub>2</sub>CF<sub>3</sub>. The C-H distances in the methyl groups vary from 0.86 to 1.26 Å.

The most disappointing factor in this structural determination was the failure to positively locate the hydridic hydrogen. Initially, all signs seemed favorable: the space group was centrosymmetric, the unit cell large, the metal was in the first row transition series, the absorption was low, the crystal stable to X-rays. The first indication of problems came when the data was being collected, when it was observed that data with  $l$  odd was significantly weaker than  $l$  even data, and, as can be seen from the final structure factor listing (Table XLVI), the amount of  $l$  odd



data observed is substantially less than  $l$  even data. The  $l$  odd levels, being weak, have higher standard deviations causing reliability factors for these levels to be higher, with the unfortunate result that the data set is not precise enough to locate the hydridic hydrogen unambiguously. The weakness of the  $l$  odd data arises in the following way: the iron atom and one of the silicon atoms lie at approximately  $y = 0.25$  which is on the glide plane perpendicular to  $c$  for space group  $Pbca$  causing the iron and silicon atoms to overlie each other at intervals of 0.5 when viewed down the  $c$  axis. For these atoms, the  $c$  glide becomes in fact a simple translation of 0.5 in the  $c$  direction, resulting in an effective halving of the unit cell and in a null contribution to the  $l$  odd planes and a maximum contribution to those for  $l$  even.

With the peak from the electron density difference map, which located all hydrogens, that seemed most appropriate for the hydridic hydrogen (one located in approximately the remaining position in the tetragonal pyramid), a refinement as a hydrogen atom was attempted. It located the hydrogen  $1.28(9) \overset{\circ}{\text{Å}}$  from the iron atom,  $2.22(8) \overset{\circ}{\text{Å}}$  from  $Si1$  and  $1.81(9) \overset{\circ}{\text{Å}}$  from  $Si2$ . The usual refined positions for hydrogen atoms place them closer to other atoms than expected, so it was decided to use the method of La Placa and Ibers<sup>66</sup> of computing difference maps limited in

$\sin\theta/\lambda$  to more accurately locate the hydrogen. The results of these calculations are shown in Table XLV where it can be seen that the peak did not behave as expected: it was too large at all levels, the iron-hydrogen distances were much shorter than the accepted 1st row transition metal-hydridic hydrogen distance of about  $1.6 \text{ \AA}$ ,<sup>27</sup> and in particular the map at  $\sin\theta/\lambda \leq 0.35$  which should give the best value for this distance is the shortest ( $1.26 \text{ \AA}$ ). In view of these discrepancies, it seems unwise to assign a definite position to this hydrogen.

A consideration was next made of the possible locations for the hydrogen atom. A graph was plotted of the silicon-hydrogen distance against the H-Fe-Si angle assuming an iron-hydrogen distance of  $1.6 \text{ \AA}$  and a H-Fe-CC<sub>p</sub> angle of  $125^\circ$  (near to that observed with the refined hydrogen position) (Figure 23). It can be seen from the graph that it is possible to locate the hydrogen in a position essentially equidistant from each silicon ( $2.08 \text{ \AA}$  with a  $\widehat{\text{H Fe Si}}$  angle projected on the cyclopentadienyl plane of  $73^\circ$ ) without it being in a bonding position with either. A similar situation exists for the trichloro analogue, with a similar graph (Figure 24) being possible.

Figure 23

Silicon-hydrogen Distances for  
 $(\pi\text{-C}_5\text{H}_5)\text{HFe}(\text{CO})[\text{Si}(\text{CH}_3)_2\text{C}_6\text{H}_5]_2$

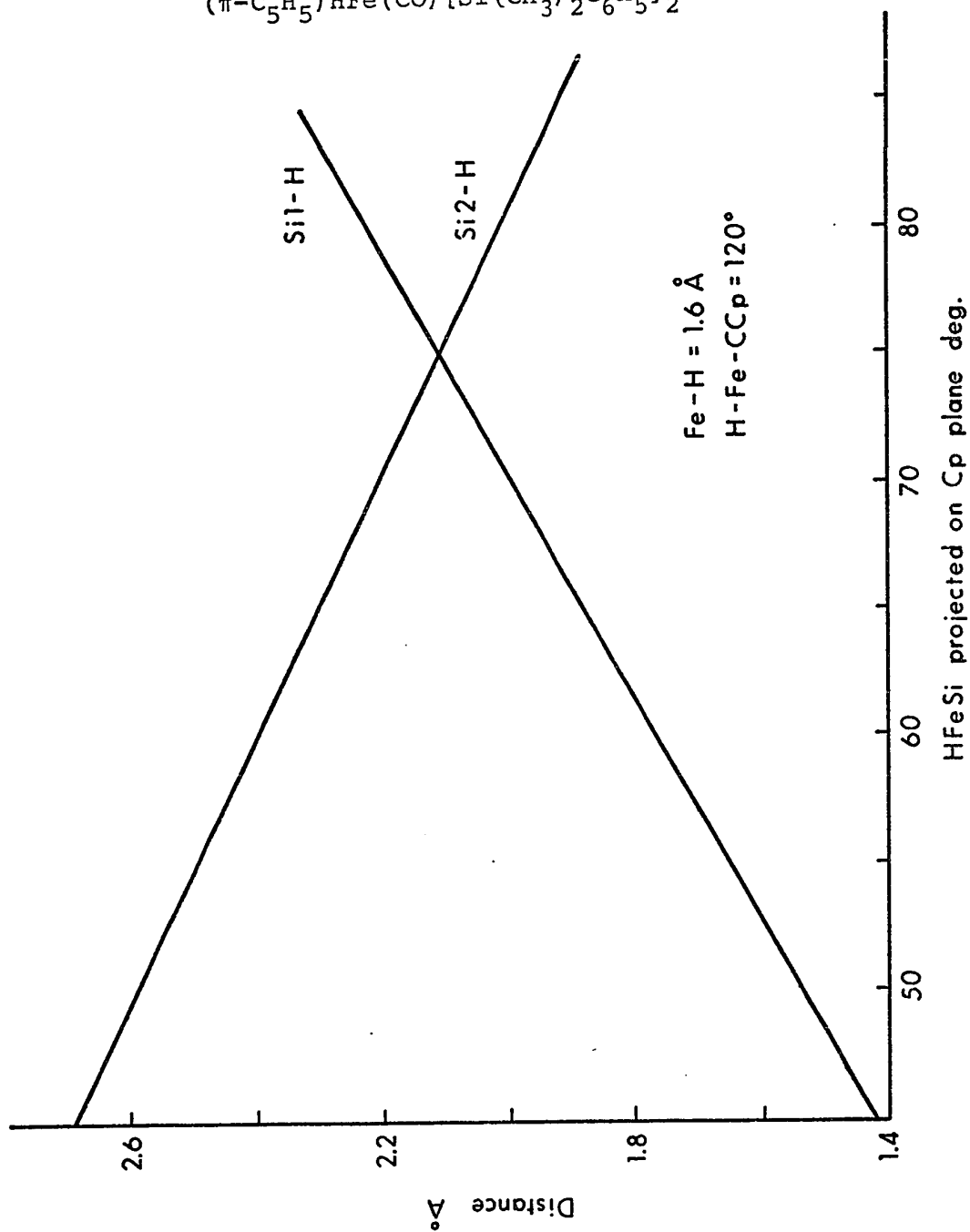
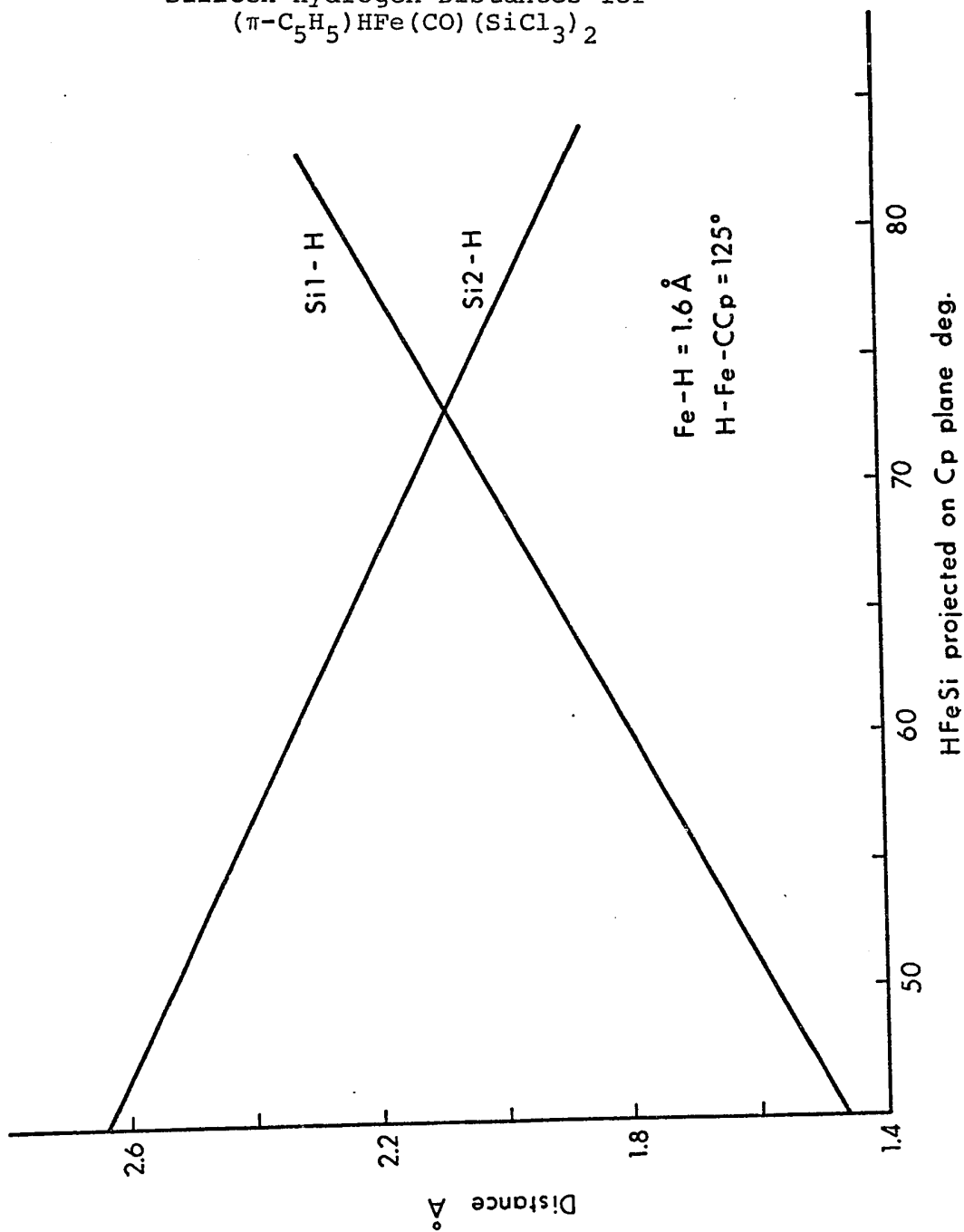


Figure 24

Silicon-Hydrogen Distances for  
 $(\pi\text{-C}_5\text{H}_5)\text{HFe}(\text{CO})(\text{SiCl}_3)_2$



## CHAPTER 7

### Summary and Conclusions

## SUMMARY AND CONCLUSIONS

The compounds whose structures have been determined during the course of this research fall into two categories: those sterically crowded,  $H_2W_2(CO)_8Si_2(C_2H_5)_4$  and  $(\pi-C_5H_5)HMn(CO)_2SiCl_2(C_6H_5)$  in which there is significant silicon-hydrogen interaction and those which are not crowded,  $HFe(CO)_4Si(C_6H_5)_3$  and  $(\pi-C_5H_5)HFe(CO)[Si(CH_3)_2C_6H_5]_2$  where silicon-hydrogen interaction is unimportant. It would perhaps be of use to discuss these compounds (and those similar ones whose structures have also been determined) in terms of chemical and spectroscopic properties. As well, some of the subtler aspects of steric crowding should be mentioned.

Beginning with the latter, it might be concluded from a cursory inspection of Figures 16 and 22 that in both  $(\pi-C_5H_5)HMn(CO)_2SiCl_2(C_6H_5)$  and  $(\pi-C_5H_5)HFe(CO)[Si(CH_3)_2C_6H_5]_2$ , the environment of the transition metal is virtually identical (silicon replacing one carbon in the former), and that if steric crowding occurs in one, it should be present in the other. However, there is reason to believe that the increased iron-silicon bond length over the manganese-carbon bond length could be sufficient to allow a non-bonded silicon-hydrogen arrangement in the disilicon species.

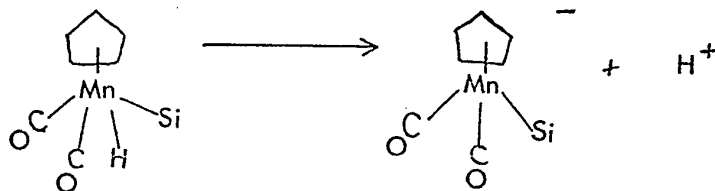
There is no evidence of inherent stability for

a weakly bridging hydrogen. On the contrary, it is only in cases of steric crowding that a close silicon-hydrogen approach occurs. There are two possible explanations for this close approach: 1) silicon could be an unusually soft atom, that is, the repulsive term for the normal potential curve is unusually small or 2) there may be a secondary minimum in the non-bonded region of the interatomic potential curve for silicon-hydrogen (see Figure 25). If the molecule is crowded, there could be a Si-H contact at the first minimum, the energy change with respect to the Si-H contact being the same as at the second minimum and at points in excess of it, but with a reduction in other interligand repulsions causing the minimum. This second explanation requires a discontinuity of Si...H contacts whereas the first does not. At present, there is insufficient evidence to separate these since only one non-crowded hydrogen has been positively located (in  $\text{HFe}(\text{CO})_4\text{Si}(\text{C}_6\text{H}_5)_3$ ) and only two hydridic hydrogens in crowded environments (in  $(\pi\text{-C}_5\text{H}_5)\text{HMn}(\text{CO})_2\text{SiR}_3$ ,  $\text{R} = (\text{C}_6\text{H}_5)_3$  and  $\text{R} = \text{Cl}_2\text{C}_6\text{H}_5$ ). All compounds, except the latter two, studied in this series can place the hydrogen so that  $\text{C}\dots\text{H} \geq 2.0$  and  $\text{Si}\dots\text{H} \geq 2.2$  Å which are in accordance with the shortest cis ligand contacts observed between atoms attached to transition metals. Where anomalous contacts have been observed with group IV elements, a pseudo five coordination exists with no angular distortion of the firmly attached atoms. The fifth inter-

action, if interpreted as a weak bond, agrees with the secondary minimum explanation and adds the requirement that the minimum lie below zero energy in keeping with the definition of a bond.

The entire question of the acidity of the hydrogen in these molecules is confused, and at the present no hard and fast correlation between acid strength and structure is apparent. In fact, the more evidence available in the form of completed structures, the more obscure becomes the acidity message. For example,  $(\pi\text{-C}_5\text{H}_5)\text{HMn}(\text{CO})_2\text{Si}(\text{C}_6\text{H}_5)_3$  is a relatively weak acid ( $\text{H}^+$  is removed only by alcoholic base) while  $\text{HFe}(\text{CO})_4\text{Si}(\text{C}_6\text{H}_5)_3$  is a stronger acid ( $\text{H}^+$  can be removed with  $\text{P}(\text{OC}_6\text{H}_5)_3$ ), the first is sterically crowded, the second not, thus, sterically crowded molecules were thought to be weak acids because of the silicon-hydrogen interaction. This hypothesis is refuted by the structure of  $\text{cis}(\pi\text{-C}_5\text{H}_5)(\text{CO})_2\text{HReSi}(\text{C}_6\text{H}_5)_3$ <sup>72</sup> which is nonetheless a weak acid, even though the increase in transition metal covalent radius reduces interligand repulsions so that the hydrogen can be in a non-interacting position with respect to the silicon. Also, the most logical thermodynamic argument suggests that, provided the other ligands can remove the electron density, the crowded molecules would be the stronger acids, since the conjugate base formed is less crowded:





The relative electronegativities of the other ligands is also a factor in determining relative acidities:  $(\pi\text{-C}_5\text{H}_5)\text{HFe}(\text{CO})(\text{SiCl}_3)_2$  is a stronger acid than  $(\pi\text{-C}_5\text{H}_5)\text{HFe}(\text{CO})[\text{Si}(\text{CH}_3)_2\text{C}_6\text{H}_5]_2$  which can most likely be accounted for by the increased electronegativities of the trichlorosilyl groups enhancing the leaving ability of the hydrogen, rather than by some change in structure. Even though neither molecule is considered sterically crowded, there is a slight possibility of weak hydrogen-silicon interaction in the latter compound, since some inconclusive evidence (Table XLV) exists that shows the hydrogen prefers to locate closer to one silicon than the other. If such interaction were to be proved in the one compound and negated in the other (by a neutron diffraction study, for example), a potential energy diagram with a double minimum could be made which would allow two energetically stable positions for the hydrogen with respect to the silicon.

The use of infrared bands for transition metal-hydrogen stretches is a routine identification procedure in the study of transition metal carbonyl hydrides with bands occurring around  $1900\text{ cm}^{-1}$  (M-D stretches at about

1300  $\text{cm}^{-1}$  if the deuterated compounds are studied). In the study of transition metal carbonyl derivatives containing silicon and hydrogen, an attempt was made to find appropriate infrared bands (which were not always present) and to correlate them with the silicon hydrogen interaction.  $(\pi\text{-C}_5\text{H}_5)\text{HMn}(\text{CO})_2\text{Si}(\text{C}_6\text{H}_5)_3$  had no band identifiable as an Mn-H stretch in the infrared while  $(\pi\text{-C}_5\text{H}_5)\text{HMn}(\text{CO})_2\text{SiCl}_3$  did (1890  $\text{cm}^{-1}$ ). The triphenyl silyl compound had a structure with silicon-hydrogen interaction and this was believed to interfere with the production of an infrared Mn-H stretch. Since the trichlorosilyl compound did show a band, supposedly there was no silicon-hydrogen interaction and an electrostatic explanation for the differences was postulated. The region for Fe-H stretch in  $\text{HFe}(\text{CO})_4\text{Si}(\text{C}_6\text{H}_5)_3$  was obscured by the carbonyl stretching frequencies, but the stretch was expected to be absent anyway since the silicon substituents were identical to those of the manganese compound where silicon-hydrogen interaction was found. As Chapter 4 has shown, no silicon-hydrogen interaction exists here, and the electrostatic arguments were dropped in favor of the steric crowding hypothesis.  $(\pi\text{-C}_5\text{H}_5)\text{HMn}(\text{CO})_2\text{SiCl}_2\text{C}_6\text{H}_5$  has a Mn-H stretch at 1895  $\text{cm}^{-1}$ ; using electrostatic or infrared arguments it should have an unbridged hydrogen; using the steric crowding hypothesis, it should contain bridged hydrogen. In fact, this molecule has a bridging hydrogen. Thus, one of the more useful tools for eluci-

dating structure, infrared spectroscopy, has been shown to be useless in predicting silicon-hydrogen interaction in compounds of this type. While there is still a possibility of coordinating the intensities of the transition metal-hydrogen stretch with the nature of the silicon substituents, this is yet to be done.

While X-ray crystallography is not an ideal technique for locating hydrogen atoms in the presence of heavy atoms, its use in determining these structures has led to a better understanding of the factors influencing the hydrogen position. Specifically, these structures have shown that the major factor influencing the nature of the silicon-hydrogen interaction is steric hindrance with electrostatic factors of less importance. To clear up the exact nature of the hydrogen silicon interaction, it would be desirable to do neutron diffraction studies on some of these hydrides. These studies would locate the hydrogen atoms much more precisely. In addition, careful spectroscopic studies to determine the potential energy curves for silicon hydrogen interactions would be very useful.

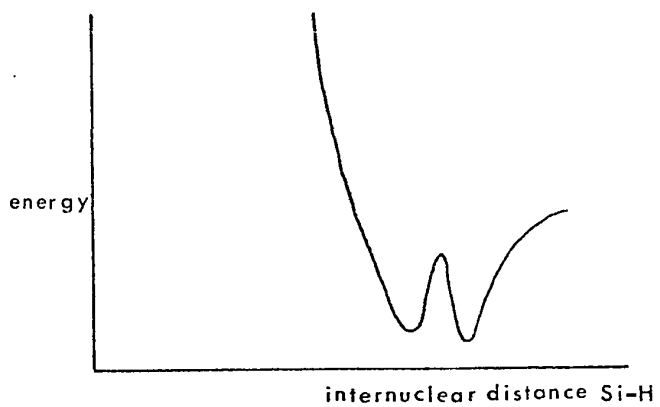


Figure 25: Potential energy diagram showing a double minimum.

REFERENCES

1. G. H. Stout and L. H. Jensen, X-Ray Structure Determination, Macmillan, New York (1968).
2. Donald E. Sands, Introduction to Crystallography, W. A. Benjamin, New York (1969).
3. D. M. Sayre, *Acta. Cryst.*, 5, 60 (1952).
4. A. E. Kitaigorodskii, The Theory of Crystal Structure Analysis, Consultants Bureau, New York (1961).
5. M. M. Woolfson, Direct Methods in Crystallography, Oxford University Press, New York (1961).
6. J. Karle in Advances in Structure Research by Diffraction Methods, R. Brill and B. Mason, eds., Wiley-Interscience, New York (1964), pp. 55-89.
7. W. C. Hamilton, *Norelco Reporter XII*, 31 (1965).
8. D. T. Cromer and J. T. Waber, *Acta. Cryst.* 18, 104 (1965).
9. D. T. Cromer, *Acta. Cryst.* 18, 17 (1965).
10. International Tables for X-Ray Crystallography, Volume III, Kynoch Press, Birmingham, England (1962).
11. R. Mason and G. B. Robertson in Advances in Structure Research by Diffraction Methods, R. Brill and B. Mason, eds., Wiley-Interscience, New York (1966).
12. R. F. Stewart, E. R. Davidson and W. T. Simpson, *J. Chem. Phys.* 42, 3175 (1964).
13. M. J. Bennett and W. L. Hutcheon, *Acta. Cryst.*, to be published.

14. W. C. Hamilton, *Acta. Cryst.* 18, 502 (1965).
15. W. Heiber and F. Leutert, *Naturwiss.*, 19, 360 (1931).
16. G. W. Coleman and A. A. Blanchard, *J. Amer. Chem. Soc.* 58, 2160 (1936).
17. G. Wilkinson and J. M. Birmingham, *J. Amer. Chem. Soc.* 77, 3421 (1955).
18. F. A. Cotton and G. Wilkinson, *Chem. and Ind.* 1956, 1305.
19. R. M. Stevens, C. W. Kern and W. N. Lipscomb, *J. Chem. Phys.* 37, 279 (1962).
20. L. L. Lohr and W. N. Lipscomb, *Inorg. Chem.* 3, 22 (1964).
21. A. D. Buckingham and P. J. Stephens, *J. Chem. Soc.* 2747, (1964).
22. R. Eisenberg and J. A. Ibers, *Inorg. Chem.* 4, 773 (1965).
23. P. G. Owston, J. M. Partridge and J. M. Rowe, *Acta. Cryst.* 13, 246 (1960).
24. P. L. Orioli and L. Vaska, *Proc. Chem. Soc.*, 333 (1962).
25. K. Knox and A. P. Ginsberg, *Inorg. Chem.* 3, 555 (1964).
26. S. C. Abrahams, A. P. Ginsberg and K. Knox, *Inorg. Chem.* 3 528 (1964).
27. S. L. La Placa, W. C. Hamilton, J. A. Ibers and A. Davison, *Inorg. Chem.* 8, 1928 (1969).
28. S. L. La Placa and J. A. Ibers, *J. Amer. Chem. Soc.* 85, 3501 (1963).

29. B. R. Davis, N. C. Payne and J. A. Ibers, *Inorg. Chem.* 8, 2719 (1969).
30. H. D. Kaesz, R. Bau and M. R. Churchill, *J. Amer. Chem. Soc.* 89, 2775 (1967).
31. R. J. Doedens, W. T. Robinson and J. A. Ibers, *J. Amer. Chem. Soc.* 89, 4323 (1967).
32. M. R. Churchill, P. H. Bird, H. D. Kaesz, R. Bau and B. Fontal, *J. Amer. Chem. Soc.* 90, 7135 (1968).
33. L. B. Handy, P. M. Treichel, L. F. Dahl and R. G. Hayter, *J. Amer. Chem. Soc.* 88, 366 (1966).
34. L. B. Handy, J. K. Ruff and L. F. Dahl, *J. Amer. Chem. Soc.* 92, 7312 (1970).
35. J. K. Hoyano, Ph.D. thesis, University of Alberta (1971),  
a) p. 63, b) p. 157.
36. W. Jetz, Ph.D. thesis, University of Alberta (1970),  
a) p. 194.
37. W. Jetz and W. A. G. Graham, *Inorg. Chem.* 10, 4 (1971).
38. A. Hart-Davis, private communication.
39. B. J. Aylett and J. M. Campbell, *Nucl. Chem. Lett.* 4,  
79 (1968).
40. B. J. Aylett and J. M. Campbell, *J. Chem. Soc. A*,  
2110 (1969).
41. E. Wood, private communication.



42. R. N. Haszeldine, R. V. Parish and D. J. Parrey,  
J. Chem. Soc. A, 683 (1969).
43. A. J. Chalk and J. F. Harrod, J. Amer. Chem. Soc. 87,  
16 (1965).
44. R. N. Haszeldine, R. V. Parish and D. J. Parrey, J.  
Organmet. Chem. 9, p. 13 (1967).
45. R. C. Taylor, C. F. Young and G. Wilkinson, Inorg.  
Chem. 5, 20 (1966).
46. J. Chatt, C. Eabon, P. N. Kapoor, J. Chem. Soc. A,  
881 (1970).
47. M. C. Baird, J. Inorg. Nucl. Chem. 29, 367 (1967).
48. A. J. Oliver and W. A. G. Graham, Inorg. Chem. 10, 1  
(1971).
49. J. K. Hoyano and W. A. G. Graham, J. Amer. Chem. Soc.,  
submitted for publication.
50. M. Elder, Inorg. Chem. 9, 762 (1970).
51. M. J. Bennett and T. E. Haas, in preparation.
52. M. J. Bennett and M. Cowie, in preparation.
53. R. J. Doedens and J. A. Ibers, Inorg. Chem. 6, 204  
(1967).
54. W. R. Busing and H. A. Levy, Acta. Cryst. 17, 142  
(1964).
55. L. F. Dahl, E. R. de Gil, R. D. Feltham, J. Amer.  
Chem. Soc. 91, 1653 (1969) and references therein.
56. V. A. Semian, Yu. A. Chapovskii, Yu. T. Struchkov and

- A. N. Nesmeyanov, *Chem. Commun.*, 666 (1968).
57. J. B. Wilford and H. M. Powell, *J. Chem. Soc. A*, 8 (1969).
58. M. E. Cradwick and D. Hall, *J. Organomet. Chem.* 25, 91 (1970).
59. M. Elder and D. Hall, *Inorg. Chem.* 8, 1273 (1969).
60. L. Pauling, *The Nature of the Chemical Bond*, Cornell University Press, Ithaca, New York (1960), a) p. 246, b) p. 256.
61. L. B. Handy, P. M. Treichel and L. F. Dahl, *J. Amer. Chem. Soc.* 88, 366 (1966).
62. M. J. Bennett and R. Mason, *Nature (London)*, 205, 760 (1965).
63. W. A. G. Graham, *Inorg. Chem.* 7, 315 (1968).
64. M. J. Bennett and W. L. Hutcheon, in preparation.
65. A. F. Wells, *Structural Inorganic Chemistry*, 3rd edition, Oxford University Press, London (1962), p. 696.
66. S. J. La Placa and J. A. Ibers, *Acta. Cryst.* 18, 511 (1965).
67. M. I. Davis and H. P. Hanson, *J. Phys. Chem.* 69, 3405 (1965).
68. H. M. Powell and R. V. G. Ewens, *J. Chem. Soc.* 1939, 286.

69. M. R. Churchill, *Inorg. Chem.* 6, 190 (1967).
70. J. Meunier-Piret, P. Piret, M. van Meerasche, *Acta. Cryst.* 19, 85 (1965).
71. M. R. Churchill and R. Bau, *Inorg. Chem.* 6, 2086 (1967).
72. R. A. Smith, private communication.
73. L. Manojlović-Muir, K. W. Muir and J. A. Ibers, *Inorg. Chem.* 9, 447 (1970).
74. A. F. Berndt and R. E. Marsh, *Acta. Cryst.* 16, 118 (1963).
75. M. J. Bennett and R. Mason, *Proc. Chem. Soc.* (1964), 395.
76. W. T. Robinson and J. A. Ibers, *Inorg. Chem.* 6, 1208 (1967).
77. K. W. Muir and J. A. Ibers, *Inorg. Chem.* 9, 440 (1970).
78. W. C. Hamilton and J. A. Ibers, Hydrogen Bonding in Solids, W.A. Benjamin, Inc., Amsterdam (1968), p. 62-63.
79. A. Faust, private communication.
80. R. W. Baker and P. Pauling, *J. Chem. Soc. D* 1495 (1969).
81. International Tables for X-ray Crystallography, Volume I, Kynoch Press, Birmingham, England (1962).
82. M. J. Bennett, *Doctoral Dissertation*, Sheffield University, 1965.
83. M. R. Churchill and J. P. Fennessy, *Inorg. Chem.* 6, 1213 (1967).

84. L. F. Dahl and R. E. Rundle, *Acta. Cryst.* 16, 419 (1963).
85. F. A. Cotton and G. Wilkinson, *Advanced Inorganic Chemistry*, Wiley, 1966, p. 105.
86. M. Tuggle, private communication.
87. W. L. Hutcheon, Ph.D. thesis, University of Alberta, 1971.
88. M. J. Bennett, F. A. Cotton, P. Legzdins and S. J. Lippard, *Inorg. Chem.* 7, 1770 (1968).
89. W. Jetz, private communication.
90. G. Wilkinson, M. Rosenblum, M. C. Whiting and R. B. Woodward, *J. Amer. Chem. Soc.* 74, 2125 (1952).
91. P. F. Eiland and R. Pepinsky, *J. Amer. Chem. Soc.* 74, 4971 (1952).
92. J. D. Dunitz and L. E. Orgel, *Nature, Lond.* 171, 121 (1953).
93. J. D. Dunitz, L. E. Orgel and A. Rich, *Acta. Cryst.* 9, 373 (1956).
94. M. J. Bennett and W. L. Hutcheon, in preparation.
95. R. K. Bohn and A. Haaland, *J. Organometal. Chem.* (Amsterdam), 5, 470 (1966).

Appendix A

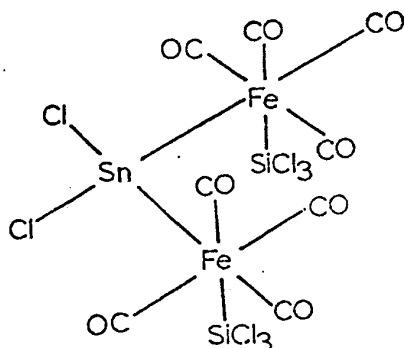
Structure of  $\text{Sn}(\text{Fe}(\text{CO})_4\text{SiCl}_3)_2\text{Cl}_2$

## EXPERIMENTAL

Yellow-orange crystals of  $\text{Sn}(\text{Fe}(\text{CO})_4\text{SiCl}_3)_2\text{Cl}_2$  were obtained in a form suitable for X-ray crystal study from W. Jetz. The parallelepiped crystals were mounted along their largest dimension and coated with shellac to retard decomposition. The preliminary photography obtained from several crystals consisted of  $\text{CuK}_\alpha$  Weissenberg's  $h0l$ ,  $h1l$ ,  $h2l$  and  $\text{MoK}_\alpha$  precession  $0kl$ . They showed the crystal to be orthorhombic with systematic absences  $0k0$ ,  $k = 2n+1$  and  $h00$ ,  $h = 2n+1$  which imply space group  $P2_12_12$ . Lattice parameters from film showed  $a = 11.82 \text{ \AA}$ ,  $b = 10.41 \text{ \AA}$ ,  $c = 9.86 \text{ \AA}$ . The observed density (2.15 gm/cc) obtained by flotation agrees with that calculated (2.174 gm/cc) for 2 molecules per unit cell, molecular weight 794.3 and unit cell volume  $1213.2 \text{ \AA}^3$ . The crystals decomposed to red-brown amorphous material in X-rays and so the structural determination was terminated at this point.

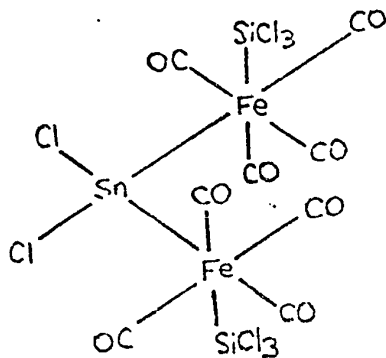
## DISCUSSION

The structure proposed for this compound<sup>89</sup> was:



This proposed structure has a mirror plane through the tin and its chlorine substituents.

For the space group  $P2_12_12$  with two molecules per unit cell, the coordinates of the equivalent positions are  $(x, y, z)$ ,  $(\bar{x}, \bar{y}, z)$ ,  $(\frac{1}{2}+x, \frac{1}{2}-y, \bar{z})$  and  $(\frac{1}{2}-x, \frac{1}{2}+y, \bar{z})$ . Thus the two tin atoms must occupy the special positions  $(0, 0, z)$  and  $(\frac{1}{2}, \frac{1}{2}, \bar{z})$ , and the remaining portion of each molecule the corresponding equivalent positions. Since these equivalent positions are related by a crystallographic 2-fold rotation axis rather than a mirror plane, the proposed structure is incorrect. A structure consistent with the crystallographic data is shown below:



Appendix B

Redetermination of the Crystal Structure of Ferrocene



## INTRODUCTION

The sandwich structure of bis-cyclopentadienyl iron (ferrocene) suggested in 1952<sup>90</sup> and confirmed by X-ray crystal structure in 1952<sup>91</sup> and 1953<sup>92</sup> was determined in detail by Dunitz, Orgel and Rich in 1956.<sup>93</sup> This appendix describes a reinvestigation of this crystal structure. A reexamination of the structure was considered desirable in order to apply some of the newer techniques to the description of the motion of the cyclopentadienyl rings, that is, to treat the rings as hindered rotors. Additionally, a comparison was wanted between ferrocene and ferrocenium picrate,  $(\text{Fe}(\text{C}_5\text{H}_5)_2^+)(\text{H}_3\text{C}_6\text{N}_3\text{O}_7^-)$ <sup>94</sup> in terms of bond distances, thermal motion, barrier to rotation and so on.

## EXPERIMENTAL

Ferrocene crystals suitable for X-ray crystallography were obtained from Dr. B. G. Kratochvil. An orange needle was mounted along the needle axis and coated with snellac. As expected, the preliminary photographs--CuK $_{\alpha}$  Weissenbergs hk0, hkl, hk2 and MoK $_{\alpha}$  precession h0 $\ell$ --showed the crystal to be monoclinic with systematic absences 0k0 for k = 2n+1 and h0 $\ell$  for h+ $\ell$  = 2n+1. These absences are characteristic of space group P2 $_1$ /n, a non-standard setting of P2 $_1$ /c. Lattice parameters a = 5.9340(13) Å, b = 7.6104(4) Å, c = 9.0437(7) Å and  $\beta$  = 93.206(16) $^{\circ}$  were obtained from least squares analysis of high angle reflections. The density by flotation was 1.49 gm/cc and is in good agreement with that calculated (1.502 gm/cc) for Z = 2, unit cell volume 407.8 Å $^3$  and molecular weight 185.1.

The crystal used for data collection was of approximate dimensions 0.35 x 0.12 x 0.15 mm and was bounded by faces of the form {011} and {100}. It was mounted with a\* coincident with the  $\phi$  axis of the diffractometer. Intensity data were collected using CuK $_{\alpha}$  radiation with a peak scan of  $2\theta$  range of 2 $^{\circ}$ , a  $2\theta$  maximum limit of 125 $^{\circ}$  and with 30 second backgrounds. Decomposition (most probably sublimation) dependent on time and  $\sin\theta/\lambda$  was observed and corrected for using the standard reflections. At the com-

pletion of data collection, the high  $\sin\theta/\lambda$  reflection had fallen to about 80% of its initial value.

An absorption correction ( $\mu = 144.8 \text{ cm}^{-1}$ ) was applied with the transmission factor range being 0.21 to 0.41. The scan data (400 reflection) after correction showed an internal consistency of  $\pm 4\%$ . Of the 647 independent reflections measured, 485 were estimated to be significantly above background using a criterion  $I/\sigma(I) \leq 3.0$ .

## SOLUTION AND REFINEMENT

The iron atom occupies the special position (0, 0, 0). The coordinates of the carbon atoms in the cyclopentadienyl ring were obtained by transforming the coordinates for the  $P2_1/a$  cell given by Dunitz, Orgel and Rich<sup>93</sup> to the  $P2_1/n$  cell. The a and c axes were interchanged on conversion from one cell to the other. The transformation effected was:

$$\begin{bmatrix} 1 & 0 & 1 \\ 0 & 1 & 0 \\ 1 & 0 & 0 \end{bmatrix} \begin{bmatrix} x_a \\ y_a \\ z_a \end{bmatrix} = (x_n \ y_n \ z_n)$$

where  $x_a, y_a, z_a$  refer to the  $P2_1/a$  cell and  $x_n, y_n, z_n$  refer to the  $P2_1/n$  cell. The coordinates so obtained were used in a least squares refinement. Two of the cyclopentadienyl carbons failed to refine, and on preparation of a model, the Dunitz et al x coordinates for  $C_4$  and  $C_5$  were found to be incorrect (Table LV). The hydrogen atoms were positioned 1 Å from the ring carbons and in the plane of the ring with isotropic temperature factors of 5.0. Neither the positions nor the temperature factors for the hydrogen atoms were refined.

With the corrected  $C_4$  and  $C_5$  coordinates and all atoms isotropic, three cycles of refinement with the twenty-

two variables gave  $R_1 = 0.137$  and  $R_2 = 0.158$ . When the carbon ring was refined as a hindered rotor and the hydrogen atoms were placed in a hindered rotor identical to that for the carbon atoms, but with the ring radius  $1 \text{ \AA}$  larger, the number of variables fell to eleven and least squares refinement gave  $R_1 = 0.119$  and  $R_2 = 0.136$ . On allowing the iron atom to have anisotropic temperature factors and taking into account its anomalous dispersion, the R factors dropped to  $R_1 = 0.077$  and  $R_2 = 0.090$  in five cycles. During the final cycle of least squares refinement, no parameters shifted by more than 0.2 of its estimated standard deviation. The final standard deviation of an observation of unit weight was 1.81.

Table LVI gives the absolute values for the observed and calculated structure factor amplitudes,  $10|F_o|$  and  $10|F_c|$ . Positional parameters and temperature factors are given in Table LVII.

Table LV

## Positional Coordinates

	$P2_1/a^{93}$			Derived $P2_1/n$ (a)			Corrected and Refined $P2_1/n$ (b)		
	$\underline{x}$ (c)	$\underline{y}$	$\underline{z}$	$\underline{x}$	$\underline{y}$	$\underline{z}$	$\underline{x}$	$\underline{y}$	$\underline{z}$
C <sub>1</sub>	0.0619	0.2613	0.0306	0.0475	0.2613	0.0169	0.0636	0.2630	0.0185
C <sub>2</sub>	0.0447	0.1767	0.2103	0.2551	0.1767	0.0447	0.2657	0.1780	0.0415
C <sub>3</sub>	0.1612	0.0590	0.0873	0.2503	0.0590	0.1612	0.2499	0.0664	0.1601
C <sub>4</sub>	0.2183	0.0787	0.1733	0.3923	0.0787	0.2183	0.0430 (d)	0.0728	0.2219
C <sub>5</sub>	0.1352	0.1963	0.2267	0.3627	0.1963	0.1352	-0.0990 (d)	0.1931	0.1454

(a) Derived by transformation of  $P2_1/a$  to  $P2_1/n$  with interchange of a and c axes.

(b) All atoms at this point were isotropic and individual.

(c) Fractional coordinates.

(d) Coordinates which were corrected.

## Table LVI

Observed and Calculated Structure Factor Amplitudes  
 $10|F_o|$  and  $10|F_c|$





Table IVII  
A) Hindered Rotor Parameters (a)

	$\underline{x}$	$\underline{y}$	$\underline{z}$	$\underline{B}$	$\underline{Bd}$	$\underline{R}$	$\underline{D}$	$\underline{E}$	$\underline{\xi}$
C ring	0.0944 (8)	0.1552 (7)	0.1156 (5)	3.6 (1)	0.75 (5)	1.204 (4)	2.321 (5)	0.485 (6)	6.04 (1)
H ring	0.0944	0.1552	0.1156	3.6	0.75	2.204	2.321	0.485	6.04

B) Hindered Rotor Atoms: Derived Positional Coordinates

	$\underline{x}$	$\underline{y}$	$\underline{z}$	Fe Temperature Factors (b)
C <sub>1</sub>	0.039 (2)	0.263 (1)	0.023 (1)	$\beta_{11}$ 0.0270 (6)
C <sub>2</sub>	0.253 (1)	0.181 (1)	0.041 (1)	$\beta_{22}$ 0.0104 (3)
C <sub>3</sub>	0.248 (1)	0.063 (1)	0.162 (1)	$\beta_{33}$ 0.0098 (2)
C <sub>4</sub>	0.031 (2)	0.073 (1)	0.219 (1)	$\beta_{12}$ -0.0009 (5)
C <sub>5</sub>	-0.098 (1)	0.196 (1)	0.133 (1)	$\beta_{13}$ -0.0002 (2)
H <sub>1</sub>	-0.005	0.353	-0.054	$\beta_{23}$ -0.0022 (3)
H <sub>2</sub>	0.385	0.202	-0.020	Equivalent B 3.144
H <sub>3</sub>	0.374	-0.013	0.201	
H <sub>4</sub>	-0.024	0.004	0.304	
H <sub>5</sub>	-0.258	0.231	0.147	

(a) These have their same meanings as in previous chapter.

(b) Anisotropic are defined by  $\exp(-\beta_{11}h^2 + \beta_{22}k^2 + \beta_{33}l^2 + 2\beta_{12}hk + 2\beta_{13}hl + 2\beta_{23}kl)$ .

## DISCUSSION

A drawing of the ferrocene molecule is given in Figure 26. The barrier to rotation of the ring implies a root mean square libration of about  $15\frac{1}{2}^\circ$ , a rather large oscillation which indicates that some errors can be expected in carbon-carbon bond lengths found using an individual atom approach. The temperature factor of the ring being just 0.44 above that of the iron suggests the motion of the ring is indeed in the plane perpendicular to the iron-ring centroid direction, another indication of the appropriateness of the hindered rotor model.

A comparison of ferrocene with the cyclopentadienyl rings as hindered rotors to ferrocene as determined in 1956 by Dunitz, Orgel and Rich is given in Table LVIII. As can be seen, the iron carbon distances average to identical values within experimental error, while the carbon-carbon distances in the hindered rotor refinement are slightly longer reflecting the inclusion of the ring motion. These carbon-carbon distances agree fairly well with those found in an electron diffraction experiment<sup>95</sup> ( $1.42(3) \text{ \AA}$ ) of ferrocene vapor at  $140^\circ\text{C}$ .

Ferrocene can also be compared with other similar compounds, and as was mentioned in the introduction, one of the purposes for this redetermination was to compare

it with ferrocenium picrate. The iron-carbon distances are longer (2.070 Å (av.)) in the latter which has eclipsed rings while the carbon-carbon distances are shorter (1.395 Å) and Hutcheon gives a detailed discussion<sup>87</sup> in terms of molecular orbitals for these differences.

In conclusion, the determination of this structure allowed the rudiments of X-ray crystallography to be learned without undue expenditure in time or money while producing some useful information.

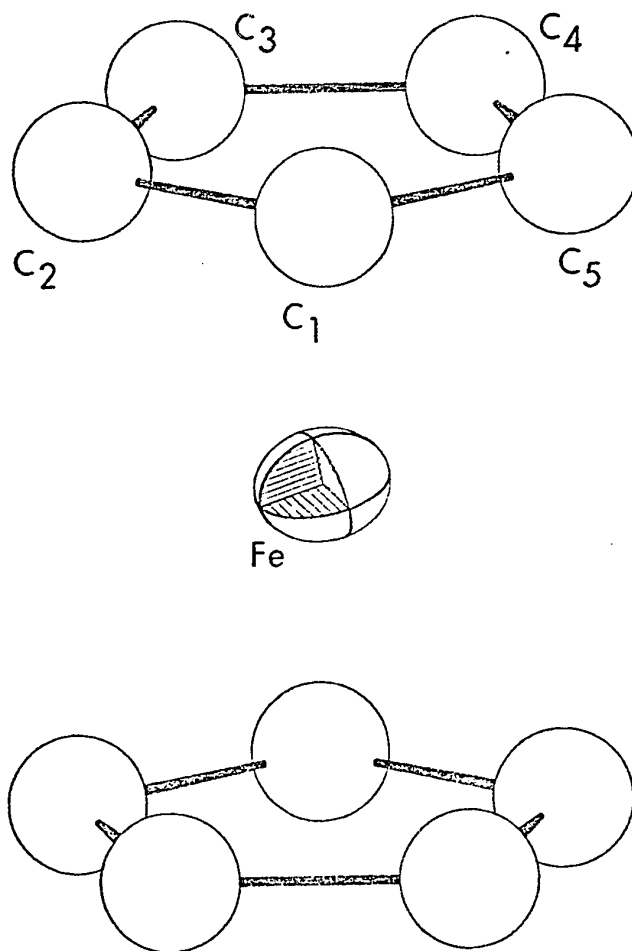


Figure 26

Perspective Drawing of Ferrocene

Table LVIII

	<u>Dunitz, Orgel, Rich Ferrocene</u>		<u>Hindered Rotor Ferrocene</u>	
	<u>Distances (Å)</u>	<u>Ring A</u>	<u>Ring B</u>	<u>Distances (Å)</u>
Fe-C1	1.994 (31)	2.010 (24)	Fe-C1	2.053 (7)
Fe-C2	2.059 (31)	2.050 (24)	Fe-C2	2.073 (7)
Fe-C3	2.078 (31)	2.069 (24)	Fe-C3	2.057 (7)
Fe-C4	2.074 (31)	2.070 (24)	Fe-C4	2.026 (7)
Fe-C5	2.034 (31)	2.024 (24)	Fe-C5	2.024 (8)
Fe-C (av.)	2.048	2.045	Fe-C (av.)	2.047 (5)
C1-C2	1.396 (35)	1.403 (40)	C-C (av.)	1.416 (4)
C2-C3	1.400 (35)	1.386 (40)		
C3-C4	1.365 (35)	1.352 (40)		
C4-C5	1.413 (35)	1.399 (40)		
C5-C1	1.471 (35)	1.476 (40)		
C-C (av.)	1.409	1.403 (40)		

Appendix C

DREFINE, a Program in FORTRAN to Obtain Accurate  
Cell Parameters

## DREF

The program DREF was written originally in order to obtain accurate cell parameters with an estimate of their standard deviations from a least-squares analysis of a number of hkl planes. It is intended for use with data obtained from the Picker manual four-circle diffractometer without the monochromator. Reflections of high  $\sin\theta/\lambda$  values are accurately centred in the window of the counter by appropriate adjustment of  $\omega$ ,  $\phi$ ,  $\chi$  and  $2\theta$ . The  $2\theta$  values of the accurately centred peaks are used in this program. Best results are obtained using  $\text{CuK}_{\alpha 1}$  radiation, with at least three reflections per parameter: for example, a minimum of 9 for an orthorhombic or 18 for a triclinic. Results can be improved by taking more planes, by having a number of widely varying hkl values, and/or by using extremely high  $2\theta$  values.

A brief discussion of the theory<sup>1</sup> involved in DREF follows. The d-spacing in a crystal can be expressed as:

$$\frac{1}{d^2} = h^2 a^{*2} + k^2 b^{*2} + l^2 c^{*2} + 2hka^*b^*\cos\gamma^* + 2hla^*c^*\cos\beta^* + 2klb^*c^*\cos\alpha^*$$

$$= f_{\text{calc}}(a^*, b^*, c^*, \alpha^*, \beta^*, \gamma^*) \quad (1)$$

It can be measured at several hkl values and is related to the  $2\theta$  angle measured on the diffractometer by Bragg's

Law:

$$2\sin\theta = n\lambda\left(\frac{1}{d}\right) \quad (2)$$

The principle of least squares states that the best values for the parameters  $a^*$ ,  $b^*$ ,  $c^*$ ,  $\alpha^*$ ,  $\beta^*$ ,  $\gamma^*$  are those which minimize the sums of the squares of the properly weighted differences between the observed and calculated values of the function for all observational points. In this case the quantity to be minimized is given by:

$$D = \sum_{r=1}^m w_r \left[ \left(\frac{1}{d}\right)_{\text{obs}}^2 - \left(\frac{1}{d}\right)_{\text{calc}}^2 \right]^2 \quad (3)$$

with  $w_r$  placing more emphasis on the highest  $\sin\theta/\lambda$  values and  $m$  being the number of observations. So the parameters  $a^*$ ,  $b^*$ ,  $c^*$ ,  $\alpha^*$ ,  $\beta^*$ ,  $\gamma^*$  are considered as variables to be adjusted to minimize this  $D$ . This is done by differentiating the right hand side of (3) with respect to each of the parameters in turn and setting the derivative to zero:

$$\sum_{r=1}^m w_r^2 \left[ \left(\frac{1}{d_r}\right)_{\text{obs}} - \left(\frac{1}{d_r}\right)_{\text{calc}} \right] \left[ \frac{\partial}{\partial p} \left(\frac{1}{d_r}\right)_{\text{calc}} \right] = 0 \quad (4)$$

$p = a^*, b^*, c^*, \alpha^*, \beta^*, \gamma^*$

These are the normal equations.

Because  $\frac{1}{d^2}$  is a non-linear function, it is necessary to approximate it by a Taylor series before attempting to solve the set of simultaneous equations given by (4):



$$f(a^*, b^*, c^*, \alpha^*, \beta^*, \gamma^*) \cong f(a^{*'}, b^{*'}, c^{*'}, \alpha^{*'}, \beta^{*'}, \gamma^{*'}) + \frac{\partial f(a^{*'} \dots \gamma^{*'})}{\partial a^*} (a^* - a^{*'}) + \dots + \frac{\partial f(a^{*'} \dots \gamma^{*'})}{\partial \gamma^*} (\gamma^* - \gamma^{*'}) \quad (5)$$

where  $a^{*'} \dots \gamma^{*'}$  are approximate values of  $a^* \dots \gamma^*$ . Application of a least-squares process to the linear equations obtained by substituting (5) into (4) will give values for  $(a^* - a^{*'}) \dots (\gamma^* - \gamma^{*'})$  such that  $a^{*'} = a^{*'} + (a^* - a^{*'}) \dots \gamma^{*' = \gamma^{*' + (\gamma^* - \gamma^{*'})}$  are better approximations to the best values for the parameters  $a^* \dots \gamma^*$  than the initial  $a^{*'} \dots \gamma^{*'}$ . Because the Taylor series was truncated at the first derivative level, the calculations outlined above must be repeated until convergence takes place. In this program, convergence is considered complete when

$$\frac{\Delta p}{\sqrt{p \sum (f_{\text{obs}} - f_{\text{calc}})^2}} \leq 0.1 \quad (6)$$

where  $\Delta p$  is the change in parameter  $p$ ,  $f_{\text{obs}}$  and  $f_{\text{calc}}$  are the observed and calculated  $\frac{1}{d}$  values for the  $hkl$  plane, the summation is over all  $hkl$  planes and  $w$  is an appropriate weighting factor.

To simplify the programming for all crystal systems and at the same time to ensure that the interrelations of the parameters  $a^* \dots \gamma^*$  are accounted for, particularly in the error terms, equation 1 was rewritten as:

$$\begin{aligned}
\frac{1}{d^2} = & h^2 (p_1 a^{*2} + p_2 b^{*2} + p_3 c^{*2}) + k^2 (p_4 a^{*2} + p_5 b^{*2} + p_6 c^{*2}) + \ell^2 (p_7 a^{*2} + p_8 b^{*2} + p_9 c^{*2}) \\
& + 2hk (p_1 a^* + p_2 b^* + p_3 c^*) (p_4 a^* + p_5 b^* + p_6 c^*) (q_1 \cos \alpha^* + q_2 \cos \beta^* + q_3 \cos \gamma^*) \\
& + 2h\ell (p_1 a^* + p_2 b^* + p_3 c^*) (p_7 a^* + p_8 b^* + p_9 c^*) (q_4 \cos \alpha^* + q_5 \cos \beta^* + q_6 \cos \gamma^*) \\
& + 2k\ell (p_4 a^* + p_5 b^* + p_6 c^*) (p_7 a^* + p_8 b^* + p_9 c^*) (q_7 \cos \alpha^* + q_8 \cos \beta^* + q_9 \cos \gamma^*) \quad (7)
\end{aligned}$$

and the least squares procedure carried out on this expanded form. The correct set of p and q vectors is generated within the program when the user selects an appropriate crystal system indicator. For example, for a monoclinic system, the indicator is 2 and  $p(i) = (100010001)$  and  $q(i) = (001010100)$  while for a rhombohedral crystal, the indicator is 5 and  $p(i) = (100010001)$  and  $q(i) = (000000000)$ .

Since both input and output is desired in the form of direct lattice parameters and equation 7 is in terms of reciprocal lattice parameters, it is necessary to convert from one to the other using the usual relationships. (See General Crystallographic Introduction Table IV)

The error terms are calculated by evaluating the derivatives of the direct lattice parameter with respect to each of the reciprocal lattice parameters, summing the squares of all terms and then taking the square root. That is,

$$\text{Error} = \left( \sum_j \frac{\partial a}{\partial p_j}^2 \right)^{1/2} \quad \text{where } p_j = a^*, b^*, c^*, \alpha^*, \beta^*, \gamma^*. \quad (8)$$

and a can be replaced by b, c,  $\alpha$ ,  $\beta$ ,  $\gamma$ .

The input to the program consists of the following:

- 1) Title card (18A4)
- 2) Cell card  $a, b, c, \alpha, \beta, \gamma$  in Å and ° respectively,  $2\theta_0$ , the input  $2\theta$  value (usually 0 and corresponding to  $2\theta_0$  for the instrument) (7F10.5)
- 3) Wavelength of radiation (F10.5)
- 4) a) Parameters to be varied:  $a, b, c, \alpha, \beta, \gamma, 2\theta_0$ ; 0 - do not vary; 1 - vary.  
b) Crystal system: 1-triclinic, 2-monoclinic, 3-orthorhombic, 4-tetragonal, 5-rhombohedral, 6-hexagonal, 7-cubic. (8I1)
- 5) Planes and  $2\theta$  values (3I4, F10.2)
- 6)  $h = 99$  terminates data set

The output gives the following information:

- 1) Title
- 2) Listing of  $hkl$  planes and corresponding values for  $2\theta_{\text{obs}}$ ,  $2\theta_{\text{calc}}$ ,  $\frac{1}{d_{\text{obs}}}$  and  $\frac{1}{d_{\text{calc}}}$
- 3) Estimate of variance
- 4) Old parameters, their shift, new parameters, and cor-

responding error terms

- 5) A repeat of 2) to 4) for each cycle until convergence is reached.

A listing of DREF, a sample set of input and the corresponding output for the monoclinic crystal system follow. The program requires only a few seconds for operation and is routinely activated from a terminal.

C  
C  
C  
C  
C  
C

\*\*\* DREF, A PROGRAM TO REFINE CELL PARAMETERS BY LEAST SQUARES

COMMON A(7),KI(7),H(3,100),FO(100),FC(100),ND,NV,J,C(6),S(6),DEL  
COMMON AN(28),V(7),VO,AS(6),CSS(6),SNS(6),WGT(100),P(9),O(9),W  
COMMON CON,RAD  
DIMENSION TEMP(7),TEM0(7),AZZ(6),AP(6),EA(3,4),SAA(6),SRT2(3)  
DIMENSION IH(3),SA(7),XA(7),AZ(6),SS(6),TITLE(18),CONV(100)

C  
C  
C

\*\*\*FORMATS

88 FORMAT (18A4)  
89 FORMAT ('1',18A4)  
90 FORMAT(3I4,F10.2)  
91 FORMAT(' VOLUME='F8.2)  
92 FORMAT (' MATRIX IS SINGULAR')  
93 FORMAT (8I1)  
94 FORMAT (7F10.5/F10.5)  
95 FORMAT (' '4F10.4)  
96 FORMAT ('0 OLD SHIFT NEW ERROR')  
97 FORMAT ('0 VARIANCE ESTIMATE IS 'E12.4)  
98 FORMAT (' '3I4,2F10.3,2F10.6)  
99 FORMAT ('0 H K L THO THC FO FC')  
100 FORMAT(' LAMDA='F7.5, ' 2\*THETA 0='F6.3)

C  
C  
C

\*\*\* READ IN DATA

RAD=180.0/3.1415927  
ND=0  
READ (5,88) TITLE  
WRITE (6,89) TITLE  
READ(5,94) (A(I),I=1,7),W  
WRITE(6,100) W,A(7)  
READ(5,93) (KI(I),I=1,7),IND

C  
C  
C

\*\*\* CHOOSE P,O VECTORS APPROPRIATE TO CRYSTAL SYSTEM

DO 101 I=1,9  
P(I)=0.0  
101 O(I)=0.0  
IF (IND.EQ.5) GO TO 1021  
DO 1020 I=3,7,2  
1020 Q(I)=1.0  
IF (IND.EQ.4.OR.IND.EQ.6.OR.IND.EQ.7) GO TO 1023  
DO 102 I=1,9,4  
102 P(I)=1.0  
GO TO 104  
1021 DO 1022 I=1,9,4  
1022 Q(I)=1.0  
1023 DO 1024 I=1,4,3  
1024 P(I)=1.0  
IF (IND.EQ.4.OR.IND.EQ.6) GO TO 1025  
P(7)=1.0  
GO TO 104

```

1025 P(9)=1.0
C
C   *** READ IN REMAINING DATA
C
104 ND=ND+1
   READ(5,90) (IH(I),I=1,3),CON
   IF(IH(1).GE.99) GO TO 120
   DO 108 I=1,3
   H(I,ND)=IH(I)
108 CONTINUE
C
C   *** WEIGHTING FUNCTION CALCULATED
C
   CONV(ND)=CON
   WGT(ND)=SIN((CON+A(7))/(2.0*PI))
   FO(ND)=(2.*WGT(ND)/W)**2
   GO TO 104
120 ND=ND-1
C   ****PREPARE CONSTANTS
   NV=0
   DO 150 I=1,7
   NV=NV+K1(I)
150 CONTINUE
235 CONTINUE
201 DO 220 I=1,3
   C(I)=COS(A(I+3)/PI)
   C(I+3)=C(I)
   S(I)=SIN(A(I+3)/PI)
   S(I+3)=S(I)
220 CONTINUE
   DO 221 I=1,3
   AS(I)=A(I)
221 AS(I+3)=AS(I)
   VO=AS(1)*AS(2)*AS(3)*SQRT(1.0-C(1)*C(1)-C(2)*C(2)-C(3)*C(3)+2.0*
1 C(1)*C(2)*C(3))
   WRITE(6,91) VO
   DO 222 I=1,3
   AS(I)=AS(I+1)*AS(I+2)*S(I)/VO
222 CSS(I)=(C(I+1)*C(I+2)-C(I))/(S(I+1)*S(I+2))
   DO 223 I=1,7,3
   TEMO(I)=Q(I)*CSS(1)+Q(I+1)*CSS(2)+Q(I+2)*CSS(3)
223 TEMP(I)=AS(1)*P(I)+AS(2)*P(I+1)+AS(3)*P(I+2)
   J=1
   JJ=7
   DO 224 I=1,3
   CSS(I)=TEMO(JJ)
   AS(I)=TEMP(J)
   J=J+3
   JJ=JJ-3
   CSS(I+3)=CSS(I)
   AS(I+3)=AS(I)
224 SNS(I)=SQRT(1.0-CSS(I)*CSS(I))
C
C   ****CONTROL RETURNS HERE TO START NEXT CYCLE
C
   DO 240 I=1,28
   AN(I)=0.0
240 CONTINUE
   DO 250 I=1,7
   V(I)=0.0

```

```

250 CONTINUE
DEL=0.0
C
C   *** LOOP THROUGH DATA
C
WRITE(6,99)
DO 300 J=1,ND
CON=CONV(J)
CALL CALC
DO 260 I=1,3
IH(I)=H(I,J)
260 CONTINUE
CC=SQRT(FC(J))*W/2.0
CC=2.*ARCSIN(CC)*RAD-A(7)
WRITE(6,98) (IH(I),I=1,3),CON,CC,FO(J),FC(J)
DEL=DEL+(FO(J)-FC(J))*2*WGT(J)
300 CONTINUE
CALL SMI(AN,NV,ISING)
IF(ISING.EQ.0) GO TO 320
WRITE(6,92)
GO TO 600
C
C   *** DEL IS VARIANCE
C
320 DEL=DEL/FLD(ND-NV)
WRITE(6,97) DEL
DO 340 I=1,NV
IJ=I
IJD=NV-I
EP=0.0
DO 335 J=1,NV
EP=EP+AN(IJ)*V(J)
IF(J-I) 330,331,332
330 IJ=IJ+IJD
IJD=IJD-1
GO TO 335
331 SA(I)=AN(IJ)
332 IJ=IJ+1
335 CONTINUE
XA(I)=EP
340 CONTINUE
C
C   *** CONVERGENCE TEST
C
KON=0
DO 350 I=1,NV
SA(I)=SQRT(ABS(SA(I))*DEL)
SS(I)=ABS(XA(I))/SA(I)
IF(SS(I).GT.0.1) KON=1
350 CONTINUE
I=0
DO 400 N=1,3
IF (KI(N).EQ.0) GO TO 390
I=I+1
AZ(N)=AS(N)+XA(I)
GO TO 400
390 AZ(N)=AS(N)
400 CONTINUE
DO 500 N=1,3
IF (KI(N+3).EQ.0) GO TO 490

```

```

I=I+1
AZZ(N)=(ARCOS(CSS(N))+XA(I))
SAA(N)=SA(I)
GO TO 500
490 AZZ(N)=ARCOS(CSS(N))
SAA(N)=0.0
500 AZZ(N+3)=AZZ(N)
DO 499 I=1,7,3
TEMP(I)=AZ(I)*P(I)+AZ(2)*P(I+1)+AZ(3)*P(I+2)
499 TEMQ(I)=COS(AZZ(I))*Q(I)+COS(AZZ(2))*Q(I+1)+COS(AZZ(3))*Q(I+2)
J=1
JJ=7
DO 501 I=1,3
AZ(I)=TEMP(J)
CSS(I)=TEMQ(JJ)
J=J+3
JJ=JJ-3
CSS(I+3)=CSS(I)
AS(I)=AZ(I)
AS(I+3)=AS(I)
SNS(I)=SQRT(1.0-CSS(I)*CSS(I))
501 SNS(I+3)=SNS(I)
VNR=AZ(1)*AZ(2)*AZ(3)*SQRT(1.0-CSS(1)*CSS(1)-CSS(2)*CSS(2)-CSS(3)
1CSS(3)+2.0*CSS(1)*CSS(2)*CSS(3))
SRT1=1.0/SQRT(1.0-CSS(1)*CSS(1)-CSS(2)*CSS(2)-CSS(3)*CSS(3)+2.0
1*CSS(1)*CSS(2)*CSS(3))
WRITE (6,96)
J=1
I=0
K=7
DO 520 N=1,3
IF (KI(N).EQ.0) GO TO 510
I=I+1
AP(N)=AS(N+1)*AS(N+2)*SNS(N)/VNR
XA(I)=AP(N)-A(N)
C
C
C
** EA ARE ERROR TERMS
EA(N,1)=SNS(N)*SRT1/(AZ(N)*AZ(N)*P(J))*SA(I)
DO 503 M=1,3
503 EA(N,M+1)=(SIN(AZZ(M))*SAA(M)*SRT1/AS(N))*(Q(K+M-1)*CSS(N)-SNS(N)*
1SRT1**2*(CSS(1)*Q(M)+CSS(2)*Q(M+3)+CSS(3)*Q(M+6)-CSS(1)*CSS(2)*Q(M
1+6)-CSS(3)*(CSS(1)*Q(M+3)+CSS(2)*Q(M))))
K=K-3
SA(I)=0.0
DO 504 JJ=1,4
504 SA(I)=SA(I)+EA(N,JJ)*EA(N,JJ)
SA(I)=SORT(SA(I))
WRITE (6,95) A(N),XA(I),AP(N),SA(I)
A(N)=AP(N)
GO TO 520
510 A(N)=AS(N+1)*AS(N+2)*SNS(N)/VNR
WRITE (6,95) A(N)
520 J=J+4
L=3
DO 550 N=4,6
IF (KI(N).EQ.0) GO TO 530
I=I+1
AP(N)=ARCCS((CSS(2)*CSS(3)-CSS(1))/(SNS(2)*SNS(3)))*RAD
XA(I)=AP(N)-A(N)

```



```

SRT2(N-3)=-1./SQRT(1.-((CSS(2)*CSS(3)-CSS(1))/(SNS(2)*SNS(3))**2))
DO 508 M=1,3
508 EA(N-3,M)=SAA(M)*SRT2(N-3)*SIN(AZZ(M))*((CSS(2)*CSS(3)-CSS(1))
1*(-CSS(3)*Q(M))/(SIN(ARCOS(CSS(2)))*SIN(ARCOS(CSS(3))))**2
2*SQRT(1.0-CSS(3)**2))-CSS(2)*Q(M+3)/(SIN(ARCOS(CSS(3))))
3*SIN(ARCOS(CSS(2)))*SQRT(1.0-CSS(2)**2))+(-CSS(2)*Q(M)-CSS(3)*
4Q(M+3)+Q(M+6))/(SIN(ARCOS(CSS(2)))*SIN(ARCOS(CSS(3))))
524 SA(I)=0.0
DO 506 J=1,3
506 SA(I)=SA(I)+EA(N-3,J)*EA(N-3,J)
SA(I)=SQRT(SA(I))*RAD
WRITE (6,95) A(N),XA(I),AP (N),SA(I)
A(N)=AP(N)
GO TO 540
530 A(N)=ARCOS((CSS(2)*CSS(3)-CSS(1))/(SNS(2)*SNS(3)))*RAD
WRITE (6,95) A(N)
540 TEM=CSS(1)
CSS(1)=CSS(N-2)
CSS(N-2)=TEM
TEM=SNS(1)
SNS(1)=SNS(N-2)
SNS(N-2)=TEM
IF (L.EQ.-3) GO TO 522
DO 521 II=1,3
TEMQ(II)=Q(II+6)
Q(II+6)=Q(II+L)
521 Q(II+L)=TEMQ(II)
L=L-3
GO TO 550
522 DO 523 II=1,3
TEMQ(II)=Q(II+3)
Q(II+3)=Q(II)
Q(II)=Q(II+6)
523 Q(II+6)=TEMQ(II)
550 CONTINUE
DO 560 I=2,3
CSS(I)=CSS(I+1)
560 SNS(I)=SNS(I+1)
CSS(4)=CSS(1)
SNS(4)=SNS(1)
IF (KI(7).EQ.0) GO TO 580
XA(NV)= 2.*XA(NV)*RAD
SA(NV)= 2.*SA(NV)*RAD
AP(NV)= A(7)+XA(NV)
WRITE(6,95) A(7),XA(NV),AP(NV),SA(NV)
A(7)= AP(NV)
DO 570 I=1,ND
WGT(I)=SIN((CCNV(I)+A(7))/(2.0*RAD))
570 FO(I)=(2.0*WGT(I)/W)**2
580 IF (KON.EQ.1) GO TO 235
600 STOP
END

```

C  
C  
C  
C  
C  
C  
C

SUBROUTINE CALC

\*\*\* CALCULATES DERIVATIVES USED IN TAYLOR EXPANSION, 1/D FUNCTION

COMMON A(7),KI(7),H(3,100),FO(100),FC(100),ND,NV,J,C(6),S(6),DEL

```

COMMON AN(28),V(7),V0,AS(6),CSS(6),SNS(6),WGT(100),P(9),Q(9),W
COMMON CON,RAD
DIMENSION HA(6),DF(7),PT(7),QT(7)
DO 200 I=1,3
HA(I)=H(I,J)
200 HA(I+3)=HA(I)
N=0
DO 210 L=1,7,3
QT(L)=0(L)*CSS(1)+Q(L+1)*CSS(2)+Q(L+2)*CSS(3)
210 PT(L)=P(L)*AS(1)+P(L+1)*AS(2)+P(L+2)*AS(3)
DO 230 I=1,3
IF (KI(I).EQ.0) GO TO 230
N=N+1
DF(N)=2.0*(AS(I)*(HA(1)*HA(1)*P(I)+HA(2)*HA(2)*P(I+3)+HA(3)*HA(3)
1*P(I+6))+HA(1)*(HA(2)*QT(1)*(PT(1)*P(I+3)+PT(4)*P(I))+HA(3)*QT(4)
1*(PT(1)*P(I+6)+PT(7)*P(I))+HA(2)*HA(3)*QT(7)*(PT(4)*P(I+6)+PT(7)
1*P(I+3)))
230 CONTINUE
DO 240 I=1,3
IF (KI(I+3).EQ.0) GO TO 240
N=N+1
DF(N)=-2.0*SNS(I)*(HA(1)*PT(1)*(HA(2)*PT(4)*Q(I)+HA(3)*PT(7)*Q(I+3)
1)+HA(2)*HA(3)*PT(4)*PT(7)*Q(I+6))
240 CONTINUE
IF (KI(7).EQ.0) GO TO 241
THETA=.5*(CON+A(7))/RAD
DF(NV)=-8./{W*W}*SIN(THETA)*COS(THETA)
241 FC(J)=HA(1)*HA(1)*(P(1)*AS(1)**2+P(2)*AS(2)**2+P(3)*AS(3)**2)+
1HA(2)*HA(2)*(P(4)*AS(1)*AS(1)+P(5)*AS(2)*AS(2)+P(6)*AS(3)*AS(3))+
2HA(3)*HA(3)*(P(7)*AS(1)*AS(1)+P(8)*AS(2)*AS(2)+P(9)*AS(3)*AS(3))+
32.0*(HA(1)*PT(1)*(HA(2)*PT(4)*QT(1)+HA(3)*PT(7)*QT(4))+HA(2)*HA(3)
4*PT(4)*PT(7)*QT(7))
N=0
DO 250 I=1,NV
DO 248 K=I,NV
N=N+1
AN(N)=AN(N)+DF(I)*DF(K)*WGT(J)
248 CONTINUE
V(I)=V(I)+(FD(J)-FC(J))*DF(I)*WGT(J)
250 CONTINUE
RETURN
END

```

C  
C  
C

SUBROUTINE SMI(AMAT,IRDER,ISING)

C  
C  
C

FORTRAN 4 VERSION-ALGORITHM 150 SYMIN2-UPPER TRI STORAGE

```

DIMENSION R000(7),AMAT(28),GAR(7),PAR(7)
LOGICAL RFOO
ISING=0
8012 DO 8013 IMAT=1,IRDER
8013 R000(IMAT)=.TRUE.

```

C  
C  
C

GRAND LOOP

C  
C  
C

DO 8096 IMAT=1,IRDER

SEARCH FOR PIVOT

```

C      BIG=0.
      DO 8020 JPP=1,IRDER
      LRP=IRDER*(JPP-1)-((JPP-1)*JPP)/2 +JPP
      IF(.NOT.(RBOO(JPP).AND.(ABS(AMAT(LRP)).GT.BIG))) GO TO 8020
8030  BIG=ABS(AMAT(LRP))
      KAT=JPP
8020  CONTINUE
      IF (BIG)8035,8100,8035
8100  ISING=1
      GO TO 8097

C      PREPARATION OF ELIMINATION STEP 1
C
C      8035 RBOO(KAT)=.FALSE.
      LRP=IRDER*(KAT-1)-((KAT-1)*KAT)/2 +KAT
      QAR(KAT)=1./AMAT(LRP)
      PAR(KAT)=1.
      AMAT(LRP)=0.
      KKAT=KAT-1
      IF (KKAT.LT.1) GO TO 8065
8037  DO 8060 JPP=1,KKAT
      LRP=IRDER*(JPP-1)-((JPP-1)*JPP)/2 +KAT
      PAR(JPP)=AMAT(LRP)
      SIG = 1.
      IF (RBOO(JPP))SIG =-SIG
      QAR(JPP)=SIG *AMAT(LRP)*QAR(KAT)
8060  AMAT(LRP)=0.
8065  KKKAT=KAT+1
      IF (KKKAT.GT.IRDER) GO TO 8094
8067  DO 8090 JPP=KKKAT,IRDER
      LRP=IRDER*(KAT-1)-((KAT-1)*KAT)/2+JPP
      SIG =-1.
      IF (RBOO(JPP)) SIG =-SIG
      PAR(JPP)=SIG *AMAT(LRP)
      QAR(JPP)=-AMAT(LRP)*QAR(KAT)
8090  AMAT(LRP)=0.

C      ELIMINATION PROPER
C
C      8094 DO 8095 JPP=1,IRDER
      DO 8095 KAT=JPP,IRDER
      LRP=IRDER*(JPP-1)-((JPP-1)*JPP)/2+KAT
8095  AMAT(LRP)=AMAT(LRP)+PAR(JPP)*QAR(KAT)
8096  CONTINUE
8097  RETURN
      END

```

222.

MONOCLINIC TEST SET SAMPLE DATA SET  
5.92 7.606 9.029 90.00 93.12 90.00 0.0  
1.5405  
11101002  
1 8 1 111.22  
4 6 2 110.89  
4 5 3 102.34  
2 7 5 121.84  
2 6 6 115.26  
3 5 6 112.64  
0 5 7 103.03  
2 4 8 115.72  
4 3 7 120.52  
2 2 8 100.87  
4 1 7 110.11  
2 1 9 112.29  
1 1 10 122.29  
99

MONOCLINIC TEST SET SAMPLE DATA SET  
 LAMDA=1.54050 2\*THETA 0= 0.0  
 VOLUME= 405.95

H	K	L	THO	THC	FO	FC
1	8	1	111.220	111.325	1.147892	1.149248
4	6	2	110.890	111.069	1.143273	1.145731
4	5	3	102.340	102.507	1.022874	1.025273
2	7	5	121.840	122.008	1.287364	1.289472
2	6	6	115.260	115.394	1.202393	1.204175
3	5	6	112.640	112.802	1.167178	1.169379
0	5	7	103.030	103.184	1.032775	1.034986
2	4	8	115.720	115.917	1.208501	1.211114
4	3	7	120.520	120.737	1.270752	1.273500
2	2	8	100.870	101.008	1.001694	1.003686
4	1	7	110.110	110.305	1.132526	1.135215
2	1	9	112.290	112.484	1.162421	1.165064
1	1	10	122.290	122.584	1.292971	1.296623

VARIANCE ESTIMATE IS 0.7158E-05

OLD	SHIFT	NEW	ERROR
5.9200	0.0140	5.9340	0.0224
7.6060	0.0044	7.6104	0.0072
9.0290	0.0147	9.0437	0.0126
89.9999			
93.1200	0.0857	93.2057	0.2812
89.9999			

VOLUME= 407.77

H	K	L	THO	THC	FO	FC
1	8	1	111.220	111.224	1.147802	1.147861
4	6	2	110.890	110.882	1.143273	1.143173
4	5	3	102.340	102.344	1.022874	1.022937
2	7	5	121.840	121.852	1.287364	1.287516
2	6	6	115.260	115.242	1.202393	1.202155
3	5	6	112.640	112.643	1.167178	1.167216
0	5	7	103.030	103.020	1.032775	1.032637
2	4	8	115.720	115.729	1.208501	1.208622
4	3	7	120.520	120.518	1.270752	1.270735
2	2	8	100.870	100.852	1.001694	1.001433
4	1	7	110.110	110.116	1.132526	1.132609
2	1	9	112.290	112.283	1.162421	1.162324
1	1	10	122.290	122.305	1.292971	1.293170

VARIANCE ESTIMATE IS 0.2348E-07

OLD	SHIFT	NEW	ERROR
5.9340	0.0000	5.9340	0.0013
7.6104	-0.0000	7.6103	0.0004
9.0437	0.0000	9.0437	0.0007
89.9998			
93.2057	0.0004	93.2061	0.0162
89.9998			